RECLAMATION

Managing Water in the West

Desalination and Water Purification Research and Development Program Report No. 189

Activated Sludge Aeration Waste Heat for Membrane Evaporation of Desalination Brine Concentrate: A Bench Scale Collaborative Study

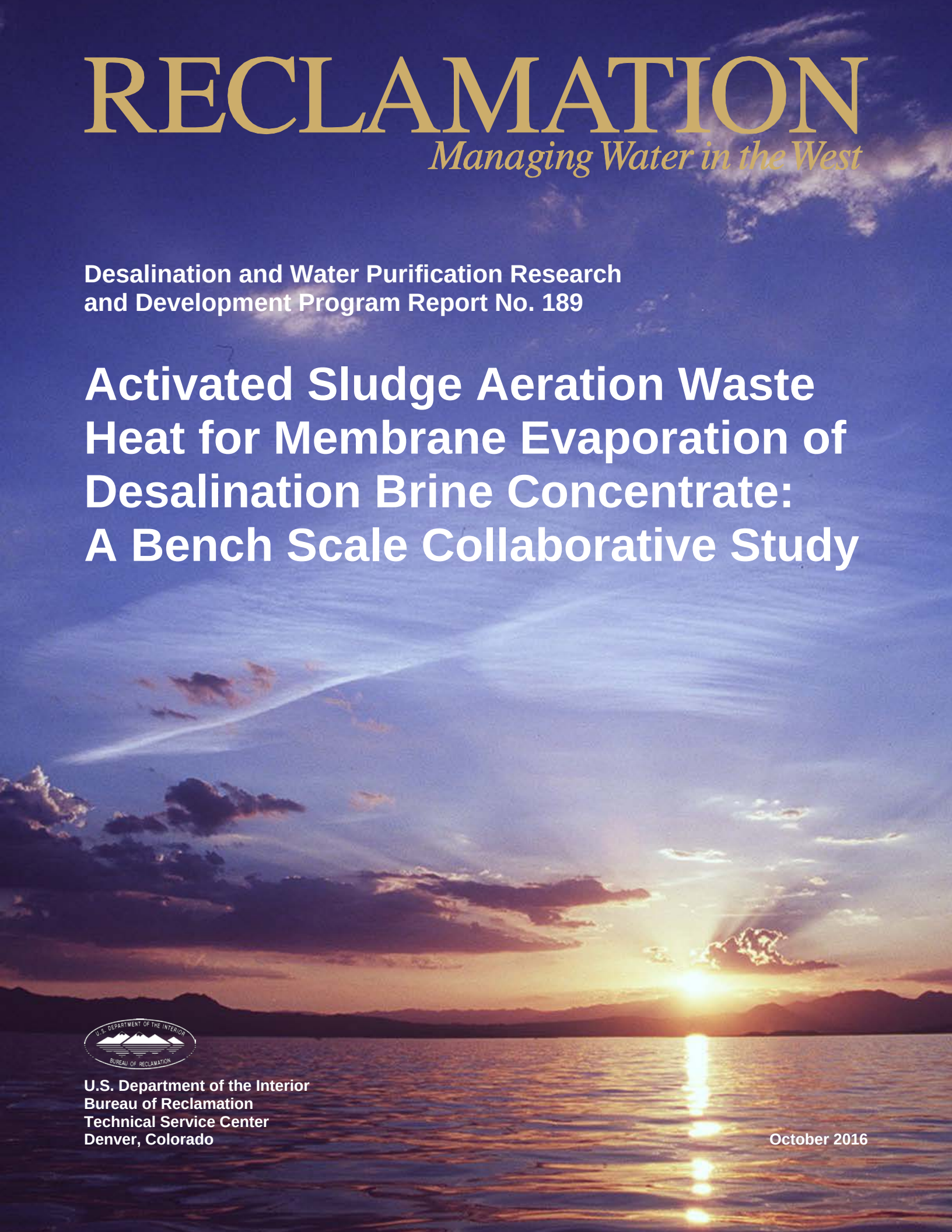

U.S. Department of the Interior
Bureau of Reclamation
Technical Service Center
Denver, Colorado

October 2016

REPORT DOCUMENTATION PAGE

Form Approved
OMB No. 0704-0188

PLEASE DO NOT RETURN YOUR FORM TO THE ABOVE ADDRESS.

1. REPORT DATE *(DD-MM-YYYY)*	**2. REPORT TYPE**	**3. DATES COVERED** *(From - To)*
30-05-2015		9/1/2014 – 6/30/2016

4. TITLE AND SUBTITLE

Activated Sludge Aeration Waste Heat for Membrane Evaporation of Desalination Brine Concentrate: A Bench Scale Collaborative Study.

5a. CONTRACT NUMBER
R14AP00172

5b. GRANT NUMBER

5c. PROGRAM ELEMENT NUMBER

6. AUTHOR(S)

Drew W. Johnson, Nayana S. Muppavarapu, Heather J. Shipley

5d. PROJECT NUMBER

5e. TASK NUMBER

5f. WORK UNIT NUMBER

7. PERFORMING ORGANIZATION NAME(S) AND ADDRESS(ES)
University of Texas at San Antonio
One UTSA Circle
San Antonio, Texas 78249

8. PERFORMING ORGANIZATION REPORT NUMBER

9. SPONSORING/MONITORING AGENCY NAME(S) AND ADDRESS(ES)

10. SPONSOR/MONITOR'S ACRONYM(S)

11. SPONSOR/MONITOR'S REPORT NUMBER(S)

12. DISTRIBUTION/AVAILABILITY STATEMENT

13. SUPPLEMENTARY NOTES

14. ABSTRACT

This study investigates the potential of coupling membrane evaporation of salt water brines with waste heat generated from activated sludge aeration blowers. To assess the efficacy of this coupling membrane, this study used parametric bench scale studies conducted with microporous hollow fiber membrane modules used to evaporate water from brine concentrate. Model predictions, derived based upon literature values for heat and mass transfer correlations, agree well with both the measured evaporated flux and brine concentrate fraction evaporated. The model was used for predicting brine concentrate evaporated fraction and flux for waste heat obtained from a full-scale wastewater aeration system. The volume of water treated was low, but economics of the process appear favorable because energy demands can be neglected when using waste heat.

15. SUBJECT TERMS

Aeration waste heat, membrane evaporation, reverse osmosis brine

16. SECURITY CLASSIFICATION OF:			**17. LIMITATION OF ABSTRACT**	**18. NUMBER OF PAGES**	**19a. NAME OF RESPONSIBLE PERSON**
a. REPORT	**b. ABSTRACT**	**c. THIS PAGE**		114	Yuliana Porras-Mendoza
U	U	U			**19b. TELEPHONE NUMBER** *(Include area code)* 303-445-2265

Desalination and Water Purification Research and Development Program Report No. 189

Activated Sludge Aeration Waste Heat for Membrane Evaporation of Desalination Brine Concentrate: A Bench Scale Collaborative Study

Prepared for the Bureau of Reclamation
Under Agreement No. R14AP00172

by

Drew W. Johnson
Nayana S. Muppavarapu
Heather J. Shipley

University of Texas at San Antonio

U.S. Department of the Interior
Bureau of Reclamation
Technical Service Center
Denver, Colorado

October 2016

Mission Statements

The Department of the Interior conserves and manages the Nation's natural resources and cultural heritage for the benefit and enjoyment of the American people, provides scientific and other information about natural resources and natural hazards to address societal challenges and create opportunities for the American people, and honors the Nation's trust responsibilities or special commitments to American Indians, Alaska Natives, and affiliated island communities to help them prosper.

The mission of the Bureau of Reclamation is to manage, develop, and protect water and related resources in an environmentally and economically sound manner in the interest of the American public.

Disclaimer

The views, analysis, recommendations, and conclusions in this report are those of the authors and do not represent official or unofficial policies or opinions of the United States Government, and the United States takes no position with regard to any findings, conclusions, or recommendations made. As such, mention of trade names or commercial products does not constitute their endorsement by the United States Government.

Acknowledgments

This work was sponsored by the Desalination and Water Purification Research and Development Program, Bureau of Reclamation. In addition, the assistance and support of the San Antonio Water System is acknowledged.

Acronyms and Abbreviations

DAQ	data acquisition
DC	direct current
DI	deionized
ED	electrodialysis
I/O	input/output
ISE	ion selective electrode
MD	membrane distillation
ME	membrane evaporation
MED	multiple effect distillation
MSF	multi-stage flash
NF	nanofiltration
PP	polypropylene
PTFE	polytetrafluoroethylene
PVDF	polyvinylidenedifluoride
RH	relative humidity
RO	reverse osmosis
SAWS	San Antonio Water System
SEM	Scanning Electron Microscopy
TDS	total dissolved solids

Measurements

°C	degree Celsius
Å	ångströms
cm	centimeter
J	joules
J $mole^{-1}$ K^{-1}	joules per mole per degree Kelvin
kg	kilograms
kg $mole^{-1}$	kilograms per molecular weight
K	degree Kelvin
kg m^{-3}	kilograms per cubic meter
kg s^{-1}	kilograms per second
kg $s^{-1}m^{-2}$	kilograms per second per square meter
kg m^{-3}	kilograms per cubic meter
kPa	kilopascal
kPa m^{-1}	kilopascals per meter
kV	kilovolts
kWh	kilowatt hour
kWh m^{-3}	kilowatt hours per cubic meter
L	liter
L d^{-1}	liters per day
L min^{-1}	liters per minute
m	meter
m s^{-1}	meters per second
m^2	square meter
m^2 s^{-1}	square meters per second
m^3	cubic meter
m^3 s^{-1}	cubic meters per second
mgL^{-1}	milligrams per liter
mL	milliliter
mL min^{-1}	milliliters per minute
mL min^{-1} m^{-2}	milliliters per minute per square meter

MLD	million liters per day
mm	millimeter
mmole L^{-1}	millimoles per liter
mol m^{-2} s^{-1}	moles per square meter per second
mS cm^{-1}	milli-siemens per centimeter
N m^{-1}	newtons per meter
N m^{-2}	newtons per square meter
N s m^{-2}	newton seconds per square meter
W	watt
W m^{-1} K^{-1}	watts per meter per degree Kelvin
W m^{-2}	watts per square meter
W m^{-2} K^{-1}	watts per square meter per degree Kelvin
W s kg^{-1} K^{-1}	watts per second per kilogram per degree Kelvin
μm	micron

Variables

A	surface area of hollow fiber membrane (m^2)
C_{p-air}	specific heat capacity of air (W s kg^{-1} K^{-1})
$C_{p-water}$	specific heat capacity of water (W s kg^{-1} K^{-1})
D	molecular and Knudsen diffusion (m^2 s^{-1})
D_{AB}	molecular diffusion (m^2 s^{-1})
D_k	Knudsen diffusion (m^2 s^{-1})
d_e	equivalent diameter (m)
d_o	hollow fiber outer diameter (m)
H_o	overall heat transfer coefficient (W m^{-2} K^{-1})
h_{bl}	heat transfer coefficient of the air boundary layer (W m^{-2} K^{-1})
h_m	membrane heat transfer coefficient (W m^{-2} K^{-1})
h_v	latent heat of vaporization latent heat of vaporization of water (W s kg^{-1})
J'	molar flux (mole m^{-2} s^{-1})
K_o	overall mass transfer coefficient (m s^{-1})
k'	thermal conductivity of air (W m^{-1} K^{-1})
k_{bl}	air boundary layer mass transfer coefficient (m s^{-1})
k'_g	thermal conductivity of saturated air (W m^{-1} K^{-1})
k_m	membrane mass transfer coefficient (m s^{-1})
k'_s	thermal conductivity of membrane material (W m^{-1} K^{-1})
L_m	length of hollow fiber membrane (m)
M_{water}	the mass flow rate of water within a single hollow fiber (kg s^{-1})
m_{air}	mass flow rate of air (kg s^{-1})
N	mass flux (kg $s^{-1}m^{-2}$)
N_f	number of hollow fibers
P_{air}	air pressure (kPa)
Pr	Prandtl number
Q	heat flux rate of heat transfer (W m^{-2})
Q_{in}	brine concentrate volumetric flowrate entering the membrane module (m^3 s^{-1})
Q_{out}	brine concentrate volumetric flowrate exiting the membrane module (m^3 s^{-1})
Q_{air}	universal gas constant (J $mole^{-1}$ K^{-1})
R	air volumetric flow rate (m^3 s^{-1})
Re_{air}	Reynold's number of airflow
r	pore radius (m)
r_{max}	largest pore size of the membrane (m)
Sc	Schmidt number
T_{air}	air temperature (K)
$T_{cold\text{-}in}$	temperature of brine concentrate entering the membrane (K)

$T_{cold\text{-}out}$	temperature of brine concentrate exiting the membrane (K)
$T_{hot\text{-}in}$	temperature of heated air entering the membrane (K)
$T_{hot\text{-}out}$	temperature of heated air exiting the membrane (K)
T_{in}	temperature on the water side at the membrane surface (K)
$T_{membrane}$	temperature at the outer surface of the membrane in contact with air (K)
T_{water}	water temperature (K)
Wc_{in}	water vapor content of air entering the membrane module (kg m^{-3})
Wc_{out}	water vapor content of air exiting the membrane module (kg m^{-3})
v	air velocity (m s^{-1})
v_{water}	water velocity (m s^{-1})
z	location along the length of the hollow fiber (m)
α	Knudsen diffusion constant
Δp	penetration pressure (N m^{-2})
ΔT_{air}	temperature difference of air upstream and the downstream along the length of the membrane (K)
δ	thickness of membrane wall (m)
σ_L i	surface tension of the liquid inside the membrane lumen (N m^{-1})
ε	porosity
θ	contact angle between liquid phase and membrane
μ	dynamic viscosity of air (N s m$^{-2)}$
v	kinematic viscosity of air (m^2 s^{-1})
ρ_a	density of humid air (kg m^{-3})
ρ_{air}	density of water vapor in air (kg m^{-3})
$\rho_{membrane}$	density of water vapor in air at the outer surface of the membrane (kg m^{-3})
ρ_{sat}	density of water vapor in air within the membrane pore just adjacent to the membrane lumen (kg m^{-3})
ρ_{water}	density of water (kg m^{-3})
σ	surface tension of liquid inside the membrane (N m^{-1})
τ	tortuosity
ϕ	membrane packing

Contents

Figures

Tables

Appendices

1. Executive Summary

This study examines a potential membrane evaporation process to reduce brine concentrate volume at the San Antonio Water System's (SAWS) 45.4 million liters per day (MLD) brackish water desalination facility in San Antonio, Texas, which is currently being constructed. This facility is a reverse osmosis (RO) process operating with 90% recovery by blending 37.9 MLD of permeate with 7.6 MLD of bypass water, producing 4.2 MLD of brine concentrate. SAWS plans to expand the facility to produce 114 MLD over the next 12 years. The brine concentrate residuals are to be disposed of through deep-well injection. The deep-well injection process is anticipated to be expensive due to well-drilling costs and maintenance costs of operating at high injection pressures.

Membrane evaporation systems are promising because they are compact systems and they can be used with low grade waste heat energy sources. This study investigates the potential of coupling membrane evaporation with waste heat generated from activated sludge aeration blowers. Blower compression of air produces significant amounts of airflow containing waste heat that can be used to drive membrane evaporation processes. This study assesses the efficacy of this coupling.

The experimental approach involved parametric bench scale studies conducted with microporous hollow fiber membrane modules used to evaporate water from brine concentrate. Oven-heated air was used under conditions simulating the waste heat available from municipal wastewater treatment aeration blowers. Results obtained from the bench scale studies were used to validate a numerical heat and mass transfer model that was used for estimating the fraction and flux of brine concentrate evaporated at full scale conditions. Bench scale testing studies were also conducted to evaluate fouling extent and possible means to control fouling.

Permeate flux and the fraction of brine concentrate that is evaporated for a membrane evaporation process were found to increase with airflow rate and air temperature and to decrease with brine concentrate flow rate. Increasing airflow rate and air temperature provides more energy to the system for evaporating water while increasing brine concentrate flow rate strips energy that could be used for evaporating brine concentrate. Model predictions, derived based upon literature values for heat and mass transfer correlations, agree well with both the measured evaporated flux and fraction of brine concentrate evaporated in the bench scale studies. For full scale conditions, the model predicted volume of water treated was low. However, the process economics appear favorable because energy demands can be neglected when using waste heat.

Operational problems are most likely to be caused by fouling. Fouling was observed in experiments for brine concentrates with and without ferrous iron. Cleaning the membranes by flushing the fibers with brine concentrate at higher flow rates was not able to alleviate this fouling. Fouling could be alleviated by adjusting the pH of the brine concentrate solution to be low for the durations of the studies conducted. Full evaluation of the process will require longer-term studies, and future studies should also consider possible sources of supplemental waste heat to increase the overall amount of water treated.

2. Introduction and Background

With increasing freshwater demands, the need to explore various water resources has been increasing. Of all the Earth's water resources, only 0.8% is available as fresh water, 96.5% percent as seawater, and the remaining as ground water, brackish water, and water covered in icecaps which are hard to recover (Gleick 1996). Thus, seawater is a promising source for coastal areas whereas brackish water can be used to overcome water scarcity for inland regions.

The salt concentration of seawater and the brackish water are reduced to potable levels by a process called desalination. Desalination removes excess minerals and salts: either by thermal energy driven processes such as multi-stage flash (MSF) distillation and multiple effect distillation (MED) or by membrane processes such as RO (Wade 1993 and Van der Bruggen and Vandecasteele 2002).

MED is the oldest method available for desalination of saltwater (Al-Shammiri and Safar 1999). The process uses the heat energy from steam condensation to evaporate brine in multiple stages. In MSF, the first stage heat from the steam is used to evaporate some of the water from the brine. The steam generated in the first stage is used for evaporating more water in the next stage which is maintained at lower pressures and the process continues till the desired percentage of removal is achieved (Wade 1993 and Van der Bruggen and Vandecasteele 2002). Different configurations and various improvements have been made since the invention of the process to improve the efficiency and reduce costs (El-Dessouky et al. 1998). It has been the most commonly used method in the Middle Eastern countries due to its low scaling capabilities (Al-Shammiri and Safar 1999 and Van der Bruggen and Vandecasteele 2002).

RO processes are relatively new technologies and are also among the most commonly used desalination methods and dominates most of the desalination facilities in the United States (Krishna 2004) because of high rejection capability at relatively low energy costs (Brehant et al. 2003). Unlike thermal desalination processes, RO does not require fuel inputs, although the energy needed for operating pressures range from 6,000 to 8,000 kilopascals (kPa), depending on the feed source (Fritzmann et al. 2007). The technology was invented around the time when MSF was in use and has been a good competitor. In RO, osmotic pressure is

applied to the seawater so that the water permeates through a membrane. In the process, 30 to 85% of the permeate is recovered as fresh water. The remaining higher concentrate effluent that leaves the system is commonly called the RO concentrate. Because of its high rejection rates and recent advancements, RO has become the optimal choice for desalination plants (Karagiannis and Soldatos 2008 and Greenlee et al. 2009).

Other types of membrane processes, such as electrodialysis (ED) (Reahl 2004) and nanofiltration (NF), are also available (Singh 1997).

All desalination processes produce highly concentrated effluent, referred to as brine concentrate. Because of the increasing number and size of desalination plants, the volume of brine concentrate has been increasing. This effluent can be disposed using different ways, depending on the location and climatic conditions of the desalination plant (Voutchkov 2011). For desalination facilities in coastal areas, effluent can be discharged into saline coastal waters. Due to presence of spent chemicals and elevated salinity (as well as high temperature for thermal desalination processes) frequent disposal can have negative impact upon the marine ecosystem. Alternatively, the effluent can be used for production of salt which can be economical in some cases. Desalination facilities in the Middle-East has been using this method since 1998 (Ravizky and Nadav 2007).

For inland brackish water desalination facilities, there are other options for concentrate disposal such as discharge into surface water bodies, solar evaporation, or deep well injection (Glater and Cohen 2003). Effluent from brackish water desalination facilities that is dumped into the nearby surface water bodies, such as lakes, can change the salinity of the water body and detrimentally impact aquatic organisms (Pérez-González et al. 2012). Furthermore, concentrate effluents may sometimes contain harmful chemicals based on the type of feed water and pose threats to aquatic organisms. Effluent requires pretreatment in these cases (Mickley 2004).

For semi-arid regions with high annual temperatures and appropriate humidity conditions, concentrated effluent can be pumped into evaporation ponds and evaporate naturally from solar energy (Ahmed et al. 2000). Even though this process is economical, it depends on climate conditions and requires large areas of evaporative ponds.

Another disposal method used by many inland desalination facilities is deep well injection (Saripalli et al. 2000). The effluent is injected several thousand meters under the ground. Injection has a high cost and controversies over potential longer-term pollution of freshwater aquifers (Leenheer et al. 1976). There are other methods such as using the concentrate for irrigation, but this raises concerns for increasing soil salinity and reducing overall crop productivity (Squire 2000).

The current study focuses on developing an alternate cost-effective technique to reduce brine concentrate volumes, which may conserve energy and reduce costs. In this process, hydrophobic hollow fiber membranes are used with micron-sized pores spread along the surface of the membrane connecting the inner and outer membrane surfaces (Kopp et al. 1997). Hollow-fiber membranes are used because they provide high surface area to volume ratios—allowing maximum energy transfer through the membrane wall. The membrane's material, diameter, pore size, and porosity impact how the membrane is used (McKelvey et al. 1997).

In membrane evaporation, the driving force is obtained by the temperature difference between fluids inside and outside the membrane. Membrane evaporation processes act similarly to heat exchangers: a cold fluid can be pumped inside the hollow membranes while exposing the outer surface of the membrane to hotter fluids flowing in a counter direction. In an application for evaporating RO brine concentrate, the brine concentrate is the cold fluid that enters inside hollow fiber lumens while exposing the outer membrane surface to low grade heat. During this process, heat is exchanged, and some of the water molecules from brine concentrate convert into vapor and escape through the membrane micro pores. The humidity of the air increases if heated air is used as the low-grade heat source. If desired, the water vapor can be collected as condensate when air leaving the membrane modules cools.

Low-grade heat sources can be used because this membrane process does not require high temperature differences to carryout mass transfer operations. An example of low-grade heat is air compressed at wastewater treatment facilities as part of their aeration process. In these operations, the compression or pressurization of the air causes an increase in air temperature (often modeled as adiabatic where heat does not enter or leave the system). This waste heat can be used to drive heat and mass transfer operations for evaporating brine concentrate from inside the membrane.

Membrane distillation is similar to membrane evaporation. However, in membrane distillation, the high temperature fluid is pumped inside the hollow membranes while outer surface is exposed to cold fluid moving in the same flow direction as hotter fluid (Lawson and Lloyd 1996 and Alkhudhiri et al. 2012). The biggest disadvantage of membrane distillation is that more energy is needed (Al-Obaidani et al. 2008) than in RO.

Finally, one should note that membrane processes such as these are widely used in other industries including the food and beverage industry (Jiao et al. 2004), and the chemical industry (Zhao et al. 2014) in addition to the water filtration industry (Roebelen et al. 1982).

One potentially problematic aspect of this membrane evaporation process is fouling. Fouling can be defined as accumulation of salts, colloids, biological material, and other solute particles on the membrane wall. Fouling affects the

overall performance of the system by clogging pores and reducing transfer performance (Schäfer et al. 2000 and Kullab and Martin 2011). The degree of fouling depends on concentration and type of solutes in the fluid and on the membrane material and pore size. Since brackish water contains high concentrations of salts, the fouling is mainly due to deposition of salts. Salts with low solubility such as calcium sulfate and calcium carbonate accumulate and pose problems in brackish water membrane treatment processes (Hasson et al. 2001). The effects of other salts, such as NaCl, have been found to be not so significant when compared to calcium salts (Drioli and Wu 1985 and Li and Elimelech 2006).

Various attempts have been made to reduce the effect of fouling by adding synthetic polymers called antiscalants to feed waters. Antiscalants work by decreasing the precipitation tendency of saturated salts. However, at high salt concentrations, antiscalants are not able to completely prevent the salts from accumulating and fouling the membrane (Bonne et al. 2000). To rectify fouling, several techniques can be used:

- Pretreatment techniques can also be beneficial to inhibit fouling such as adding acids to feed water to lower the pH and increase the solubility of salts resulting in a decreased fouling rate (Isaias 2001).

- Membrane cleaning uses cleaning agents to wash off the accumulated salt inside the membrane to make it reusable.

- Low pH (≈ 2) solutions from hydrochloric acid addition can be used for cleaning (Bonne et al. 2000). At low pH, the solubility of salts increases and the accumulated salts are dissolved in the solution.

- Backwashing is another physical technique, where permeate is pumped in the opposite direction at high flow rates to wash off salt build up inside the membrane (Yiantsios and Karabelas 2001).

3. Conclusions and Recommendations

The results obtained from bench scale experimental studies agree well with predictions for evaporated flux and the fraction of brine concentrate that is evaporated, derived based upon literature values for heat and mass transfer correlations. Brine concentrate is the brine remaining after RO treatment. The fraction of brine concentrate evaporated (< 0.0012) and the amount of condensate collected (~5,000 liters per day [L d^{-1}]) would be negligible if the system were operated at full-scale condition (4.2 10^6 L d^{-1}). The system brine concentrate flow rate is too high, and the membranes act like heat exchangers with little evaporation occurring. If the brine concentrate flow rate were reduced to 50,000 L d^{-1}, approximately 40% of the brine concentrate could be recovered as condensate at ~ 20,000 L d^{-1}.

Evaporating 20,000 L d^{-1} of brine concentrate and given the current cost of membranes at approximately $13 per square meter ($m^2$) with 1,120 m^2 needed for the full-scale membrane area, and an assumed membrane life time of 3 years, equates to an unamortized membrane treatment cost of $0.66 per cubic meter ($m^3$) of brine concentrate evaporated. Other costs may be incurred for acid addition, but the cost of treatment is likely to be favorable because the system uses waste heat and energy costs can be neglected.

It is important to note that the membrane evaporation process used in this study has dual benefits obtained for the cost incurred. The brine concentrate volume requiring disposal is reduced while high quality permeate is produced.

Operational problems are likely to be caused by fouling, as fouling occurred in experiments for brine concentrates with and without ferrous iron. Cleaning the membranes by flushing the fibers with brine concentrate at higher flow rates was not able to alleviate this fouling. Fouling could be alleviated by adjusting the pH of the brine concentrate solution to be low for the durations of the studies conducted. Full evaluation of the process will require longer-term studies than those conducted in this study, and future studies should also consider possible sources of supplemental waste heat to increase the overall amount of water treated.

4. Theory

Membrane processes such as membrane evaporation (ME) and membrane distillation (MD) act as type of heat exchangers. One side of the membrane is exposed to hot fluid, and the other side is exposed to cold fluid with both fluids flowing parallel along the membrane wall. The difference between heat exchangers and membrane process is that mass transfer doesn’t take place in heat exchangers, whereas membrane process allows both heat and mass transfer.

A membrane can be either flat sheet or a hollow fiber. The pores in the membrane wall allow the flow of mass from one side of the surface to the other side, depending on the driving force. ME or MD processes usually requires a hollow fiber membrane as depicted in Figure 1. In ME processes, cold fluid is pumped inside the fiber lumen while the outer surface of the membrane is exposed to the hotter fluid, whereas in MD, hot fluid is pumped inside the membrane and cold fluid is pumped outside the membrane.

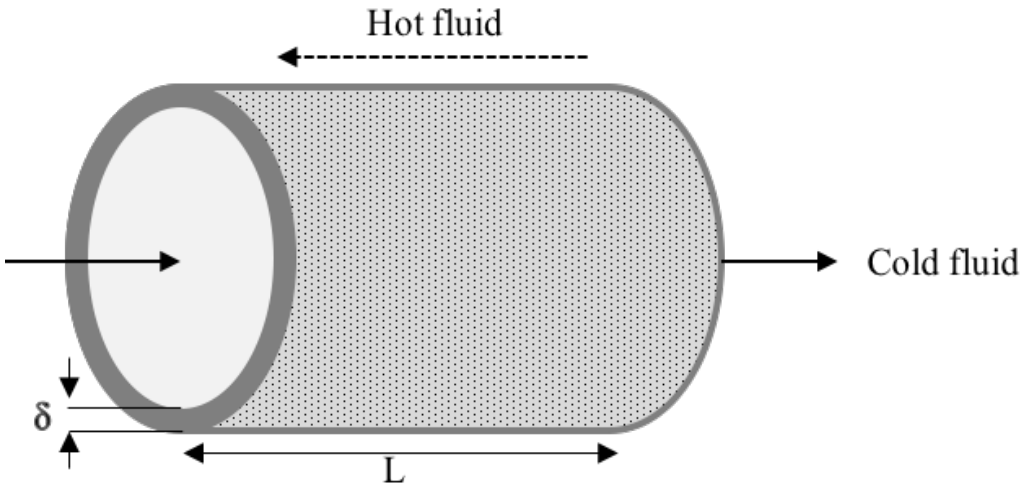

**Figure 1: Hollow fiber membrane in membrane evaporation process.
δ: wall thickness of membrane fiber and L_m: length of hollow fiber membrane (m).**

4.1. Membrane Performance Characteristics

For a desalination ME process, the cold fluid is brine concentrate and the hot fluid is air. An ideal membrane should allow maximum permeate flux through the membrane while using low grade heat energy and should have minimum membrane wetting tendency. This depends on the various features of the membrane material. Most polymer membranes are low surface energy materials and hence if unmodified, are hydrophobic. Hydrophobic membrane materials include polytetrafluoroethylene (PTFE), polypropylene (PP) and polyvinylidenedifluoride (PVDF) (Lawson and Lloyd 1997). The membrane is also characterized by other parameters such as its pore size and porosity. The pore size should be small enough to prevent the brine concentrate inside the membrane from leaking into the air side and it should be large enough to allow water vapor flux. The pore size usually ranges from as small as 100 ångströms (Å) to as high as 1 micron (μm). The relation between molar flux through the membrane pores and average pore size of a membrane is given in Equation 1:

$$J' \propto \frac{(r^{\alpha})\varepsilon}{\tau\delta} \qquad (1)$$

Where:
J' is molar flux (mole per square meter per second [mole m^{-2} s^{-1}])
r is pore radius (meter [m])
α is a constant (for Knudsen diffusion α=1 and for viscous fluids α=2)
ε is porosity
τ is tortuosity
δ is thickness of membrane wall (m)

From Equation 1, it can be said that the molar flux increases with pore size and membrane porosity and decreases with tortuosity and membrane wall thickness. Porosity can be defined as number of pores per unit surface area. Even though increasing the pore size increases the molar flux, there is a maximum size until which feed doesn't leak through the pores. This phenomenon of the feed inside the membrane lumen penetrating into the air side, as shown in Figure 2, is called membrane wetting.

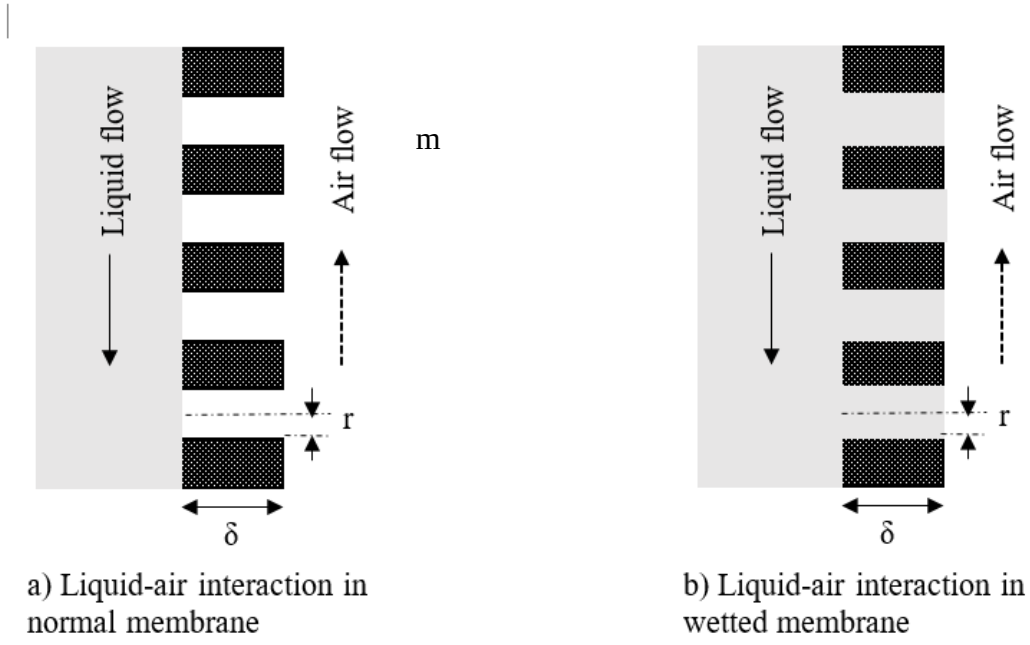

Figure 2: Membrane wetting phenomenon.

The relation between membrane wetting and the maximum allowable pore size can be described by Equation 2, the Laplace-Young equation (Yan, Fang et al. 2007, Lv, Yu et al. 2010):

$$\Delta p = -\frac{2\sigma_L cos\theta}{r_{max}} \qquad (2)$$

Where:
Δp is penetration pressure (newtons per square meter [N m^{-2}])
σ_L is the surface tension of the liquid inside the membrane lumen (newtons per meter [N m^{-1}])
θ is the contact angle between liquid phase and the membrane
r_{max} is the largest pore radius of the membrane (m)

Membrane wetting occurs when the pressure difference between liquid phase and gas phase exceeds the penetration pressure. As seen from Equation 2, the wetting phenomenon not only depends upon membrane's properties but also on the liquid properties. The higher the surface tension of the liquid, the larger the penetration pressure with which the membrane wetting can occur.

4.2. Heat and Mass Transfer Relations

It is well established that membrane evaporation is a membrane separation process where permeate flux across the membrane wall is driven by vapor pressure differences corresponding to differences in water content and fluid temperatures across the membrane. In membrane evaporation, cold fluid flows inside the membrane lumen while hot air flows outside the membrane surface—which means that heat flux and the permeate flux occurs in opposite direction as shown in Figure 3.

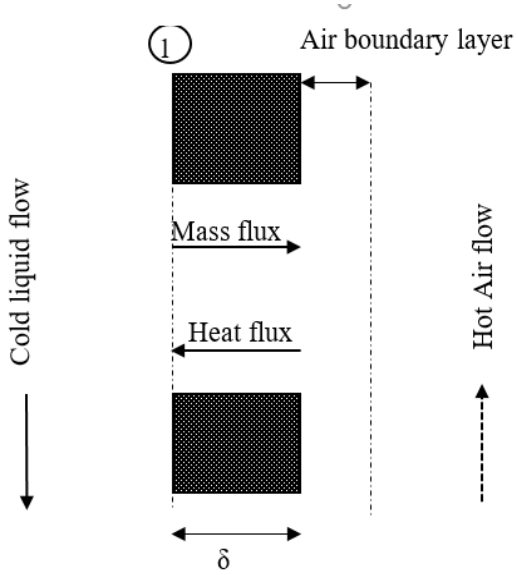

Figure 3: Interaction of cold fluid and hot air at the membrane wall in membrane evaporation.

Cold liquid inside the membrane lumen and the hot air outside the membrane flow in the counter flow direction. As hot air flows outside the membrane surface, the heat energy from the bulk air is transferred to the air boundary layers, through the membrane wall and into the cold liquid at the surface (surface 1 in Figure 3). The cold liquid in contact with the inside of the membrane wall absorbs the heat energy and increases in temperature. The water or any relatively volatile content in the feed then converts into vapor, leaving the salts behind and diffuses in opposite direction of the heat transfer through the pores of membrane, through the air boundary layer and enters into the bulk air. As the air flows along the length of membrane and is cooled from this heat transfer process, the water vapor content inside the bulk air may condense.

Temperature profiles of air and liquid along the length of the membrane in the direction of flow are shown in Figure 4. The liquid and air flow in the counter flow directions inside and outside membrane fiber respectively. The liquid or brine concentrate at ambient temperature enters inside the membrane at 0^{th} position, which is colder than the air side, represented by $T_{cold\text{-}in}$ (degrees Kelvin [K]) in Figure 4. The air at higher temperature, $T_{hot\text{-}in}$ (K) flows from the other end of the membrane outside on its surface. As the brine concentrate flows along the length of the membrane, the temperatures increase by absorbing the heat from the air side. As the brine concentrate reaches the other end, it reaches the highest temperature, $T_{cold\text{-}out}$ (K) on the brine concentrate side. However, the temperature of the brine concentrate is still lower than the temperature on the air side because of heat loss. As the air flows towards the 0^{th} position, the temperature in the air side decreases down to $T_{hot\text{-}out}$ (K) due to heat transfer to the brine concentrate side.

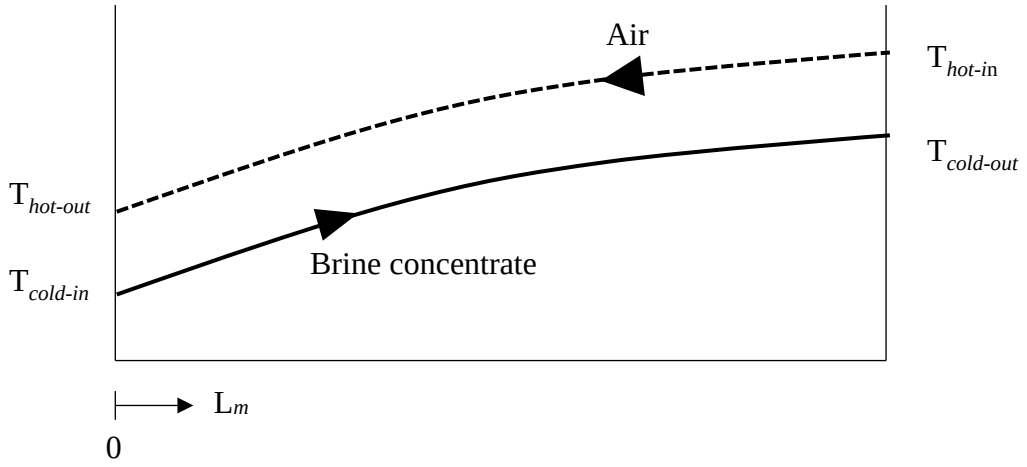

Figure 4: Temperature profiles of the air and brine concentrate along the length of the hollow fiber membrane.

Water vapor profiles of the air outside the membrane and the liquid water flow rate inside the membrane are shown in Figure 5. The water vapor content of air entering the membrane module, represented by Wc_{in} ,(kilograms per cubic meter [kg m^{-3}]) is due to the relative humidity of source air. As air flows along the membrane, it entrains water vapor diffused through the membrane pores. By the time it reaches the other end of the membrane module, the water vapor content reaches a maximum, Wc_{out} (kg m^{-3}). Q_{in} (cubic meters per second [$m^3 s^{-1}$]) is brine concentrate volumetric flowrate entering the membrane module. Q_{out} ($m^3 s^{-1}$) is the brine concentrate volumetric flowrate exiting the membrane module. Brine concentrate flow rates decrease along the length of membrane module because water (as a vapor) is moving across the membrane along the length of membrane.

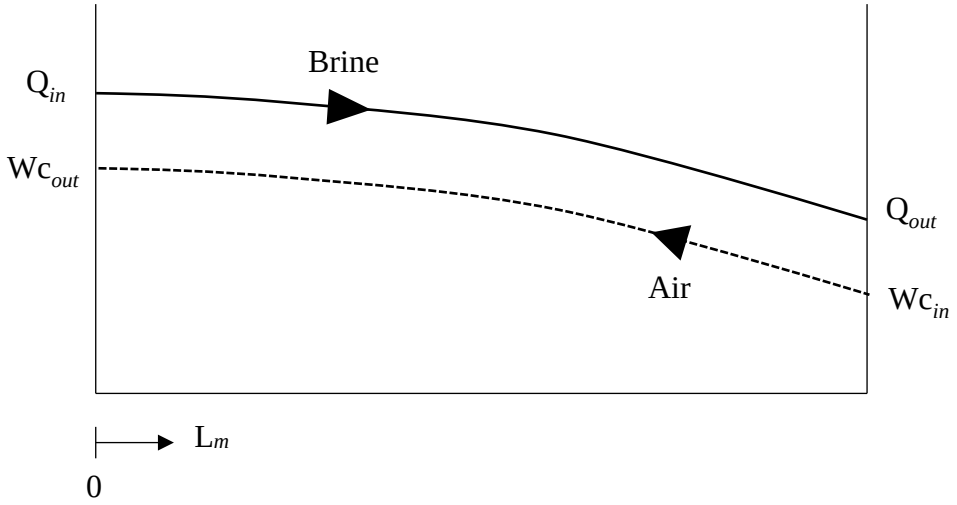

Figure 5: Water content profiles in the air side and brine concentrate side along the length of hollow fiber membrane.

4.2.1. Mass Transfer Across the Membrane

The mass transfer across the membrane occurs by diffusion of water vapor through membrane pores from the liquid side to the air side. The driving force is obtained by water vapor pressure difference across the membrane wall. The mass transfer profile across the membrane is shown in Figure 6. The vapor pressure difference is shown in terms of densities. The resistance in mass transfer occurs in series through the membrane wall and the air boundary layer as shown in Figure 6. The rate at which water vapor escapes through the pores in the membrane wall is given by Equation 3 (Schofield et al. 1987):

$$NA = k_m A(\rho_{sat} - \rho_{membrane}) \quad (3)$$

Where:
N is mass flux which is defined as the rate at which water vapor escapes through micro porous membrane per unit surface area (kilograms per second per square meter [kg $s^{-1}m^{-2}$])

A is lateral surface area of hollow fiber (m^2)

k_m is the membrane mass transfer coefficient (meters per second [m s^{-1}])

ρ_{sat} is density of water vapor in air (kilograms per cubic meter [kg m^{-3}]) within the membrane pore just adjacent to the membrane lumen and can be calculated assuming the air is at 100% relative humidity based upon T_{in}, temperature on the water side at the membrane surface (K)

$\rho_{membrane}$ is density of water vapor in air (kg m^{-3}) at the outer surface of the membrane

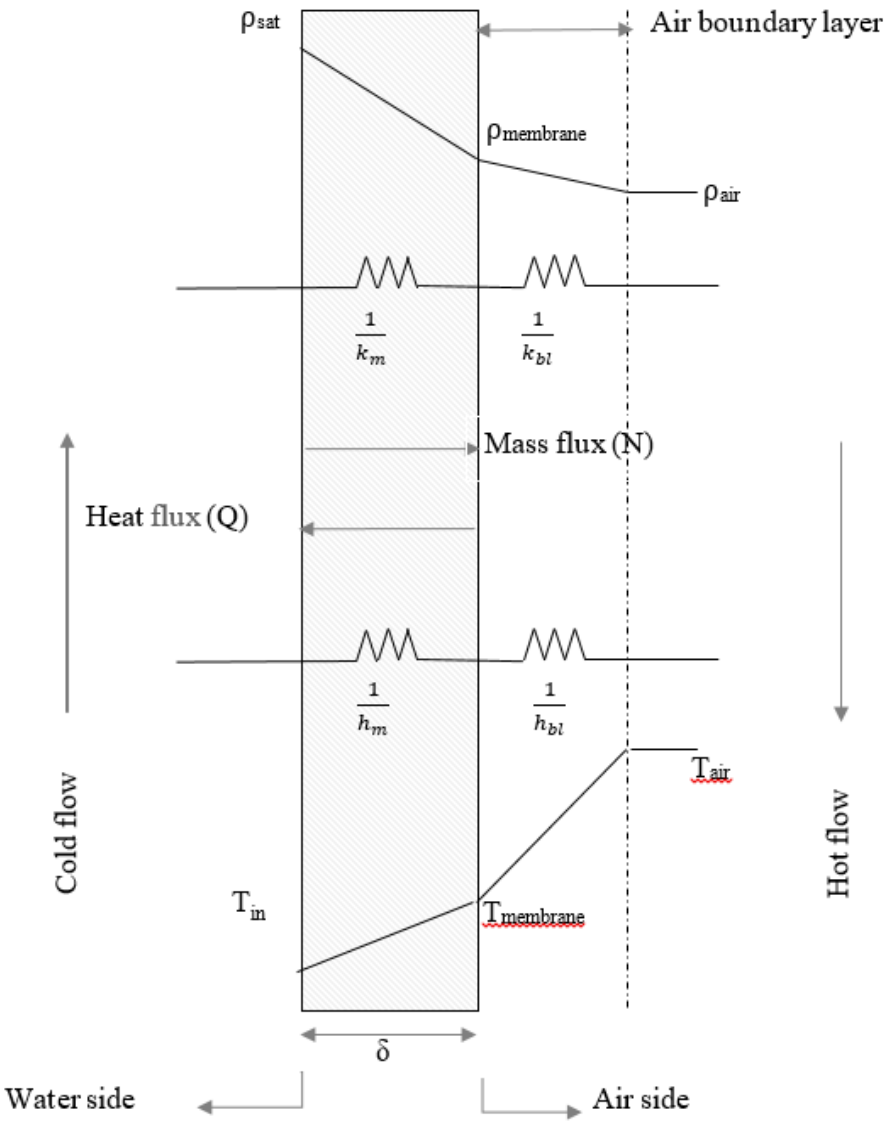

Figure 6: Temperature and vapor profiles across the membrane wall.

The rate of water diffusion through the air boundary layer is given in Equation 4:

$$NA = k_{bl}A(\rho_{membrane} - \rho_{air}) \quad (4)$$

Where:
k_{bl} is the air boundary layer mass transfer coefficient (m s^{-1})
ρ_{air} is the density of water vapor in the bulk air (kg m^{-3})

Equations 3 and 4 can be combined as shown in Equation 5:

$$\mathrm{NA} = K_o A(\rho_{sat} - \rho_{air}) \quad (5)$$

Where:
K_o is the overall mass transfer coefficient through membrane and air boundary layer (m s^{-1}) and can be written as resistance in series as shown in Equation 6:

$$\frac{1}{K_o} = \frac{1}{k_m} + \frac{1}{k_{bl}} \quad (6)$$

4.2.2. Heat Transfer Across the Membrane

Similar to the mass transfer process, heat transfer occurs across the membrane but in the opposite direction and from the air side to the liquid side. The driving force is temperature difference across the membrane wall. The heat transfer profile across the membrane is shown in Figure 6. The resistance in heat transfer occurs in series through the membrane wall and the air boundary layer as shown in Figure 6. Equation 7 is for the rate of heat transfer across the membrane wall, QA (watts [W])

$$QA = h_m A(T_{membrane} - T_{in}) \quad (7)$$

Where:
Q is heat flux which is defined as the rate at heat transfer per unit surface area (watts per square meter [W m^{-2}])
h_m is membrane heat transfer coefficient (watts per square meter per degree Kelvin [W m^{-2} K^{-1}])
T_{in} is the temperature on the water side at the membrane surface (K)
$T_{membrane}$ is the temperature at the outer surface of the membrane in contact with air (K)

The rate of heat transfer through the air boundary layer is given by Equation 8:

$$\mathrm{QA} = h_{bl}\mathrm{A}(\mathrm{T}_{air} - \mathrm{T}_{membrane}) \quad (8)$$

Where:
h_{bl} is the heat transfer coefficient of the air boundary layer (W m^{-2} K^{-1})

T_{air} is the air temperature (K).

Equations 7 and 8 can be combined to write the overall rate of heat transfer as shown in Equation 9.

$$QA = H_o A(T_{air} - T_{in}) \quad (9)$$

Where:
H_o is the overall heat transfer coefficient (W m^{-2} K^{-1}) through the membrane and the air boundary layer, which can be written mathematically as resistance in series as shown in Equation 10:

$$\frac{1}{H_o} = \frac{1}{h_m} + \frac{1}{h_{bl}} \quad (10)$$

The overall rate of heat transfer across the membrane wall should be equal to the heat extracted from the air shown mathematically in Equation 11:

$$QA = m_{air} C_{p-air} \Delta T_{air} \quad (11)$$

Where:
m_{air} is the mass flow rate of air (kilograms per second [kg s^{-1}])
C_{p-air} is specific heat capacity of air (watts second per kilogram per degree Kelvin [W s kg^{-1} K^{-1}])

ΔT_{air} is difference in temperature (K) of air upstream and the downstream along the length of the membrane

4.3. Model Development

In the present analysis, a counter-current parallel flow membrane contactor configuration is used and the lumen side water mass balance is provided in Equation 12 (obtained from Equation 5 for a single hollow fiber).

$$\frac{dM_{water}}{dz} = K_o \pi d_o (\rho_{air} - \rho_{sat}) \quad (12)$$

The accompanied change in shell side water density in air from all of the membrane fibers in the module is provided in Equation 13:

$$\frac{d\rho_{air}}{dz} = \frac{\partial M_{water}}{\partial z} * \frac{N}{Q_{air}} \quad (13)$$

As the water evaporates, the water inside the membrane is cooled and heat is extracted from the air with the resulting change in lumen side water temperature as provided in Equation 14:

$$\frac{dT_{water}}{dz} = \frac{\frac{\partial M_{water}}{\partial z} * h_v + H_o \pi d_o (T_{air} - T_{water})}{M_{water} C_{p-water} T_{water}} \quad (14)$$

The accompanied change in air temperature from all of the membrane fibers is provided in Equation 15.

$$\frac{dT_{air}}{dz} = \frac{H_o N_f \pi d_o (T_{air} - T_{water})}{Q_{air} C_{p-air} \rho_a} \quad (15)$$

In Equations 12 - 15:
M_{water} is the mass flow rate of water within a single hollow fiber (kg s^{-1})

z is the location along the length of the hollow fiber (m)

d_o is the hollow fiber outer diameter (m)

N_f is the number of hollow fiber membranes within the module

Q_{air} is the air volumetric flow rate passing through the membrane module (cubic meters per second [m^3 s^{-1}])

h_v is the latent heat of vaporization of water (W s kg^{-1} K^{-1}) which can be defined as energy required to convert from saturated liquid phase to vapor phase at constant temperature

T_{air} is the air temperature that varies with distance (K)

T_{water} is the water temperature that varies with distance (K)

$C_{p\text{-}water}$ is the specific heat of water (W s kg^{-1} K^{-1})

ρ_a is the mass per volume density of air within the membrane shell (kg m^{-3})

Liquid water is incompressible. Therefore, the liquid water parameters depend on water temperature (T_{water}) but not on water pressure. Air and water vapor within air is compressible and, therefore, the air phase parameters in Equations 12 - 15 depend upon both air temperature (T_{air}) and air pressure (P_{air}). Air pressure changes along the length of the membrane module due to frictional losses as the airflow through the membrane shell. During experiments, inlet and outlet air pressures were monitored and the polynomial relationship shown in Equation 16 represented the change of air pressure with Reynold's number (Re_{air}) along the length the membrane module. Air pressure has units of kilopascals (kPa) and length is expressed in meters. Therefore, Equation 16 has units of kilopascals per meter (kPa m^{-1}).

$$\frac{dP_{air}}{dz} = 3.10^{-08}Re_{air}{}^{2} + 8.10^{-05}Re_{air} - 0.0138 \quad (16)$$

The membrane heat transfer coefficient can be calculated from the membrane thickness and thermal conductivity of gas and solid as shown in Equation 17; including membrane thickness (δ) and porosity (ε).

$$h_m = \frac{\varepsilon k_g' + (1-\varepsilon)k_s'}{\delta} \quad (17)$$

Where:
k_g' is the thermal conductivity (watts per meter per degree Kelvin [W m^{-1} K^{-1}]) of the saturated air in the membrane pores

k_s' is thermal conductivity of membrane material (W m^{-1} K^{-1}).

Water vapor diffusion through the membrane is a function of molecular diffusion, Knudsen diffusion, and membrane characteristics; including membrane thickness (δ), tortuosity (τ), and porosity (ε). The membrane mass transfer coefficient can then be described mathematically in Equation 18:

$$k_m = \frac{D\varepsilon}{\tau\delta} \quad (18)$$

D (square meters per second [m^2 s^{-1}]) represents the combined molecular and Knudsen diffusion and is calculated as shown in Equation 19:

$$\frac{1}{D} = \frac{1}{D_k} + \frac{1}{D_{AB}} \quad (19)$$

D_{AB} is the molecular diffusion of water vapor in air and can be estimated using the Fuller, Schettler, and Giddings method. Knudsen diffusion, D_k, can be expressed mathematically in Equation 20:

$$D_k = \frac{2r}{3}\left(\frac{8RT_{air}}{\pi MW}\right)^{1/2} \quad (20)$$

Where:
R is the universal gas constant (joules per mole per degree Kelvin [J $mole^{-1}$ K^{-1}])

MW= molecular weight of air (kilograms per mole [kg mole^{-1}])

Estimates of the air boundary layer mass transfer coefficient (k_{bl}) can be obtained from correlations in the literature for parallel flow membrane contactors. We used the correlation of Prasad and Sirkar (1988), provided in Equation 21, because it provides significant concurrence in geometric similarity.

$$k_{bl} = 5.85 \frac{D_{AB}}{d_e} Re_{Air}^{0.6} Sc^{0.33} \frac{d_e}{L_m}(1 - \emptyset) \quad (21)$$

Where:
ϕ is membrane packing

The Reynold's number is a dimensionless term used to determine the flow characteristics, and for the airflow it can be calculated using velocity and density as given in Equation 22:

$$Re_{air} = \frac{\rho_a \mathrm{v} d_e}{\mu} \quad (22)$$

Where:
ρ_a is the density of humid air (kg m^{-3})
v is the air velocity (m s^{-1})
μ is the dynamic viscosity of air (newton seconds per square meter [N s m^{-2}])
d_e is the equivalent diameter (m)

The equivalent diameter is defined as Equation 23:

$$d_e = \frac{4(cross\ sectional\ area\ of\ flow)}{(wetted\ perimeter)} \quad (23)$$

The mass and heat transfer boundary layer coefficients (k_{bl} and h_{bl}) can be linked by using the Chilton-Colburn Analogy, which is used to find the heat transfer coefficient through the boundary layer as shown in Equation 24:

$$k_{bl} = \frac{h_{bl}}{\rho_a C_{p-air}} \left(\frac{Pr}{Sc}\right)^{\frac{2}{3}} \quad (24)$$

Where:
Pr is the Prandtl number
Sc is the Schmidt number

Both Pr and Sc are dimensionless terms.

The Prandtl number is defined in Equation 25:

$$Pr = \frac{v}{k'/\rho_a C_{p-air}} \quad (25)$$

Where:
ν is the kinematic viscosity of air ($m^2 s^{-1}$)
k' is the thermal conductivity of air ($W m^{-1} K^{-1}$)

The Schmidt number is defined in Equation 26:

$$Sc = \frac{v}{D_{AB}} \quad (26)$$

Equations 12 - 26 were solved simultaneously with known boundary conditions of inlet air and water flow rates, inlet air and water temperatures and inlet air humidity (water vapor content) and also inlet air pressure. We used Mathcad Software (Mathsoft Inc., Cambridge, Massachusetts) and used the @Air Software add-on for Mathcad (Techware Engineering Applications, Inc., Ringwood, New Jersey) to account for the changes in air and water temperatures and air pressure with module length. Solving Equation 12 enables the rate of water evaporated through a single hollow fiber membrane to be determined. This result, multiplied by the number of fibers within the membrane module, enables the rate of water evaporation to be calculated and compared to results obtained from membrane modules studied during laboratory experiments.

4.4. Membrane Fouling

Usually, water with salinity concentrations between 1,000 - 10,000 milligrams per liter (mgL^{-1}) of total dissolved solids (TDS) is considered brackish water. For comparison, the salinity of seawater is greater than 10,000 mgL^{-1} TDS and goes as high as 35,000 mgL^{-1} (Wilf and Klinko 2001). Cations such as Na^+, Mg^{2+}, Ca^{2+}, and anions such as Cl^-, SO_4^{2-}, CO_3^{2-}, HCO_3^- and silica are the most common components of brackish groundwater (Jurenka and Chapman-Wilbert 1996). Biological components are usually rare in brackish groundwater but are found in high concentration in brackish surface water. Due to the presence of carbonates, the brackish water is alkaline with pH greater than 7. The cations and anions react with each other to form salts such as $CaSO_4$, $CaCO_3$, and NaCl.

Because the brine concentrate is highly concentrated, often solute particles precipitate and get deposited inside the fiber lumen in the feed side in which gypsum ($CaSO_4.2H_2O$) is usually dominant. These deposits increase the resistance for heat and mass transfer processes and thereby decreasing the overall effectiveness of the system. This process is referred to as fouling.

5. Materials and Methods

5.1. Membrane Module Construction

Membrane modules were made by packing a required number of hollow fiber membranes in a pipe of suitable diameter. In this study, a micro porous hydrophobic hollow membrane fabric made of polypropylene manufactured by Membrana was used. The properties of the membrane are summarized in Table 1.

The preparation of the module is shown in the Figure 7 (a) through (d). A weaved fabric sheet of approximately 60 fibers was carefully cut from the supply roll using a sharp knife. The excess strands were removed from the membrane to obtain 50 fibers. The weaved sheet of 50 fibers was rolled and inserted into stainless steel tubing of 6.35 millimeters (mm) in diameter with length of 0.35 m with both ends fitted with two T-fittings (Swagelok, Solon, Ohio). The rest of the membrane (hanging out from the ends of the steel pipe) was glued inside small steel pipes of approximately 0.05 m long. The glue, a low viscosity casting plastic (Alumalite Corp., Kalamazoo, Michigan), was applied at the end of the steel pipe in a way that the hollow fiber membrane lumens were open and the gap in the steel pipe was sealed as shown in Figure 8.

The module was then allowed to sit for 24 hours to harden the glue before setting into the main experimental apparatus. The membrane surface area for each modules was 0.014 m^2.

Table 1: Hollow Fiber Membrane Properties

Fiber inner radius	110 μm
Fiber outer radius	150 μm
Pore radius	0.02 μm
Porosity	0.4
Tortuosity	2.8
Bubble point	1,379 kPa

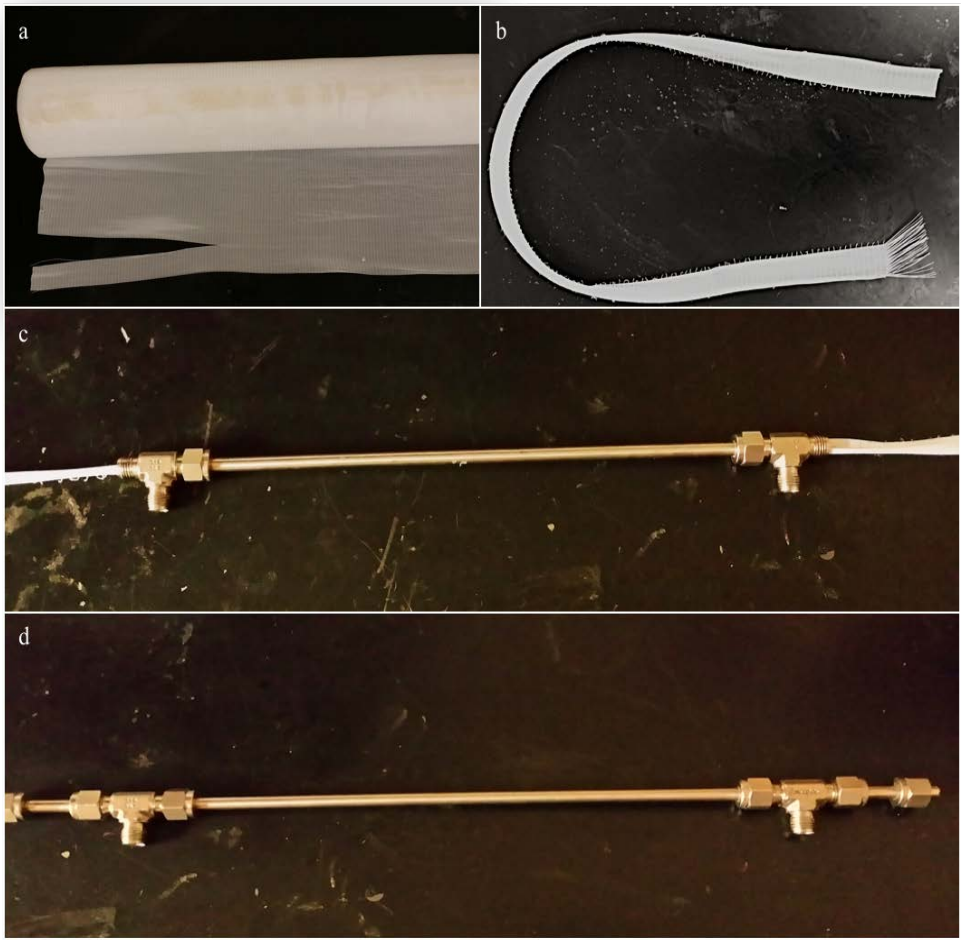

Figure 7: Preparation of membrane module. (a) Supply roll of micro porous membrane as provided by the manufacturer. (b). A weaved sheet of 50 fibers cut from the supply roll, ready to go inside the module. (c) Steel pipe fitted with T-connections for air flow entrance inside the module. (d) The final membrane module ready to set up in the main experimental apparatus.

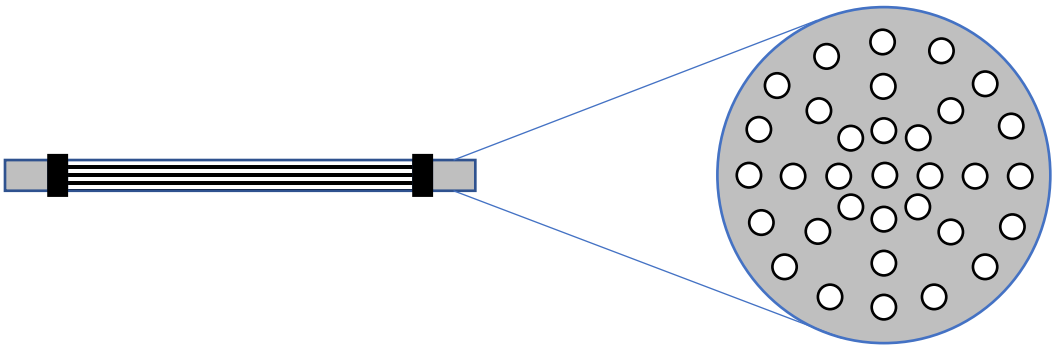

Figure 8: A hollow fiber membrane with the ends glued so that only the hollow fibers are open to the water as seen in the cross-section.

5.2. Heat Loss Concerns at the Facility

Experiments were initially set up at the SAWS wastewater facility as shown in Figure 9 to use waste heat generated on-site. A 6.35 mm diameter steel pipe about 4 meters (m) long conveyed air from blower piping into the experimental membrane module. While the air temperature inside the blower was about 80 ^{o}C, due to the heat loss, the room temperature was reduced to about 23 ^{o}C as air reached to the module. To alleviate and compensate for heat loss, the experimental set up was moved to a laboratory where blower conditions could be simulated using laboratory hood air and a heating oven.

Figure 9: Experimental set up at the full scale facility.

5.3. Experimental Apparatus

The membrane modules prepared were used for running different tests. The module was attached to a system of flow meters, thermocouples, pressure gauges, and weighing balances to continuously monitor temperatures pressures, water flow, and air flow along the membrane. The experimental set up at the laboratory is shown in Figure 10. The apparatus is illustrated in detail in Figure 11. The apparatus was set up in a way that the membrane module could be easily replaced between the tests without having to dismantle the whole system. The experimental setup is comprised of two independent flow systems: water flow and air flow. The water flow system is represented by solid line in Figure 11 and a dotted line represents air flow.

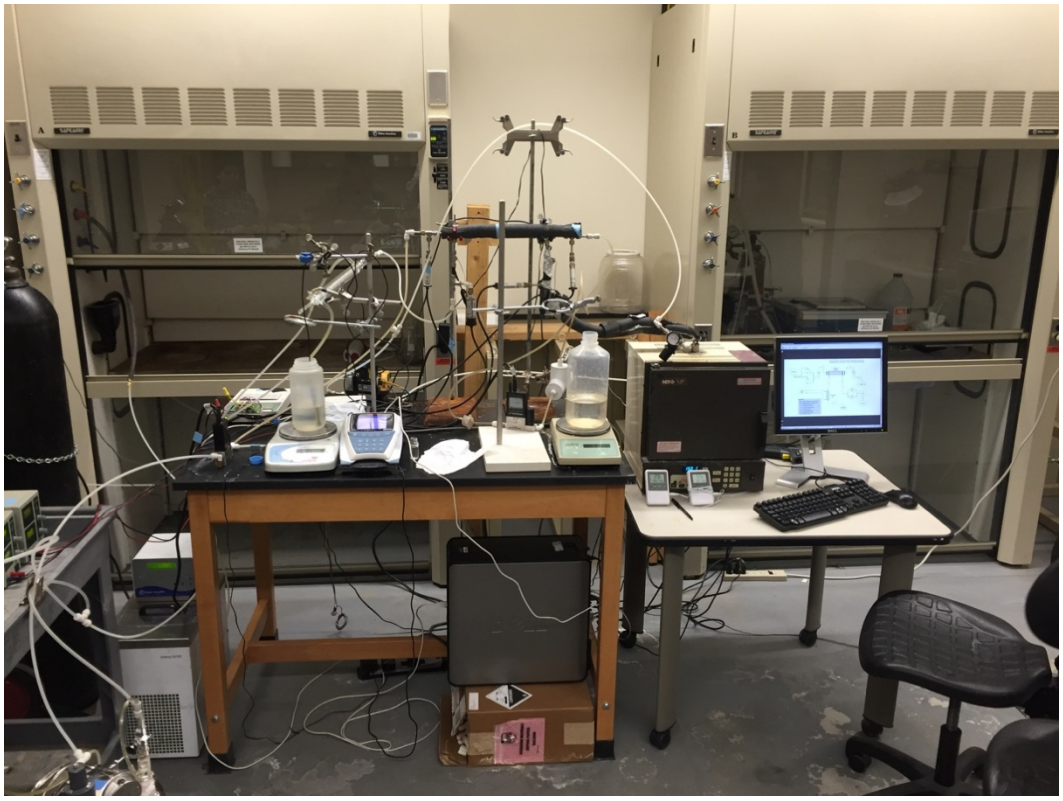

Figure 10: Experimental set up at the laboratory.

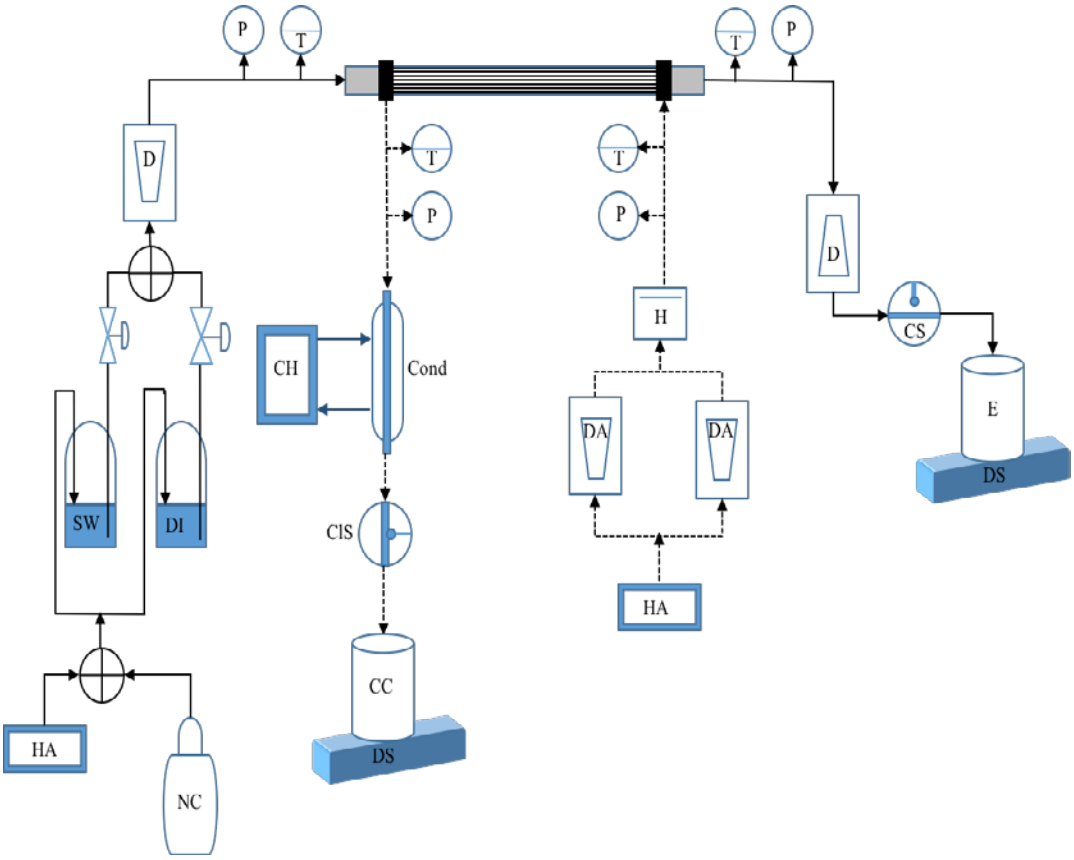

Figure 11: Schematic of test apparatus. NC: Nitrogen cylinder; HA: Hood air; SW: Salt water; DI: Deionized water; D: Digital flowmeter/control; P: Pressure transmitter; T: Thermocouple; CS: Conductivity sensor; E: Effluent; DS: Digital scale; Cond: Condenser; CH: Chiller; DA: Digital air flow meter/control; ClS: Chloride concentration sensor; CC: Condensation collection.

5.3.1. The Water Flow System

The water flow side begins with two pressurized water tanks. The two stainless steel cylindrical tanks, one with 60 liters (L) capacity (Alloy Product Corporation, Model 73-16) was filled with deionized (DI) water and the second vessel of 20 L capacity (Alloy Product Corporation, Model 73-05) was filled with synthetic brine concentrate solution. Each tank is represented by DI and SW in Figure 11. The two tanks were pressurized with air from the laboratory fume hoods (Fisher Scientific SafeAire) or with the nitrogen cylinder when testing brine concentrates containing ferrous iron. The larger tank can withstand pressures as high as 415 kPa while the small tank can withstand pressures only up to 275 kPa. Pressurizing the water tanks allows water to flow with certain pressure without use of external pumps. The two tanks are connected with dual shutoff valves to allow for switching between DI water and synthetic brine concentrate without having to stop the process run.

The water stream leaves the source tank and flows through a digital water flow control valve (Cole Parmer, Model 32907-43) that is set fully open and enters inside the lumens of the hollow fiber membrane inside the module. The water flow rate was controlled by the digital water flow control valve at the output side of the module to maintain pressure and avoid cavitation on the water side of the membrane module. The digital water flow can measure and control water flow ranging from 1 milliliters per minute (mL min^{-1}) through 50 mL min^{-1}. Pressure transmitters (Cole-Parmer Instrument Company, Model 07356-03) which can measure pressures ranging from 0 to 690 kPa were installed in-line: one at the water input side of the module and one at the water output side of the module before the digital outflow control valve. As the water flows through the module and exits through the digital flow control valve, the water pressure drops down to atmospheric pressure and enters a reservoir with conductivity sensors (Cole Parmer, Model 19504-02, which can measure water conductivity as high as 100 milli-siemens per centimeter ($mScm^{-1}$). The reservoir retains a volume of approximately 180 milliliters (mL) and continually reads the average conductivity in the reservoir. The water exits the conductivity sensing reservoir and was dripped into a 1000 mL container that was positioned on a digital scale (Setra EL-4100D) which continuously measures the mass of the container and collected evaporated brine concentrate.

5.3.2. The Airflow System

The airflow side begins with air sourced from a laboratory fume hood (Fisher Scientific SafeAire). The air from the hood was at ambient temperature (22 °C). At 1 atmosphere of pressure the fume hood air has a relative humidity (RH) of 8% as determined using a humidity sensor (Hygrodat 20, Rosemount Analytical). The air from the fume hood is then fed into two airflow control valves (Aalborg GFC17 Mass Flow Transducer) connected in parallel. Each flow valve has a maximum flow rate measuring capacity of 15 liters per minute (L min^{-1}) and combined therefore provides a maximum total airflow of 30 L min^{-1} when both are fully open. The air exiting the airflow control valves flowed into the oven (Ney2-525 Series II Muffle Furnace) that consists of heat exchanger coiled copper tubing that is 3 meters (m) long and 6 millimeters (mm) in diameter.

The heated air exiting the oven and heat exchanger is monitored by an in-line air pressure transmitter (Cole-Parmer Instrument Company, Model 07356-03) and inline air temperature sensor (Control Company, Cat #4127) before entering the membrane module. The air and water interface is counter current, where the air flows into the module through T-fitting at the water outflow side of the module, and flows counter current on the external side of the membrane hollow fibers, exiting at the water inflow side of the module as shown in Figure 11. As the air passes through the module, it collects water vapor evaporated from the water side of the module into the air side.

The air exiting the module is monitored by an in-line air temperature sensor (Control Company, Cat #4127), followed by an inline air pressure transmitter (Cole-Parmer, Model 07356-03) before being fed into the condenser tube (Fisher Scientific, EISCO, Liebig Condenser Tube). The condenser tube uses a water chiller system (Fisher Scientific Isotemp 3016D Digital Refrigerated Bath) that circulates water at 4 degree Celsius (°C) through the condenser shell. As the air is cooled, it becomes supersaturated with water vapor, which condenses in the condenser inner tube and drips into a 1,000 millilter (mL) container positioned on a digital scale (Setra SI-4100D), which reads the amount of water being condensed from the supersaturated air. The water collected from the output of the condenser tube was monitored for chloride content using an ion selective electrode (ISE) submerged in the collection container. The presence of chloride in the condensate is an indicator for brine concentrate solution leaking through the membrane and into the air side of the system. The time and rate of increase in chloride content provide data of when the leak occurred and the intensity of the leak.

System operating parameters were monitored and recorded in the Labview project application. Monitored parameters included: input and output water flow rates and pressure, input airflow rates and pressure, water conductivity, and chloride content in the condensate. Two direct current (DC) regulated power supplies (ExTech Model 382200 and Model 382202) provided power to the flow valves and pressure sensors within the framework of two Data Acquisition Terminal blocks (DAQ, NI-USD-6229 and NI-USD-6230 pinouts). The air temperature sensors were self-contained battery-operated thermometers with external probes encased and sealed within the airflow lines. These air temperature readings were manually recorded and were independent of the LabVIEW interface. The digital scales and ISE (chloride) sensor were not connected to the data acquisition (DAQ) terminal blocks but were individually connected to the computer using R232 cables. While digital scales were monitored as input/output (I/O) devices within the LabVIEW interface, the data from the ISE sensor were recorded into HyperTerminal communications in the Windows operating system.

5.4. Data Analysis Procedures

Brine concentrate evaporation rates through the experimental modules were determined based on the measured rate of condensate collection. The liquid mass flow meters that monitored flow into and out of the membrane module also could have been used to calculate evaporation rates based upon flow differences, but this proved problematic as the manufacturer reported that the measurement uncertainty of the meters was 1% of the full range (0.5 milliliters per minute [mL min^{-1}]), resulting in propagated flow uncertainties of 1 mL min^{-1}—which in some cases exceeded measured flow differences. Measured rates of condensate collection had to be corrected for air water vapor content entering and leaving the experimental apparatus. The air entering the experimental apparatus had a measured relative humidity (RH) of 8% at 22 °C and thus contained water vapor

not added by the membrane. In contrast, air leaving the condenser portion of the apparatus was at 100% RH at 4 °C and contained water vapor not collected by the condenser apparatus. These contributions of water vapor content were subtracted and added to the measured rate of condensate collection respectively to enable calculation of the rate of water evaporation across the membrane module as shown in Equation 27:

$$Rate\ of\ evaporation\ (\text{mL min}^{-1}) = Condensate\ collection\ rate\ (\text{mL min}^{-1}) + Q_{air}\ (\text{L min}^{-1}) * 4.6 * 10^{-3} \quad (27)$$

The numerical value $4.6 * 10^{-3}$ in Equation 27 gives the condensation correction for the amount of water in the corresponding airflow rate. The measured fraction of evaporation is calculated as ratio of corrected condensate collection to the feed flow rate given in Equation 28. Permeate flux (milliliters per minute per square meter [mL min^{-1} m^{-2}]) is the rate of evaporation per unit area which can be mathematically calculated as shown in Equation 29:

$$Fraction\ evaporated = \frac{Rate\ of\ evaporation\ (mL\ min^{-1})}{(Q_{out} + Rate\ of\ evaporation)(mL\ min^{-1})} \quad (28)$$

$$Permeate\ Flux\ (mL\ min^{-1} m^{-2}) = \frac{Rate\ of\ evaporation\ (mL\ min^{-1})}{Area\ of\ membrane\ module\ (m^2)} \quad (29)$$

Conductivity of effluent was monitored throughout experiments testing brine concentrate solutions. The conductivity measurement apparatus was at the liquid effluent for the experimental apparatus and had to be corrected for residence time spent within the 29 mL of tubing. The residence time was calculated from the ratio of tubing volume to effluent flow rate—where the tubing was assumed to be plug flow. The conductivity of effluent when near steady state can be correlated to fraction of water evaporated using Equation 30.

$$Fraction\ evaporated = 1 - \frac{Initial\ conductivity}{Steady\ state\ conducitvity} \quad (30)$$

5.4.1. Calibration of Digital Water Flow Meters

The effluent mass flow meter was used to control and set constant effluent flow during testing runs. To ensure that the effluent flow rate used was accurate, scale readings were used to calibrate the digital flowmeter readings. To perform flow meter calibrations, the inflow and outflow digital water flow meters were connected in series along with digital scale at the end without connecting any pressure or temperature sensors. Then the digital outflow meter was used to

control the flow through this calibration system. When the flow on the digital outflow meter was set to a certain value, the corresponding values on the digital inflow meter and the digital scale were recorded. A few sets of values were recorded at that flow rate for an accuracy check. The procedure was repeated for different water flow rates. Then, the data were plotted with digital scale values on the x-axis and the corresponding digital flow meter values on the y-axis with a linear line of best fit used a calibration correction equation. This calibration was repeated before new membrane modules were placed into the experimental apparatus.

5.5. Experimental Conditions

Most of the operating conditions used in this study were based on the aeration blower conditions at the local wastewater treatment facility for the San Antonio Water System (SAWS). Full scale operation parameters at SAWS and scaled laboratory testing operating parameters are provided in Table 2. As shown in the table, temperature, humidity, pressure and brine concentrate conductivity are direct equivalents between the laboratory and full-scale facility operations. These values are representative of measured full-scale conditions or ambient air condition during testing. Flow rates of air and brine concentrate tested in the laboratory must be scaled based upon equivalent membrane module Reynold's numbers (Re) for the full-scale airflow conditions as defined in Equation 22.

The laboratory modules tested have much smaller diameters (0.48 centimeters [cm]) than what would be expected if used full scale piping sized modules (119 cm). However, using a typical 20% membrane packing fraction (where the membranes occupy 20% of the interval volume) for the laboratory modules, the equivalent diameter (d_e) is equivalent for a full-scale module with a packing fraction of 25%. At equivalent d_e, *Re* in Equation 22 can be interpreted as operating at similar air velocities and their corresponding airflow rates in laboratory and full-scale operations.

Table 2: Operating Parameters

Parameter	Full-scale wastewater facility	Equivalent laboratory conditions
Air temperature after blowers	72 °C	72 °C
Inlet air relative humidity	60%	60%
Air pressure after blowers	75 kPa	75 kPa
Brine concentrate conductivity	14.4 - 16.2 mS cm^{-1}	14.9 mS cm^{-1}
Module diameter	119 cm	0.48 cm

Membrane length	30.5 cm	30.5 cm
Number of membrane fibers	3.9×10^6	50
Membrane packing	25%	20%
Equivalent diameter	0.92 mm	0.92 mm
Blower air flow rate	$1{,}400 \times 10^6$ L d^{-1}	16.5 L min^{-1}
Module air velocity	19.4 m s^{-1}	19.4 m s^{-1}
Air Reynold's number	1,450	1,450
Brine concentrate flow rate	4.2×10^6 L d^{-1}	37 mL min^{-1}

L min^{-1} liters per minute
mS cm^{-1} = milli-siemens per centimeter

Using these packing fractions for membrane modules, the laboratory brine concentrate flow rates can also be scaled to match the wastewater facility conditions. Membrane module length is a direct equivalent between laboratory and full-scale membrane modules.

5.5.1. Experimental Methodology Using Deionized Water

Initial studies were carried out by running deionized (DI) water through membrane modules. The evaporation rates were studied for three different settings:

(1) Variable water flow rates at constant airflow rates and constant air temperature

(2) Variable airflow rate at constant water flowrate and constant air temperature

(3) Variable air temperature at constant water flowrate and constant air flowrate

Evaporation rate data were collected at varying water flow rates. The airflow rate and temperature were set constant on the airside using digital airflow control value and oven respectively. The flow rate of DI water inside the system was controlled by the digital outflow control meter. DI water was pumped at a pressure of 138 kPa, a higher pressure than the air pressure on the airflow side of the module. The DI water tank was pressurized using laboratory fume hood air, and the pressure was regulated with the help of a regulator. Calibration data were

used to set flow rate according to digital scale using the digital outflow meter. At constant air temperature of 60 °C and the constant airflow rate of 20 L min^{-1} (Re_{air} of 1,268), the evaporation data was collected at a DI water flow rate of 0.38, 1, 1.5, 2 and 3 mL min^{-1} readings, corresponding to water Reynold's Numbers (Re_{water}) of 0.7, 1.9, 2.9, 3.9 and 5.8 based on the digital scale readings when using the digital outflow meter as a control valve.

The water Reynold's Number is defined as shown in Equation 31

$$Re_{water} = \frac{\rho_{water} v_{water} d_e}{\mu_{water}} \tag{31}$$

Where:
ρ_{water} is density of water (kg m^{-3})
v_{water} is the water velocity (m s^{-1})
μ_{water} is the dynamic viscosity of water (N s m^{-2})

At each water flow rate, the system was set to stabilize for about an hour and all parameters (including: pressure at water inlet and outlet side, pressure at air inlet and outlet side, water inflow, and outflow readings on the digital flow meters, and digital scale readings for effluent and condensation collection) were monitored continuously and recorded at 1-minute intervals using the LabVIEW interface. The temperatures at the air inlet and outlet were recorded manually for every 10 minutes throughout the experiment until the temperature was confirmed to be essentially steady state.

A second set of data was collected at varying airflow rates. The water flow rate and the temperature at the air inlet was set at a constant rate using the digital water outflow control value and the hot air oven respectively. At a constant air temperature of 60 °C and the constant water flow rate of 0.4 mL min^{-1} reading on from the digital scale, the evaporation data was collected at the airflow rate of 5, 10 15, 20, 25, and 30 L min^{-1}; corresponding to Re_{air} of 317, 634, 951, 1268, 1584 and 1901. Stabilization times and data monitoring processes were the same as described for the varying DI water flow rate studies.

The third set of data was collected at varying airflow temperatures at the air inlet side. The water flow rate on the airside and the airflow rate was set at a constant rate using the digital water outflow control valve and the digital airflow meters connected in parallel, respectively. At a constant airflow rate of 20 L $min^{-1}$and a constant water flow rate of 0.4 mL min^{-1} reading on digital scale, the evaporation data were collected at the airflow temperatures of 23 °C (ambient temperature), 45 °C, 60 °C, 70 °C, and 80 °C measured via thermocouple at the air inlet. The desired temperatures were obtained through trial and error iterations of oven set point temperatures. Stabilization times and data monitoring processes were the same as described for the varying DI water flow rate studies.

5.5.2. Experimental Methodology Using a Synthetic Brine Concentrate

As discussed in the introduction and background sections, fouling is a concern. As part of this study, we conducted experiments to determine fouling rates and fouling control and membrane module cleaning options when testing brine concentrate.

Unlike the DI water experiments, these tests were run for longer time periods and used a synthetic brine concentrate. Stabilization times and data monitoring processes were the same as described for the varying DI water flow rate studies. The system data for airflow rates, air pressures, water flow rates, water pressures, conductivity of evaporated brine concentrate, and the chloride concentration of condensation were monitored continuously using LabVIEW until the module showed signs of fouling.

Fouling was indicated by a number of operating conditions that were monitored during these longer-term tests:

- An increase in the water pressure drop across the membrane was thought to indicate internal membrane fouling. As the membrane fouls, water pressure along the membrane module drops more due to solids accumulation in the membrane.

- The trend in the conductivity data can also be useful to indicate fouling. Since conductivity was measured in real time, the initial conductivity of the brine concentrate solution at time zero corresponded to the start of the experiment and then increased and reached a steady state value. If the rate of evaporation were constant, the conductivity of the effluent stayed constant. If the rate of evaporation decreased, the conductivity of the effluent also decreased, which indicates fouling.

- Decreases in the rate of condensate collected from the humid air stream and decreases in the rate of evaporation of brine concentrate were perhaps the most obvious signs of fouling.

In addition to monitoring for fouling aspects, we also monitored system operation for possible leaking of brine concentrate through the membrane. Signs of membrane leaking or wetting can be observed by monitoring the air pressure drop across the membrane. Air pressure drop increasing indicated that salts were accumulating on the shell side of the membrane. Chloride concentration of the condensation data was also used to monitor for brine concentrate leakage across the membrane. As liquid brine concentrate enters the air stream, it contaminated the condensate collection vessel, and chloride values increased in the condensate.

The brine solution used in these experiments was synthetically prepared in the laboratory. The recipe is based upon data obtained from the local water treatment facility, San Antonio Water Systems (SAWS) where they measured the effluent brine properties when conducting pilot scale experiments. The chemical properties of the brine solution obtained from SAWS is summarized in Table 3 The chemical composition used in the laboratory based on the Table 3 is listed in Table 4. The ferrous iron listed in the table was only used for one of the fouling studies and eliminated from the rest. Mineral scaling was expected to foul the membrane and reduce the rate of evaporation and possibly clog the membrane lumens. To avoid precipitation and to reduce the effect of fouling, calculations were carried using Visual Minteq to operate at 70 °C without scale formation, with results indicating that the pH of the brine solution should be at 6.0. Brine with this pH was obtained by titrating with the appropriate amount of HCl as determined from monitoring brine solution pH.

Table 3: Brine Concentrate Water Quality, units are mgL^{-1} except where provided

Total hardness	1,730-2,160
Total alkalinity	1,030-1,460
Specific conductance ($mS\ cm^{-1}$)	14,400-16,200
TDS (parts per trillion)	11.4-12.9
pH	7.2-7.5
Na^{+}	2,690-4,020
Mg^{+2}	199-276
K^{+}	99.2-100
Ca^{+2}	337-471
Fe^{+2}	1.78-1.98
Cl^{-}	1,900-2080
SO_4^{-2}	4,480-6,060
NO_3^{-} and NO_2^{-}	Non-detectable

Table 4: Total Ion Concentration in the Brine Concentrate Solution

Ion	**Concentration (millimoles per liter [mmole L^{-1}])**
Na^{+}	146
Ca^{2+}	10
Mg^{2+}	10
K^{+}	26
Fe^{2+}	0.034
Cl-	56
SO_4^{2-}	55
CO_3^{2-}	11

The fouled membranes were saved for Scanning Electron Microscopy (SEM) imaging for analysis at the conclusion of the fouling studies. Prior to being imaged, membranes were air dried within the testing module. Fouled membranes were removed from the module and cut into slices and fastened onto a sample holder with carbon tape before SEM imaging (Hitachi, South San Francisco, California, S – 5500) at 16 - 18 kilovolts (kV).

An airflow temperature of 60 °C was used in the fouling studies with four different experimental conditions as summarized in Table 5 to consider the effects of brines with and without iron, brine pH, airflow rate, and brine flow rate. The effect of fouling on the membrane was also studied at three different brine concentrate pH values of 6.25, 5.75 and 4.0 and airflow rates of 20 L min^{-1} or 15 L min^{-1}.

Table 5: Experimental Conditions when Testing with Brine Concentrate

Module test #	Testing conditions
1	Brine concentrate flow rate = 0.38 mL min^{-1}, pH = 6.25 Airflow rate = 20 L min^{-1} Fe = 0 mgL^{-1}
2	Brine concentrate flow rate = 0.38 mL min^{-1}, pH = 6.25 Airflow rate = 15 L min^{-1} Fe = 5 mgL^{-1}
3	Brine concentrate flow rate = 0.23 or 3.0 mL min^{-1} , pH = 5.75 Airflow rate = 15 L min^{-1} Fe = 0 mgL^{-1}
4	Brine concentrate flow rate = 0.38 mL min^{-1} pH = 4 Airflow rate = 15 L $min^{-1,}$ Fe = 0 mgL^{-1}

With the exception of module test 3, all studies were conducted with the brine effluent flow rate held constant by the effluent flow controllers at 0.38 mL min^{-1}. For module test 3, a lower brine flow rate of 0.23 mL min^{-1} was used. After fouling developed, the effluent flow controller was set fully open to allow and brine flow rate of 3.0 mL min^{-1} to encourage flushing of foulants from within the fiber lumens. After 90 minutes of flushing, the module was returned to service with its original flow rate to determine time required for secondary fouling.

6. Results and Discussion

6.1. Effect of Water Flow Rate on the Rate of Evaporation for DI Water

The study was carried out by varying exit flow rate conditions and by keeping the airflow rate and the inlet airflow temperature on the shell side constant. The observed data and line of best fit is given in Appendix I for different water flow rates. The plot for the observed fraction evaporated and corresponding flux is shown in Figure 12.

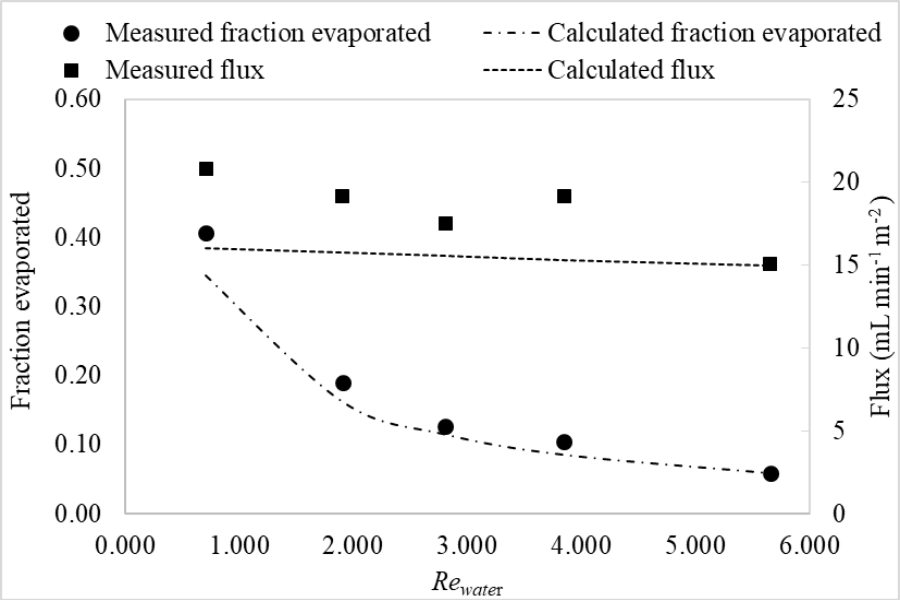

Figure 12: DI water evaporation rate with varying water flow rates at constant airflow rate and constant airflow temperature.

The airflow rate was fixed at a Re_{air} of 1,268 and the airflow temperature at the air inlet was fixed at 60 °C. As shown in Figure 12, the evaporative flux and fraction evaporated for modeled and measured values decreases with Re_{water} inside the membrane. This is contrary to what is observed in membrane distillation processes where permeate flux increases with increasing flow rate (Laganà et al. 2000, Li et al. 2003, Cath et al. 2004, and Alklaibi and Lior 2005). In membrane distillation, this phenomenon is explained by a combination of a thinning boundary layer on the feed side in addition to an increased heat loading to the system. In membrane evaporation, the heat flux occurs from air side to the feed side and as a result, the heat energy from the hot air outside the membrane fiber lumens—while still absorbed by the water—provides less of a water temperature increase when compared to lower water flow rates with lower retention time inside the fiber lumens. At higher water flow conditions, the water can act as a heat exchanger without a significant increase in water temperature or evaporation rates. Measured values and model results agree reasonably well for both the fraction of evaporated and evaporative flux, and the model adequately explains the influence of water side Reynold's Number on evaporation performance.

6.2. Effect of Airflow Rate on the Rate of Evaporation for DI Water

The fraction evaporated and corresponding permeate flux across the membrane obtained at varying airflow rates (i.e., at different Re_{air} values) while keeping the airflow temperature entering and the feed flow exiting the membrane module constant are shown in Figure 13.

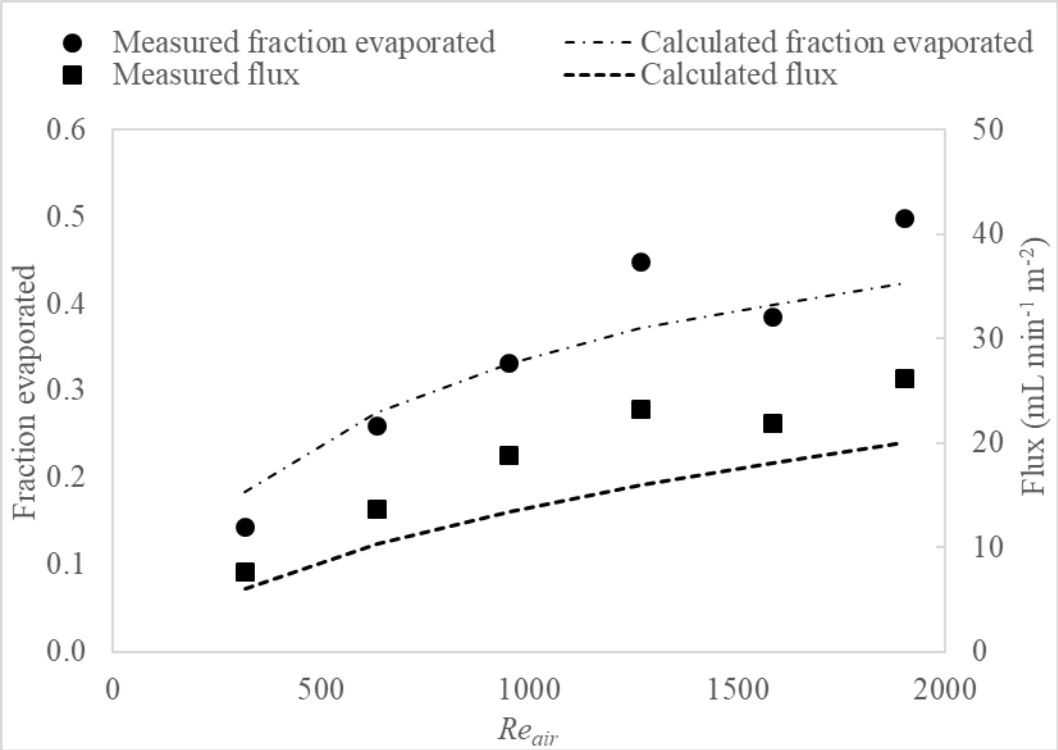

Figure 13: DI water evaporation rate with varying airflow rate at constant water flow rate and constant airflow temperature.

The airflow temperature was fixed at 60 °C and the water flow rate exiting the membrane was fixed at 0.38 mL min^{-1}. The observed data for different airflow rates are in Appendix II. Both the flux and the fraction of brine evaporated increases with Re_{air} (Figure 13). These results are similar to that of membrane distillation studies. In membrane distillation, the permeate flux increased with increase in air velocities (Khayet et al. 2000, García-Payo et al. 2002, Khayet et al. 2003, and Khayet et al. 2012). This can be explained by the phenomenon of decreasing air boundary layer thickness (increasing mass transfer coefficient) with increasing air Re number (García-Payo et al. 2002). Furthermore, as airflow rates increase, the amount of heat provided to evaporate water also increases, allowing the driving force to increase.

Model predictions are also shown in Figure 13. The measured values agree reasonably well for both the fraction evaporated and the evaporative flux and the model adequately explains the influence of Re_{air} on evaporation performance, considering that the model uses dimensionless correlations rather than fitted correlations for the heat and mass transfer coefficients obtained from literature.

6.3. Effect of Air Temperature on the Rate of Evaporation for DI Water

The DI water fraction evaporated obtained at various air inlet temperatures while keeping the airflow rate and the water flow rate exiting the membranes constant is shown in Figure 14.

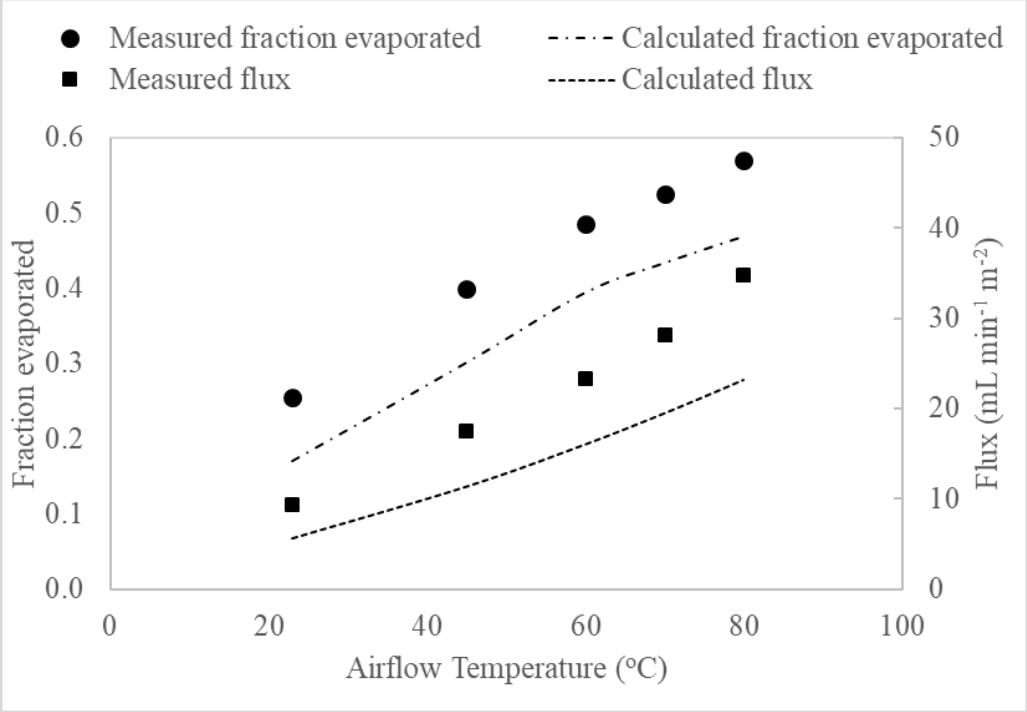

Figure 14: DI water evaporation rate with varying air temperature at constant feed flow rate and the constant airflow rate.

The airflow rate was fixed at a Re_{air} of 1,268 and the exit water flow rate was fixed at 0.38 mL per minute (Re_{water} of 0.7). The observed data is provided in Appendix III for different air temperatures. The water fraction evaporated and the evaporative flux increase with an increase in the airflow temperature. This is analogous to the effect of feed temperature on the permeate flux in membrane distillation where heat transfer occurs from feed side to the permeate side (Gryta and Tomaszewska 1998, Martínez-Díez and Vazquez-Gonzalez 1999, Phattaranawik and Jiraratananon 2001, and El-Bourawi et al. 2006) and the more heat that is added, the greater the permeate flux. In membrane evaporation, as the temperature of the air increases, more energy is available to drive the water evaporation process. In addition, the water vapor holding capacity of the air increases with increasing temperature, and the air is less likely to be at water vapor saturation at higher air temperatures. Model predictions also show good agreement between the model and measured values (Figure 14) and the model adequately explains the influence of air temperature on evaporation performance.

6.4. Fouling Studies with Brine Concentrate Solutions

The fouling behavior was observed with run time for conditions listed in Table 5 for four membrane module tests. The data observed for the four modules is given in Appendix IV, Appendix V, Appendix VI, and Appendix VII. The effect of operating conditions on the fraction of brine concentrate evaporated and the rate of fouling can be seen in Figure 15. The brine concentrate fraction evaporated for module 1 and module 3 is greater at time zero when compared to other modules. This is attributed to the higher airflow rate of 20 L min^{-1} used for module test 1 and the lower brine concentrate flow rate at 0.23 mL min^{-1} used for module test 3. These conditions can be related to the results obtained from DI water studies where the higher the airflow rate, the higher the fraction of water evaporated and lower water flow rates inside the membrane result in a higher water fraction evaporated. Different rates of fouling for the different testing conditions used, as indicated by the decreasing fraction of brine concentrate evaporated with run time, are shown in Figure 15. Module test 1 had the quickest fouling where the brine concentrate fraction evaporated was reduced to half its initial value after only 14 hours of run time. This is attributed to its high initial brine concentrate fraction evaporated along with being run with a higher pH brine concentrate and thus more susceptible to scale fouling.

Due to the high initial brine concentrate fraction evaporated, the concentration of brine concentrate solution inside the membrane lumen increases as it moves towards the end of the module. This leads to the precipitation of salts at a higher rate. As Gryta (2008) observed in one membrane distillation study, low feed flow rates have high fouling rates and efficiency decreased by 30% when feed flow rate decreased from 1.2 to 0.35 mL min^{-1} when used with tap water. Even though module 3 starts at higher fraction evaporated, the rate of fouling is slower—taking approximately 24.5 hours to reach half of the initial evaporation fraction

This extended run time for module 3 was possible because it was run at a pH of 5.75 (compared to pH of 6.25 for module 1). The effect of pH can also be observed in module test 4, the pH was lower yet (pH=4), and essentially no fouling was observed over the 58-hour test duration. Similar pH effects have been seen in ultrafiltration studies (Lee et al. 2007).

Module test 2 was the only testing done with a brine concentrate that contained ferrous iron. Iron appears to have negligible effect on the fouling performance curves. Module test 2 fouled at a rate slightly slower than module test 1 that contained no iron. The slightly slower module 2 fouling rate may be attributed to the lower airflow rate used for module test 2 and may not necessarily be due to the presence of iron in the brine concentrate.

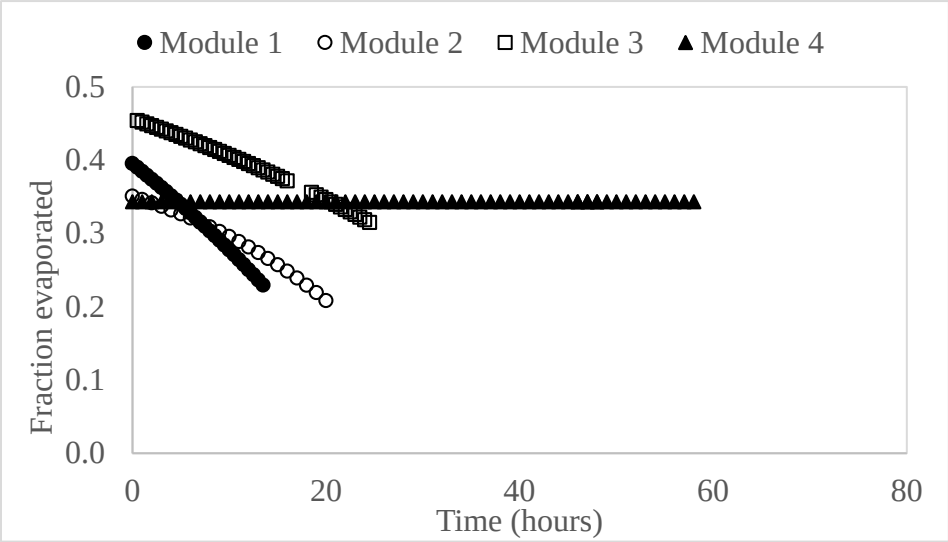

Figure 15: Fraction evaporated for modules under different conditions.

Similar conclusions for the influence of operating conditions on the evaporation fraction of brine concentrate can be obtained from examining and interpreting the changes in effluent conductivity values shown in Figure 16. For module test 4 (that exhibited no fouling), measured evaporated brine concentrate conductivity reached a steady state value of 22.4 mS cm^{-1} after approximately 5 hours of run time. Using a simple mass balance (Equation 30), this increase in conductivity from the initial 14.9 mS cm^{-1} value equates to a brine concentrate fraction evaporated of 0.34. This value is in agreement with the values shown in Figure 15 for module test 4 of 0.34 over the entire testing duration.

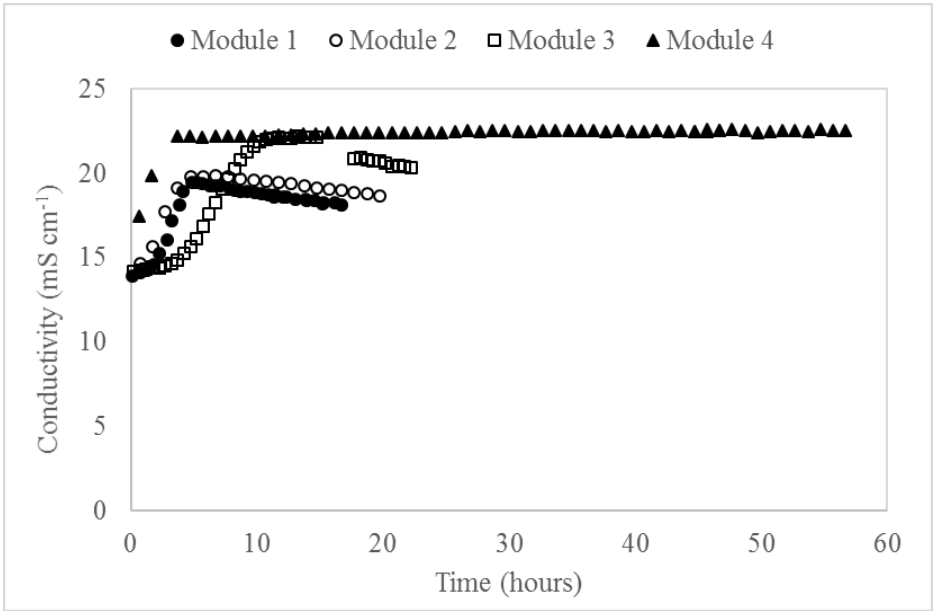

Figure 16: Conductivity of effluent for modules under different conditions.

It should be noted that the time to reach steady state for module 4 and the general conductivity trends with time observed for all modules are influenced by the volume of the conductivity reservoir used to hold the conductivity sensor. Initially, the reservoir contained untreated brine concentrate. The increase in conductivity with run time observed in Figure 16 for all modules indicates that concentrated effluent is entering the conductivity reservoir. While the conductivity reached a steady state value for module 4, fouling occurred in the other module tests, and the initial trend of increasing conductivities measured with time reversed as evaporated brine concentrate conductivities decreased as smaller fractions of brine concentrate were evaporated with the fouled modules.

Changes in brine concentrate and air pressure across the membrane modules with run time are shown in Figure 17 and Figure 18 respectively. The brine concentrate pressure differences across the membranes represent the pressure drop required to force the brine concentrate to flow through the membrane lumens. As seen in Figure 17, unfouled membranes required between 3.5 - 4.7 kPa of pressure drop, depending on the brine concentrate flow rate used. As the membranes fouled, pressure drop increased, requiring up to nearly 16 kPa to force the brine concentrate to flow through the membranes for modules 1 and 2. This pressure drop is attributed to solid precipitates plugging the modules. Figure 19 shows SEM images of an unfouled membrane lumen exposed to brine concentrate and membrane lumens from modules tests 1 and 2.

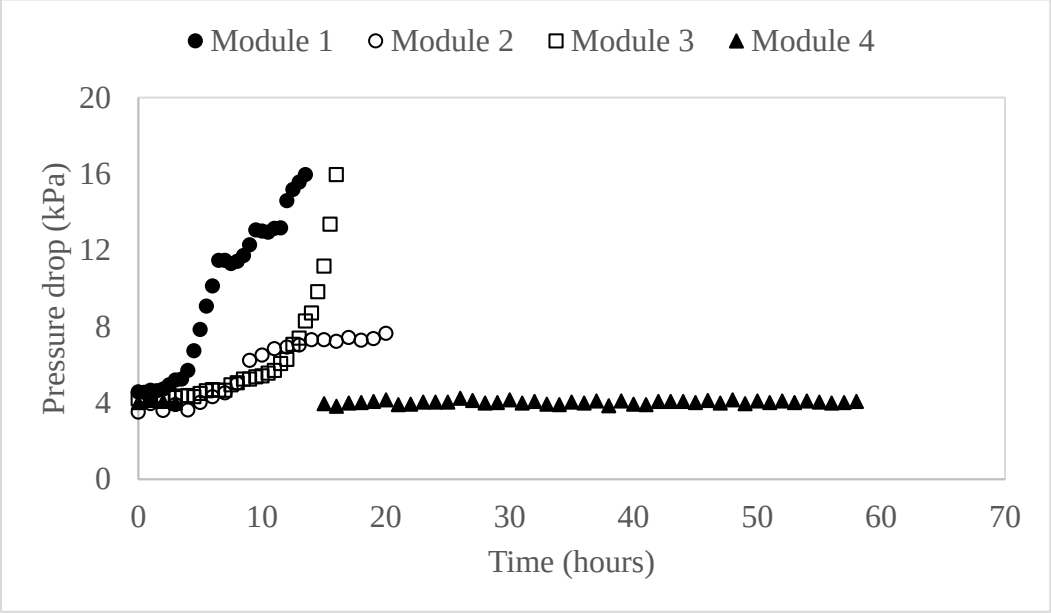

Figure 17: Water pressure drop along the membrane for modules under different conditions.

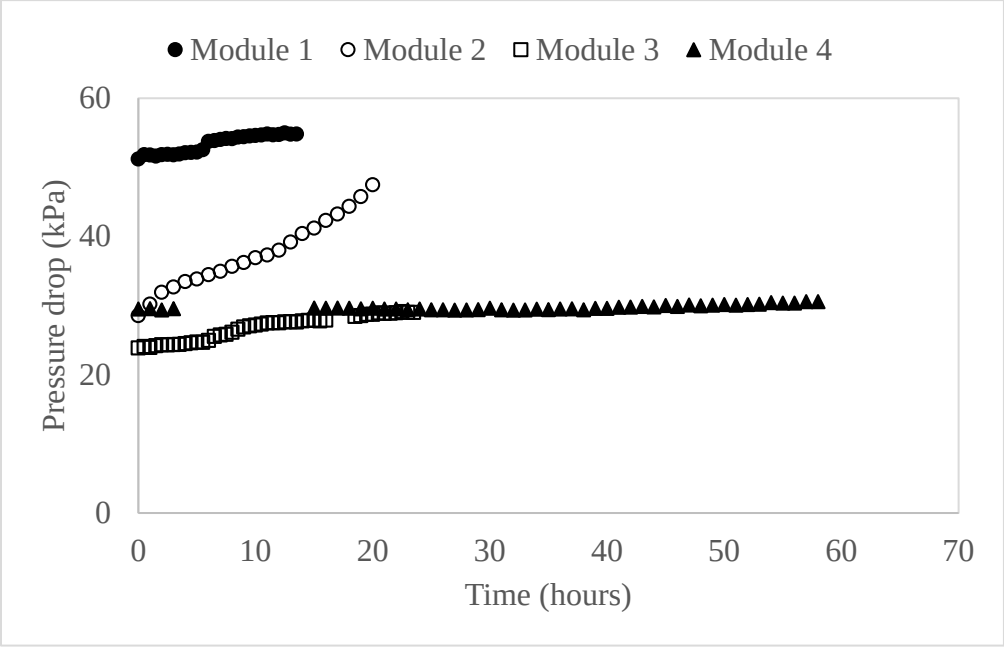

Figure 18: Air pressure drop in the membrane module under different conditions.

The membranes for module tests 1 and 2 appear to be severely plugged, with large volumes of precipitates apparent within the fiber lumens. The analogous air side pressure drops across the exterior side of the membranes are shown in Figure 18. The air pressure drop is used for monitoring the brine concentrate solution leakage into the airside along with the chloride content measurement in the condensation collection. The air pressure drops were ranged from 25 to 50 kPa, depending upon airflow rates used, and the air pressure drops were relatively constant throughout the testing durations for all modules—with the exception of module test 2. In module test 2, the air pressure drop increased with run time, starting at 30 kPa at zero hours and increasing to 50 kPa by the end of 20 hours. The increasing air pressure drop with run time for module 2 may indicate brine concentrate leakage across the membrane as salts accumulated and caused plugging within the air shell side of the module.

It should be noted that salt rejection was one (1.0) for all modules and that no chloride was found in the condensate collection for any of the modules. For module 2, this may be because of brine concentrate leaking in small quantities evaporated before it could travel and carry chloride into the condensate tube to be detected by chloride sensor. Hence, the evaporative fraction values obtained for module test 2, while in-line with other tests, should be interpreted with some caution due to the possibility that module leakage or wetting of the membrane with brine concentrate solution may have occurred during this test.

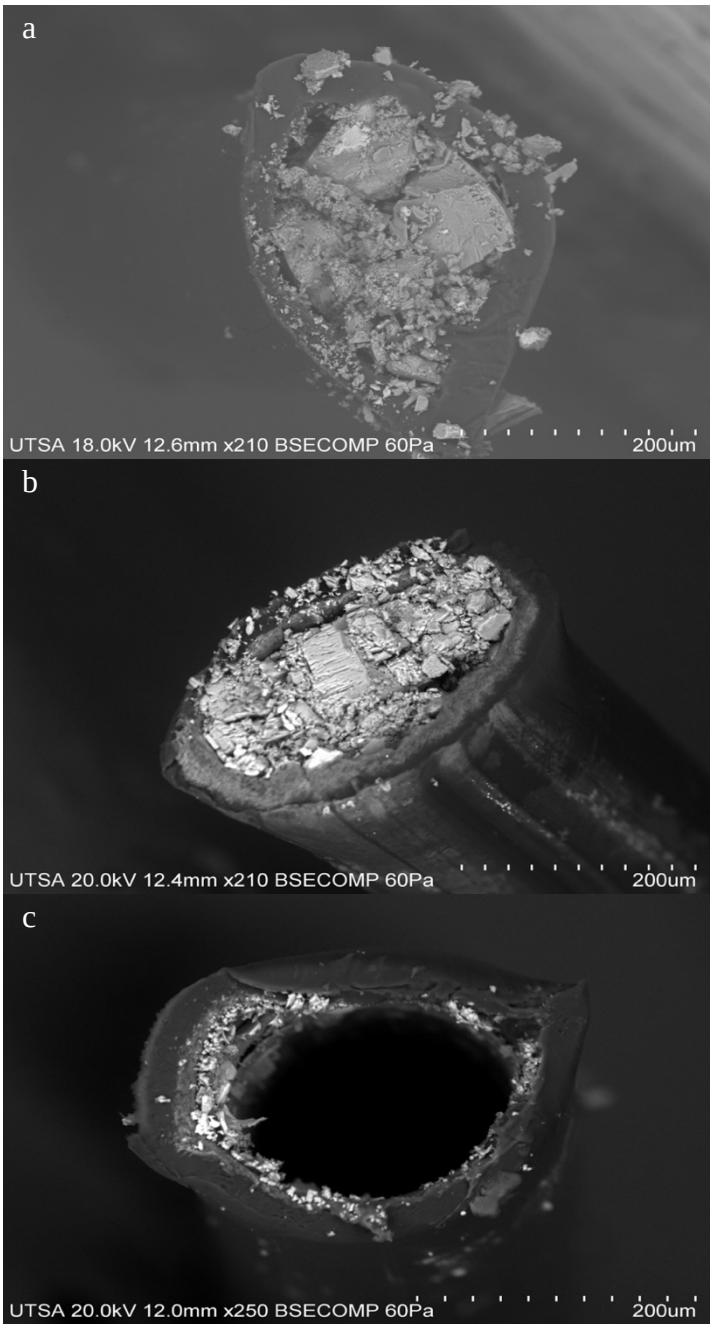

Figure 19: SEM image of fouled membrane (a) module 1, (b) module 2, and (c) membrane exposed to brine.

It is also important to note that the pressure drops associated with using membranes to evaporate the brine concentrate (25 - 50 kPa) are not negligible in comparison to pressure values used for aeration processes. Pressure ranges necessary for aeration processes vary between 55 - 207 kPa gauge (Tchobanoglous et al. 2003).

At SAWS, the air pressure inside the blower pipe is 74 kPa, and steps would be required to ensure that the resulting pressures after the membrane module is retrofitted into the blower pipe remain suitably high for aeration processes.

6.5. Cleaning Studies

A flushing study was conducted when testing module 3. As shown in Figure 15, module 3 was allowed to foul until 16 hours of operating time. At this point, the brine concentrate flow control valve was set fully open and the brine concentrate was allowed to flow at 3 mL min^{-1} for 90 minutes. This time interval is seen in Figure 15 as missing data for the fraction evaporated from module 3. After this flushing process, the outflow control was resumed at the initial effluent flow rate of 2.3 mL min^{-1}. Despite this flushing process, the extent of fouling remained unchanged. When the module was returned to service, the rate of fouling appeared to continue unabated. Module flushing appears to be ineffective for cleaning the membrane of foulants for the conditions studied.

7. Application of Results

The experimental results presented in Figure 12 - Figure 19 were obtained using bench-scale testing methods. These results can be used to validate the modeling approach. Once validated, the model can be used to extend findings to full scale operating conditions. For model validation purposes, the model calculated and measured values for the DI water studies are presented as parity plots in Figure 20 for brine concentrate fraction evaporated and Figure 21 for evaporated water flux. Overall, the model slightly under-predicts the measured values but appears suitable for making conservative performance estimates for the full-scale conditions shown in Table 2. Predictions for the full-scale conditions for the fraction of brine concentrate evaporated and the amount of condensate collected are shown in Figure 22 for various brine concentrate feed flow rates to the module.

The fraction of brine concentrate evaporated (< 0.0012) and the amount of condensate collected (~5,000 L d^{-1}) would be negligible if the system were operated with the 4.2 MLD for the full-scale conditions. The condensation collection is limited by the total heat available at the full-scale facility (either in the form of airflow rate or the temperature of the blower air). The system brine concentrate flow rate is too high and the membranes act like heat exchangers with little evaporation occurring. If the brine concentrate flow rate were reduced to 50,000 L d^{-1}, approximately 40% of the brine concentrate could be recovered as condensate at ~ 20,000 L d^{-1}.

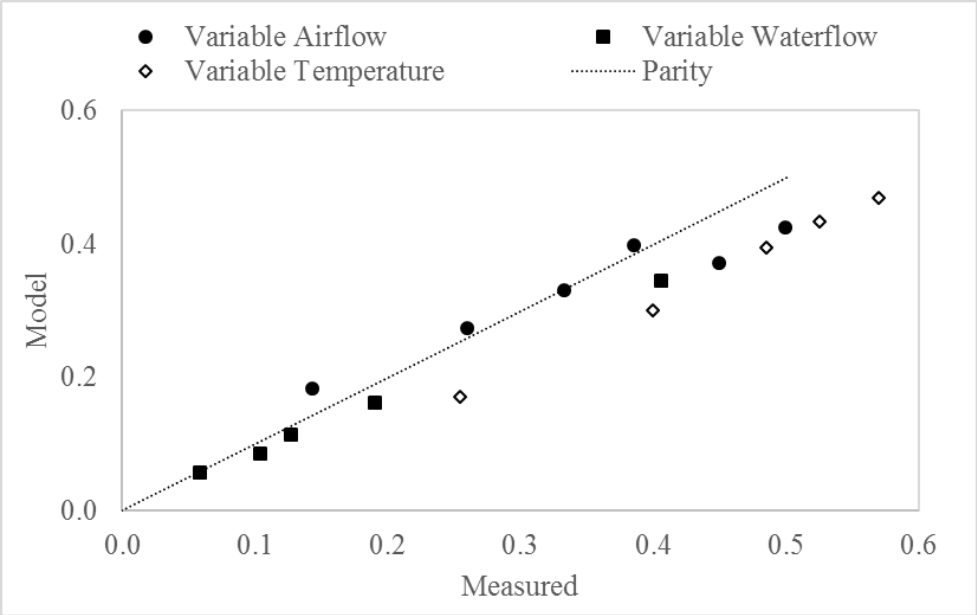

Figure 20: Parity plot between model and measured fraction evaporation.

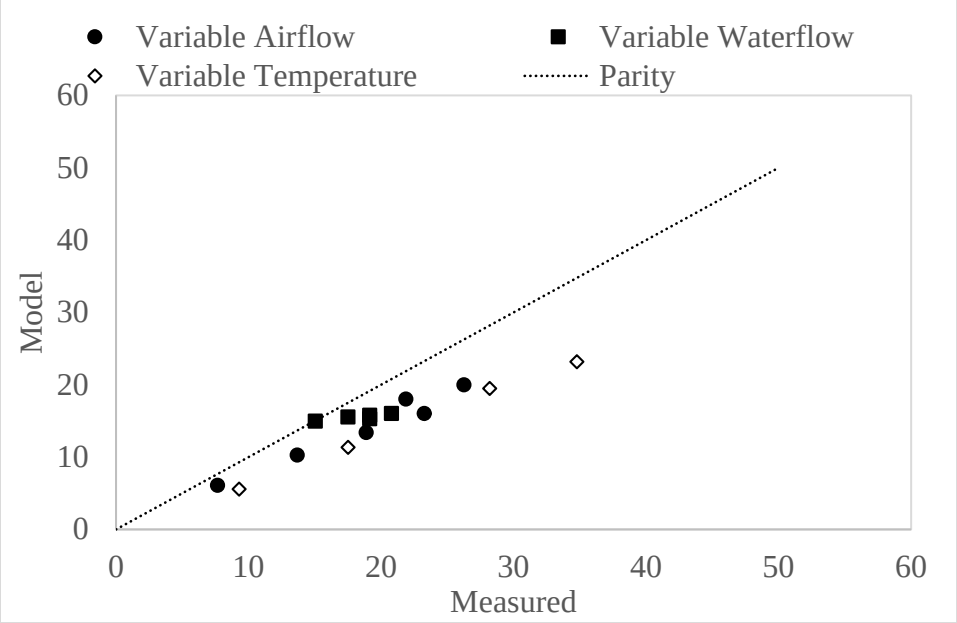

Figure 21: Parity plot between model and measured permeate flux.

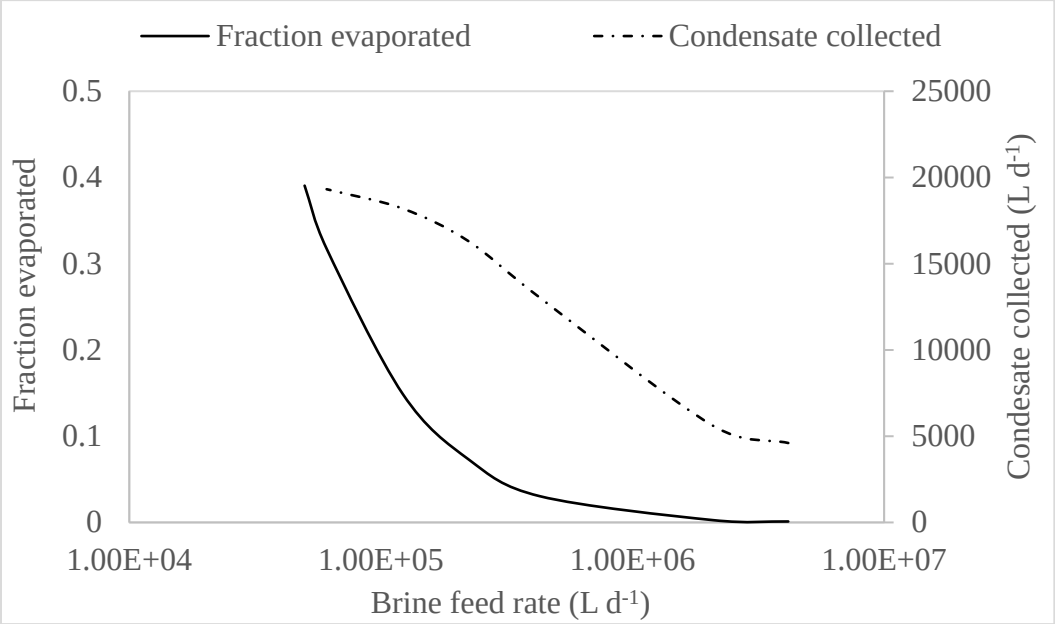

Figure 22: Fraction evaporation and condensate collection prediction for full scale facility.

Evaporating 20,000 L d^{-1} of brine concentrate with the current cost of membrane at approximately \$13 m^2, a required full-scale membrane area of 1,120 m^2 and assumed life time of 3 years, equates to an unamortized membrane treatment cost of \$0.66 per m^3 of brine concentrate, which gives total condensation collection values of 21.9 million liters (assuming no fouling occurs during the membrane's life time). Other costs may be incurred for acid addition. However, the cost of treatment is likely to be favorable because the system uses waste heat and energy costs are assumed to be zero.

Energy costs for membrane desalination process vary with the conductivity of source water treated. For source waters of 8.4 mS cm^{-1} (Walha et al. 2007) estimated energy consumption of 1.09 kilowatt hours per cubic meter (kWh m^{-3}) for RO and 1.5 kWh m^{-3} for electrodialysis (ED). Assuming an electricity cost of \$0.10 per kilowatt hour (kWh), this equates to \$0.05 m^{-3} for RO and \$0.15 m^{-3} for ED. These costs would likely increase for the concentrated brine of 14.9 mS cm^{-1} treated in this study, and these treatment processes must also account for membrane costs. For RO, Sweet (2008) reports desalination costs, including the membrane, to be \$0.81 m^{-3}, which is comparable to the \$0.66 m^{-3} found in this study for membrane evaporation. Finally, it is important to note that the membrane evaporation process used in this study has dual benefits obtained for the cost incurred. The brine concentrate volume requiring disposal is reduced while high quality permeate is produced.

8. Summary and Conclusions

Permeate flux and fraction of brine concentrate evaporated for a membrane evaporation process were found to increase with air flow rate and air temperature and to decrease with brine concentrate flow rate used. Increasing the air flow rate and air temperature provides more energy to the system for evaporating water, while increasing brine concentrate flow rate results in increasing water temperatures and reduced mass flow across the membrane. Model predictions, derived based upon literature values for heat and mass transfer correlations, agree well with both the measured evaporated flux and brine concentrate fraction evaporated. The model was used for predicting brine concentrate evaporated fraction and flux for waste heat obtained from a full-scale wastewater aeration system. The volume of water treated was low, but economics of the process appear favorable because energy demands can be neglected when using waste heat.

Operational problems associated with fouling are likely to be problematic as fouling occurred in experiments for brine concentrates with and without ferrous iron. Cleaning the membranes by flushing the fibers with brine concentrate at higher flow rates was not able to alleviate this fouling. Fouling could be alleviated if the pH of the brine concentrate was adjusted to be low for the durations of the studies conducted. Full evaluation of the process will require longer-term studies than those conducted in this study and future studies should also consider possible sources of supplemental waste heat to increase the overall amount of water treated.

9. References

Ahmed, M., W. H. Shayya, D. Hoey, A. Mahendran, R. Morris, and J. Al-Handaly (2000). "Use of evaporation ponds for brine disposal in desalination plants." Desalination 130(2): 155-168.

Al-Obaidani, S., E. Curcio, F. Macedonio, G. Di Profio, H. Al-Hinai, and E. Drioli (2008). "Potential of membrane distillation in seawater desalination: thermal efficiency, sensitivity study and cost estimation." Journal of Membrane Science 323(1): 85-98.

Al-Shammiri, M. and M. Safar (1999). "Multi-effect distillation plants: state of the art." Desalination 126(1–3): 45-59.

Alkhudhiri, A., N. Darwish, and N. Hilal (2012). "Membrane distillation: A comprehensive review." Desalination 287: 2-18.

Alklaibi, A. and N. Lior (2005). "Membrane-distillation desalination: status and potential." Desalination 171(2): 111-131.

Bonne, P., J. Hofman, and J. Van Der Hoek (2000). "Scaling control of RO membranes and direct treatment of surface water." Desalination 132(1): 109-119.

Brehant, A., V. Bonnelye, and M. Perez (2003). "Assessment of ultrafiltration as a pretreatment of reverse osmosis membranes for surface seawater desalination." Water Science and Technology: Water Supply 3(5-6): 437-445.

Cath, T. Y., V. D. Adams, and A. E. Childress (2004). "Experimental study of desalination using direct contact membrane distillation: a new approach to flux enhancement." Journal of Membrane Science 228(1): 5-16.

Drioli, E. and Y. Wu (1985). "Membrane distillation: An experimental study." Desalination 53(1–3): 339-346.

El-Bourawi, M., Z. Ding, R. Ma, and M. Khayet (2006). "A framework for better understanding membrane distillation separation process." Journal of Membrane Science 285(1): 4-29.

El-Dessouky, H., I. Alatiqi, S. Bingulac, and H. Ettouney (1998). "Steady-state analysis of the multiple effect evaporation desalination process." Chemical Engineering and Technology 21(5): 437.

Fritzmann, C., J. Löwenberg, T. Wintgens, and T. Melin (2007). "State-of-the-art of reverse osmosis desalination." Desalination 216(1): 1-76.

García-Payo, M., C. Rivier, I. Marison, and U. Von Stockar (2002). "Separation of binary mixtures by thermostatic sweeping gas membrane distillation: II. Experimental results with aqueous formic acid solutions." Journal of Membrane Science 198(2): 197-210.

Glater, J. and Y. Cohen (2003). "Brine disposal from land-based membrane desalination plants: A critical assessment." Prepared for the Metropolitan Water District of Southern California.

Gleick, P. (1996). Water Resources in Encyclopedia of Climate and Weather. New York, University Press.

Greenlee, L. F., D. F. Lawler, B. D. Freeman, B. Marrot, and P. Moulin (2009). "Reverse osmosis desalination: Water sources, technology, and today's challenges." Water Research 43(9): 2317-2348.

Gryta, M. (2008). "Fouling in direct contact membrane distillation process." Journal of Membrane Science 325(1): 383-394.

Gryta, M. and M. Tomaszewska (1998). "Heat transport in the membrane distillation process." Journal of Membrane Science 144(1): 211-222.

Hasson, D., A. Drak, and R. Semiat (2001). "Inception of $CaSO_4$ scaling on RO membranes at various water recovery levels." Desalination 139(1): 73-81.

Herron, J. and R. Salter (2003). Membrane assisted evaporation process and device for brine concentration. Google Patents.

Hickman, K. C. (1959). Multiple effect distillation. Google Patents.

Isaias, N. P. (2001). "Experience in reverse osmosis pretreatment." Desalination 139(1): 57-64.

Jiao, B., A. Cassano, and E. Drioli (2004). "Recent advances on membrane processes for the concentration of fruit juices: a review." Journal of Food Engineering 63(3): 303-324.

Jurenka, R. and M. Chapman-Wilbert (1996). "Maricopa Ground Water Treatment Study: Water Treatment Technology Program Report No. 15." US Department of the Interior, Bureau of Reclamation, Denver, CO.

Karagiannis, I. C. and P. G. Soldatos (2008). "Water desalination cost literature: review and assessment." Desalination 223(1): 448-456.

Khayet, M., C. Cojocaru, and A. Baroudi (2012). "Modeling and optimization of sweeping gas membrane distillation." Desalination 287: 159-166.

Khayet, M., M. Godino, and J. Mengual (2003). "Possibility of nuclear desalination through various membrane distillation configurations: a comparative study." International Journal of Nuclear Desalination 1(1): 30-46.

Khayet, M., P. Godino, and J. I. Mengual (2000). "Theory and experiments on sweeping gas membrane distillation." Journal of Membrane Science 165(2): 261-272.

Kopp, C. V., R. J. Streeton, and P. S. Khoo (1997). Hollow fiber membranes. Google Patents.

Krishna, H. J. (2004). "Introduction to desalination technologies." Texas Water Development 2.

Kullab, A. and A. Martin (2011). "Membrane distillation and applications for water purification in thermal cogeneration plants." Separation and Purification Technology 76(3): 231-237.

Laganà, F., G. Barbieri, and E. Drioli (2000). "Direct contact membrane distillation: modelling and concentration experiments." Journal of Membrane Science 166(1): 1-11.

Lawson, K. W. and D. R. Lloyd (1996). "Membrane distillation. II. Direct contact MD." Journal of Membrane Science 120(1): 123-133.

Lawson, K. W. and D. R. Lloyd (1997). "Membrane distillation." Journal of Membrane Science 124(1): 1-25.

Lee, C., S. Bae, S. Han, and L. Kang (2007). "Application of ultrafiltration hybrid membrane processes for reuse of secondary effluent." Desalination 202(1): 239-246.

Leenheer, J. A., R. L. Malcolm, and W. R. White (1976). "Investigation of the reactivity and fate of certain organic components of an industrial waste after deep-well injection." Environmental Science and Technology 10(5): 445-451.

Li, J.-M., Z.-K. Xu, Z.-M. Liu, W.-F. Yuan, H. Xiang, S.-Y. Wang, and Y.-Y. Xu (2003). "Microporous polypropylene and polyethylene hollow fiber membranes. Part 3. Experimental studies on membrane distillation for desalination." Desalination 155(2): 153-156.

Li, Q. and M. Elimelech (2006). "Synergistic effects in combined fouling of a loose nanofiltration membrane by colloidal materials and natural organic matter." Journal of Membrane Science 278(1): 72-82.

Lv, Y., X. Yu, S.-T. Tu, J. Yan, and E. Dahlquist (2010). "Wetting of polypropylene hollow fiber membrane contactors." Journal of Membrane Science 362(1): 444-452.

Martínez-Díez, L. and M. I. Vazquez-Gonzalez (1999). "Temperature and concentration polarization in membrane distillation of aqueous salt solutions." Journal of Membrane Science 156(2): 265-273.

McKelvey, S. A., D. T. Clausi, and W. J. Koros (1997). "A guide to establishing hollow fiber macroscopic properties for membrane applications." Journal of Membrane Science 124(2): 223-232.

Mickley, M. (2004). "Review of concentrate management options." The future of desalination in Texas. Volume 2. Texas Water Development Board, December 2004. 1-14.

Pérez-González, A., A. Urtiaga, R. Ibáñez, and I. Ortiz (2012). "State of the art and review on the treatment technologies of water reverse osmosis concentrates." Water Research 46(2): 267-283.

Phattaranawik, J. and R. Jiraratananon (2001). "Direct contact membrane distillation: effect of mass transfer on heat transfer." Journal of Membrane Science 188(1): 137-143.

Prasad, R. and K. Sirkar (1988). "Dispersion-free solvent extraction with microporous hollow-fiber modules." AIChE Journal 34(2): 177-188.

Ravizky, A. and N. Nadav (2007). "Salt production by the evaporation of SWRO brine in Eilat: a success story." Desalination 205(1): 374-379.

Reahl, E. (2004). Half a Century of Desalination with Electrodialysis. General Electric Company.

Roebelen, G. J., G. F. Dehner, and H. E. Winkler (1982). Thermoelectric integrated membrane evaporation water recovery technology, SAE Technical Paper.

Saripalli, K., M. Sharma, and S. Bryant (2000). "Modeling injection well performance during deep-well injection of liquid wastes." Journal of Hydrology 227(1): 41-55.

Schäfer, A., A. G. Fane, and T. Waite (2000). "Fouling effects on rejection in the membrane filtration of natural waters." Desalination 131(1): 215-224.

Schofield, R., A. Fane, and C. Fell (1987). "Heat and mass transfer in membrane distillation." Journal of Membrane Science 33(3): 299-313.

Singh, R. (1997). "A review of membrane technologies: reverse osmosis, nanofiltration, and ultrafiltration." Ultrapure Water 14(3): 21-29.

Squire, D. (2000). "Reverse osmosis concentrate disposal in the UK." Desalination 132(1–3): 47-54.

Squire, D., J. Murrer, P. Holden, and C. Fitzpatrick (1997). "Disposal of reverse osmosis membrane concentrate." Desalination 108(1–3): 143-147.

Sweet, P. (2008). "Desalination gets a serious look." In Las Vegas Sun, March 21 2008. https://lasvegassun.com/news/2008/mar/21/desalination-gets-serious-look.

Tchobanoglous, G., F. Burton, and D. Stensel (2003). Wastewater Engineering, Treatment and Reuse: Metcalf & Eddy. Boson, Massachusetts, Mc Graw Hill.

Van der Bruggen, B. and C. Vandecasteele (2002). "Distillation vs. membrane filtration: overview of process evolutions in seawater desalination." Desalination 143(3): 207-218.

Voutchkov, N. (2011). "Overview of seawater concentrate disposal alternatives." Desalination 273(1): 205-219.

Wade, N. M. (1993). "Technical and economic evaluation of distillation and reverse osmosis desalination processes." Desalination 93(1): 343-363.

Walha, K., R. B. Amar, L. Firdaous, F. Quéméneur, and P. Jaouen (2007). "Brackish groundwater treatment by nanofiltration, reverse osmosis and electrodialysis in Tunisia: performance and cost comparison." Desalination 207(1): 95-106.

Wilf, M. and K. Klinko (2001). "Optimization of seawater RO systems design." Desalination 138(1): 299-306.

Yan, S.-p., M.-X. Fang, W.-F. Zhang, S.-Y. Wang, Z.-K. Xu, Z.-Y. Luo, and K.-F. Cen (2007). "Experimental study on the separation of CO 2 from flue gas using hollow fiber membrane contactors without wetting." Fuel Processing Technology 88(5): 501-511.

Yiantsios, S. and A. Karabelas (2001). "An experimental study of humid acid and powdered activated carbon deposition on UF membranes and their removal by backwashing." Desalination 140(2): 195-209.

Zhao, S., P. H. Feron, Z. Xie, J. Zhang, and M. Hoang (2014). "Condensation studies in membrane evaporation and sweeping gas membrane distillation." Journal of Membrane Science 462: 9-16.

Appendix I: Data record for variable water flow rate (DI water) at air temperature 60 °C

1. Water flow rate: 0.38 mL min^{-1}

Time	Airflow (L min^{-1})		Water flow (mL min^{-1})		Outflow scale (g)	Air pressure (psi)		Water pressure (psi)		Condensed mass (g)	Calibrated water flow (mL min^{-1})	
	I	II	In	Out		In	Out	In	Out		In	Out
14:21	10	10	1.17	0.56	627.85	6	0	50	49	99.46	0.68	0.38
14:26	10	10	1.17	0.56	629.72	6	0	50	49	100.28	0.67	0.37
14:31	10	10	1.18	0.56	631.7	6	0	50	49	101.1	0.69	0.38
14:36	10	10	1.17	0.56	633.48	6	0	50	49	101.86	0.68	0.38
14:41	10	10	1.15	0.56	635.31	6	0	50	49	102.67	0.66	0.38
14:46	10	10	1.14	0.56	637.27	6	0	50	49	103.41	0.65	0.38
14:51	10	10	1.15	0.56	639.05	6	0	50	49	104.11	0.66	0.38
14:56	10	10	1.16	0.56	640.94	6	0	50	49	104.97	0.67	0.38
15:01	10	10	1.14	0.56	642.75	6	0	50	49	105.75	0.65	0.38

g =grams
psi = pounds per square inch

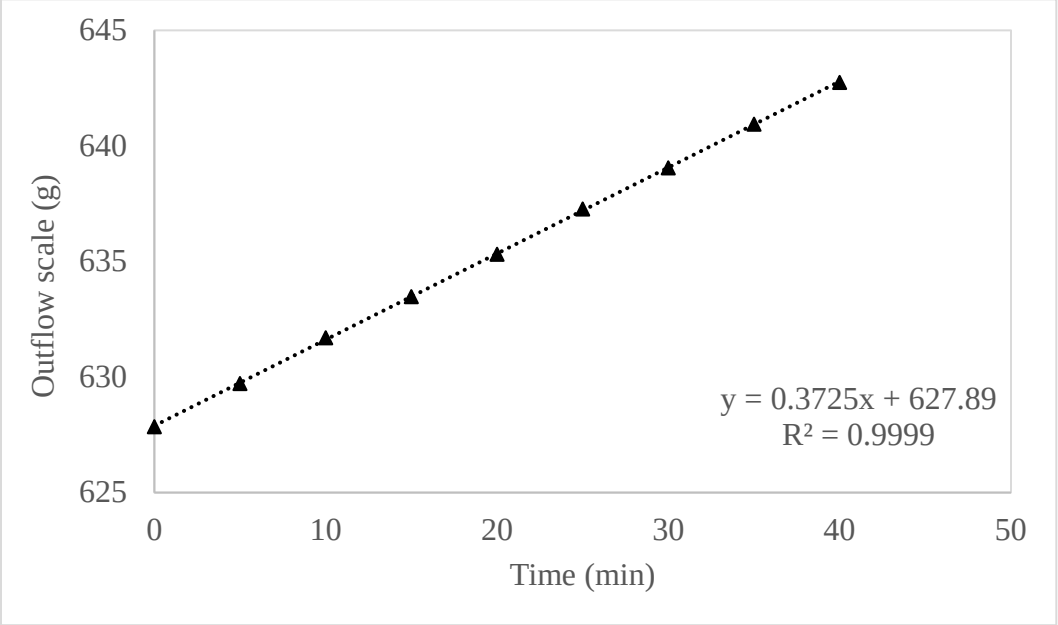
645
640
635
630
625
Outflow scale (g)
0
10
20
30
40
50
Time (min)
y = 0.3725x + 627.89
R² = 0.9999

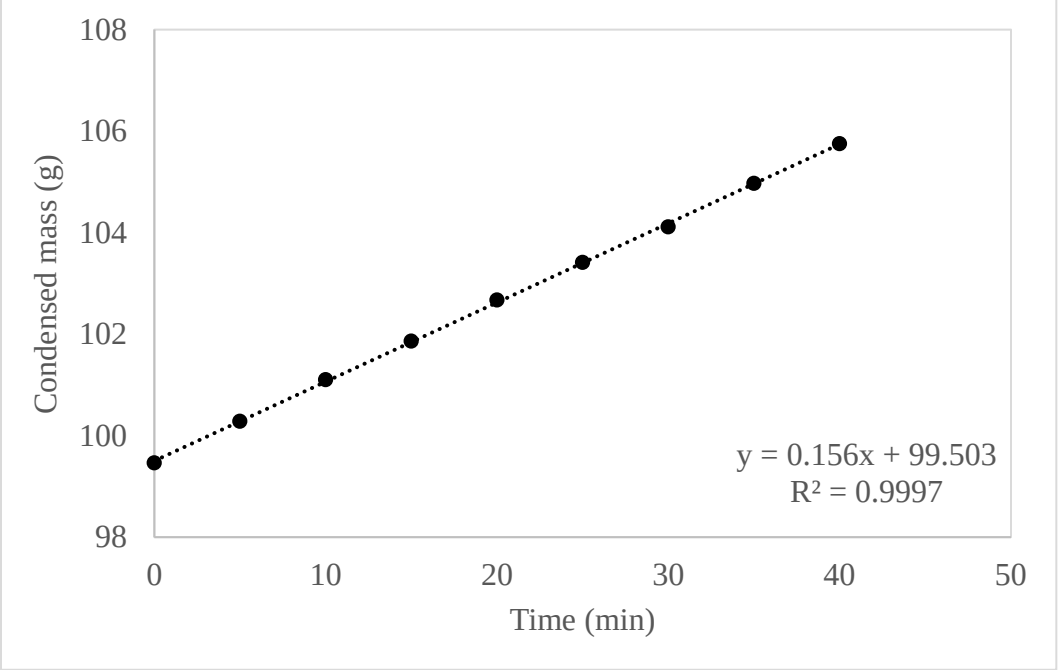
108
106
104
102
100
98
Condensed mass (g)
0
10
20
30
40
50
Time (min)
y = 0.156x + 99.503
R² = 0.9997

2. Water flow rate: 1.0 mL min^{-1}

Time	Airflow (L min^{-1})		Water flow (mL min^{-1})		Outflow scale (g)	Air pressure (psi)		Water pressure (psi)		Condensed mass (g)	Calibrated water flow (mL min^{-1})	
	I	II	In	Out		In	Out	Inlet	Outlet		In	Out
15:08	10	10	1.78	1.25	645.46	6	0	50	48	106.86	1.29	1.00
15:18	10	10	1.73	1.26	655.55	6	0	49	48	108.46	1.24	1.01
15:28	10	10	1.69	1.25	665.18	6	0	49	48	109.93	1.21	1.00
15:38	10	10	1.65	1.26	675.1	6	0	49	48	111.3	1.17	1.01
15:48	10	10	1.67	1.25	685	6	0	49	48	112.84	1.18	1.00
15:58	10	10	1.65	1.25	694.95	6	0	49	48	114.1	1.17	1.00
16:08	10	10	1.66	1.25	704.98	6	0	50	49	115.46	1.17	1.00
16:18	10	10	1.65	1.26	714.95	6	0	50	49	116.85	1.16	1.01
16:28	10	10	1.66	1.27	724.93	6	0	50	49	118.26	1.17	1.01

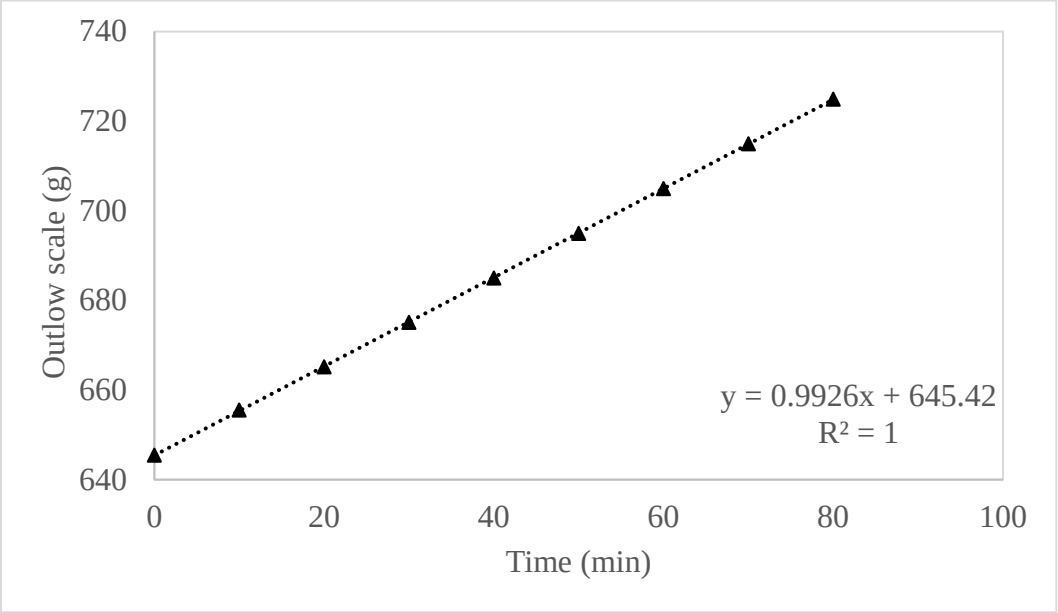
740
720
700
680
660
640
Outlow scale (g)
0
20
40
60
80
100
Time (min)
y = 0.9926x + 645.42
R² = 1

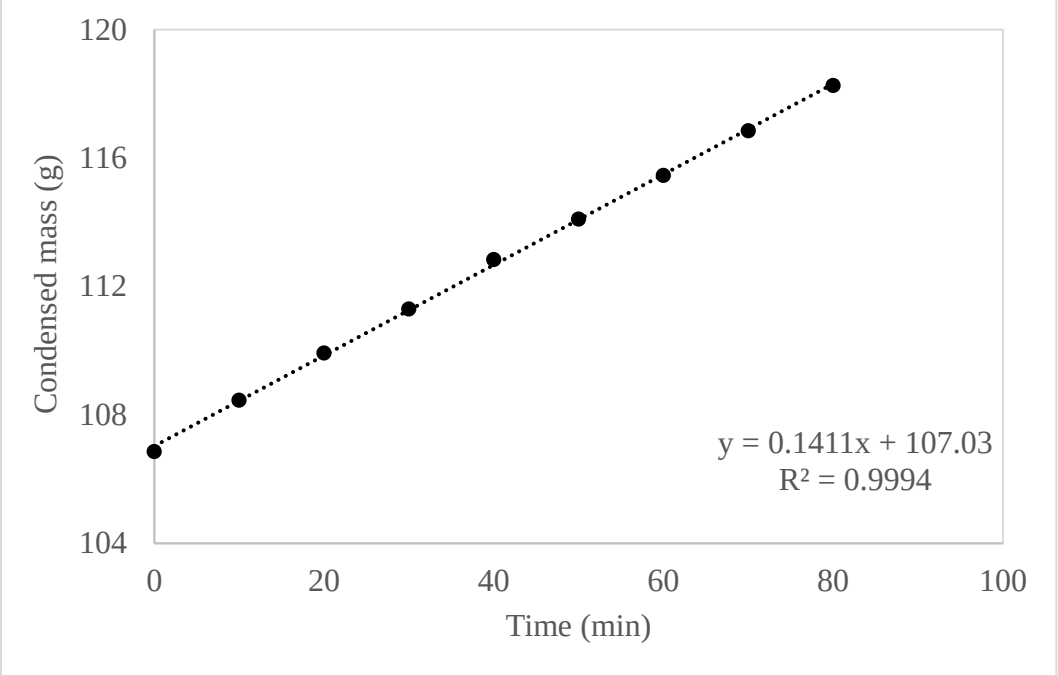
120
116
112
108
104
Condensed mass (g)
0
20
40
60
80
100
Time (min)
y = 0.1411x + 107.03
R² = 0.9994

3. Water flow rate: 1.5 mL min^{-1}

Time	Airflow (L min^{-1})		Water flow (mL min^{-1})		Outflow scale (g)	Air pressure (psi)		Water pressure (psi)		Condensed mass (g)	Calibrated water flow (mL min^{-1})	
	I	II	In	Out		In	Out	In	Out		In	Out
20:56	10	10	2.25	1.81	253.86	6	0	37	36	81.53	1.77	1.50
21:01	10	10	2.19	1.81	261.11	6	0	37	35	82.15	1.71	1.50
21:06	10	10	2.14	1.81	268.36	6	0	37	35	82.68	1.67	1.50
21:11	10	10	2.13	1.81	275.7	6	0	37	35	83.44	1.65	1.50
21:16	10	10	2.14	1.81	282.98	6	0	37	35	83.88	1.66	1.50
21:21	10	10	2.13	1.82	290.3	6	0	37	35	84.51	1.65	1.51
21:26	10	10	2.14	1.81	297.59	6	0	37	36	85.04	1.66	1.50

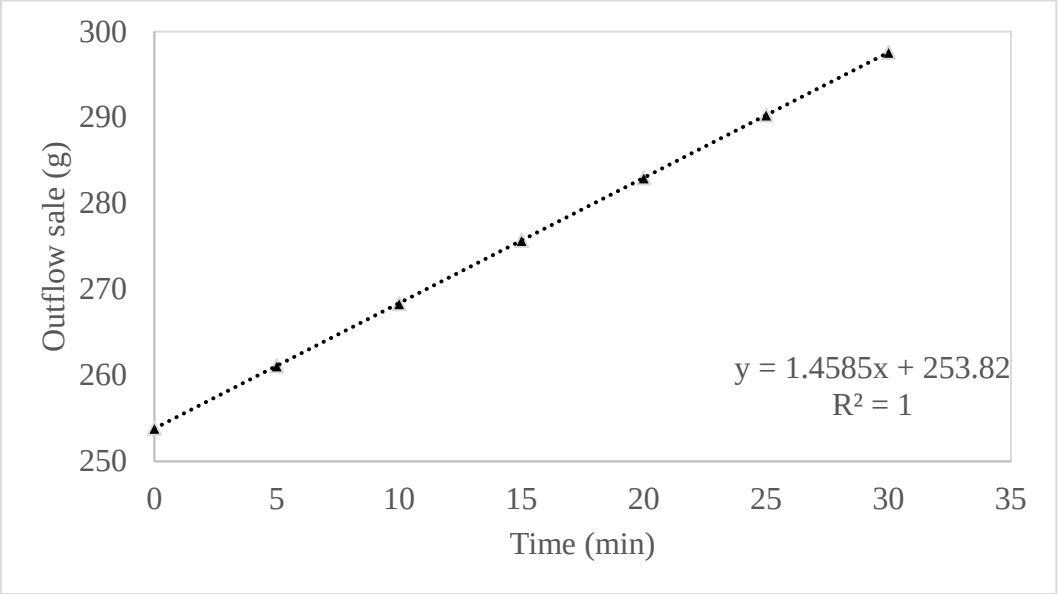
300
290
280
270
260
250
Outflow sale (g)
0
5
10
15
20
25
30
35
Time (min)
y = 1.4585x + 253.82
R² = 1

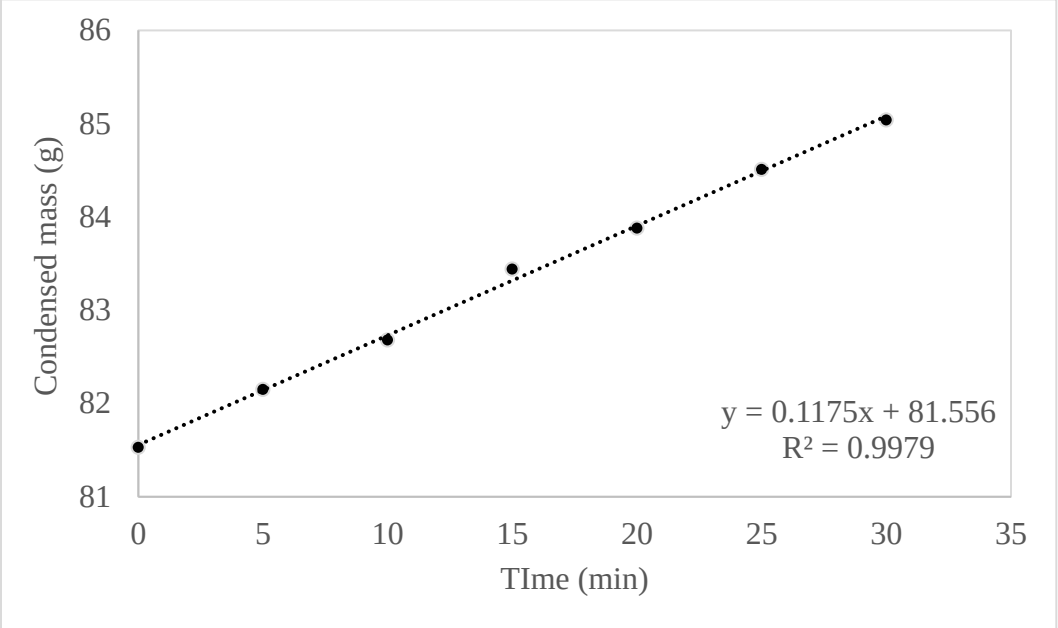
86
85
84
83
82
81
Condensed mass (g)
0
5
10
15
20
25
30
35
TIme (min)
y = 0.1175x + 81.556
R² = 0.9979

4. Water flow rate: 2.0 mL min^{-1}

Time	Airflow (L min^{-1})		Water flow (mL min^{-1})		Outflow scale (g)	Air pressure (psi)		Water pressure (psi)		Condensed mass (g)	Calibrated water flow (mL min^{-1})	
	I	II	In	Out		In	Out	In	Out		In	Out
16:31	10	10	2.67	2.37	729.01	6	0	50	48	118.74	2.20	2.00
16:41	10	10	2.63	2.37	748.97	6	0	50	48	119.97	2.16	2.00
16:51	10	10	2.60	2.37	769.08	6	0	50	48	121.28	2.13	2.00
17:01	10	10	2.58	2.38	789.08	6	0	50	48	122.77	2.11	2.01
17:11	10	10	2.56	2.37	809.13	6	0	50	48	124.14	2.08	2.01
17:21	10	10	2.58	2.37	829.1	6	0	50	48	125.6	2.11	2.01

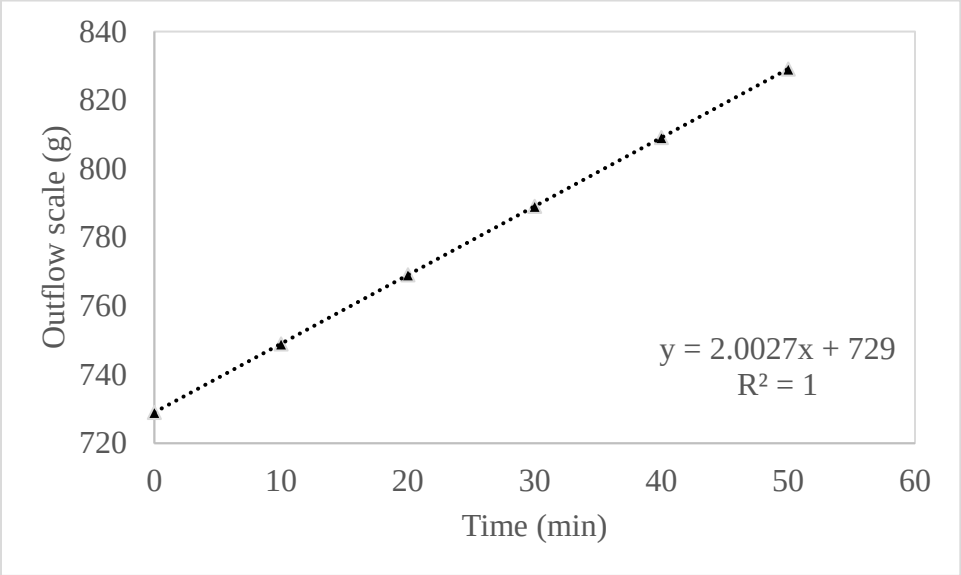
840
820
800
780
760
740
720
Outflow scale (g)
0
10
20
30
40
50
60
Time (min)
y = 2.0027x + 729
R² = 1

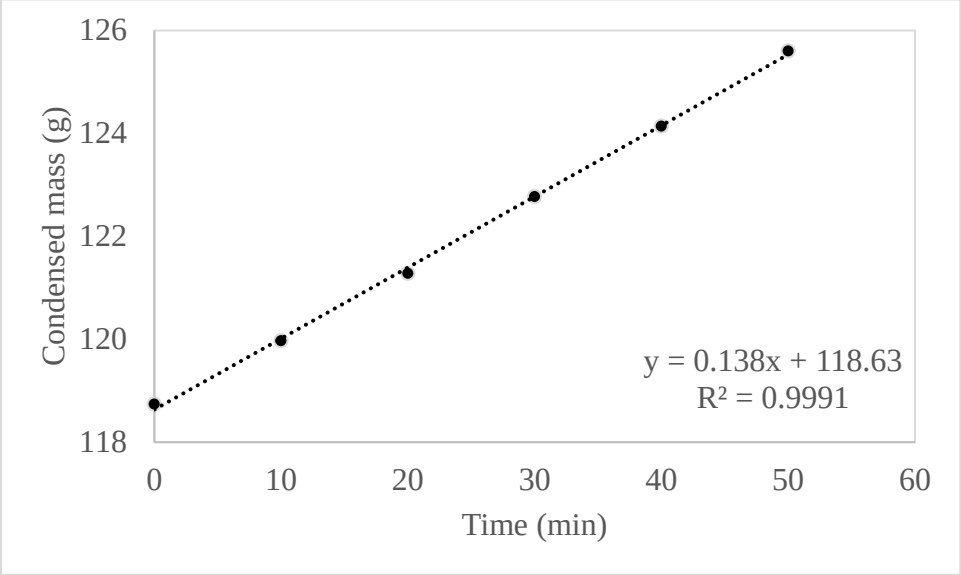
126
124
122
120
118
Condensed mass (g)
0
10
20
30
40
50
60
Time (min)
y = 0.138x + 118.63
R² = 0.9991

5. Water flow rate: 3.0 mL min^{-1}

Time	Airflow (L min^{-1})		Water flow (mL min^{-1})		Outflow scale (g)	Air pressure (psi)		Water pressure (psi)		Condensed mass (g)	Calibrated water flow (mL min^{-1})	
	I	II	In	Out		In	Out	In	Out		In	Out
21:34	10	10	3.56	3.49	311.62	6	0	37	34	85.89	3.10	3.01
21:39	10	10	3.50	3.49	326.27	6	0	37	35	86.43	3.04	3.00
21:44	10	10	3.48	3.48	340.92	6	0	37	35	87.03	3.02	3.00
21:49	10	10	3.43	3.49	355.59	6	0	37	35	87.43	2.97	3.01
21:54	10	10	3.46	3.49	370.28	6	0	37	35	87.7	3.00	3.00
21:59	10	10	3.45	3.49	384.97	6	0	37	35	88.3	2.99	3.01
22:04	10	10	3.44	3.48	399.67	6	0	37	35	88.58	2.99	3.00
22:09	10	10	3.44	3.48	414.38	6	0	37	34	88.91	2.99	3.00
22:14	10	10	3.43	3.49	429.08	6	0	37	35	89.54	2.98	3.01

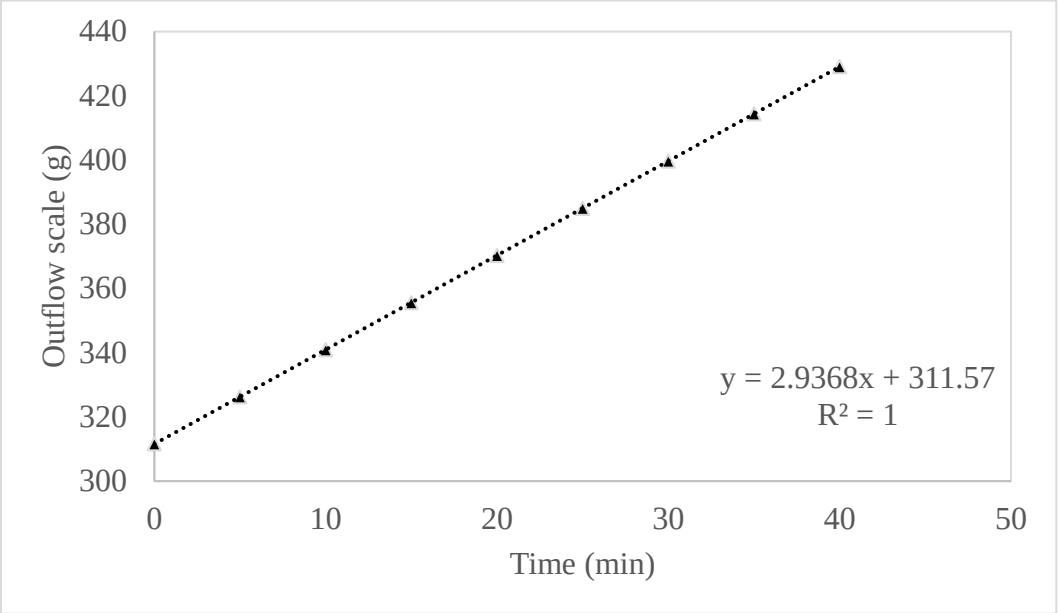
440
420
400
380
360
340
320
300
Outflow scale (g)
0
10
20
30
40
50
Time (min)
y = 2.9368x + 311.57
R² = 1

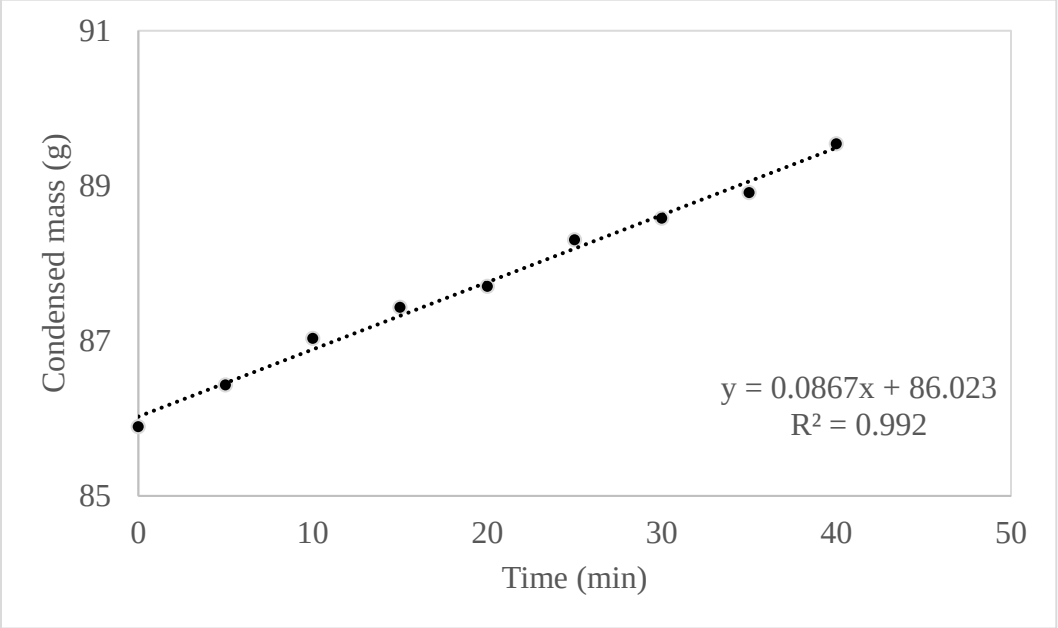
91
89
87
85
Condensed mass (g)
0
10
20
30
40
50
Time (min)
y = 0.0867x + 86.023
R² = 0.992

Appendix II: Data record for variable airflow rate (DI water) at air temperature 60 °C

1. Airflow rate: 5 L min^{-1}

Time	Airflow (L min^{-1})		Water flow (mL min^{-1})		Outflow scale (g)	Air pressure (psi)		Water pressure (psi)		Condensed mass (g)	Calibrated water flow (mL min^{-1})	
	I	II	In	Out		In	Out	In	Out		In	Out
17:37	2.5	2.5	0.94	0.56	264.54	1	0	37	36	70.48	0.44	0.38
17:47	2.5	2.5	0.94	0.56	267.72	1	0	37	36	71.02	0.44	0.38
17:57	2.5	2.5	0.93	0.56	270.91	1	0	37	36	71.96	0.44	0.38
18:07	2.5	2.5	0.93	0.56	274.05	1	0	37	36	72.65	0.43	0.38
18:17	2.5	2.5	0.92	0.56	277.24	1	0	37	36	73.31	0.42	0.38
18:27	2.5	2.5	0.89	0.56	280.48	1	0	37	36	74.27	0.40	0.38
18:37	2.5	2.5	0.92	0.56	283.62	1	0	37	36	75.12	0.42	0.38
18:47	2.5	2.5	0.91	0.56	286.81	1	-1	37	36	75.86	0.41	0.38

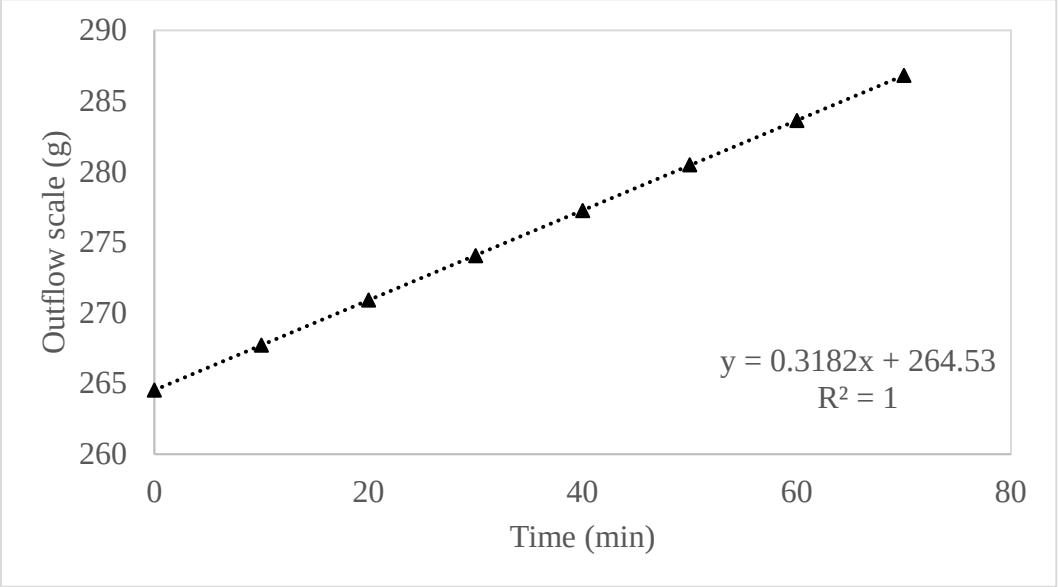
290
285
280
275
270
265
260
Outflow scale (g)
0
20
40
60
80
Time (min)
y = 0.3182x + 264.53
R² = 1

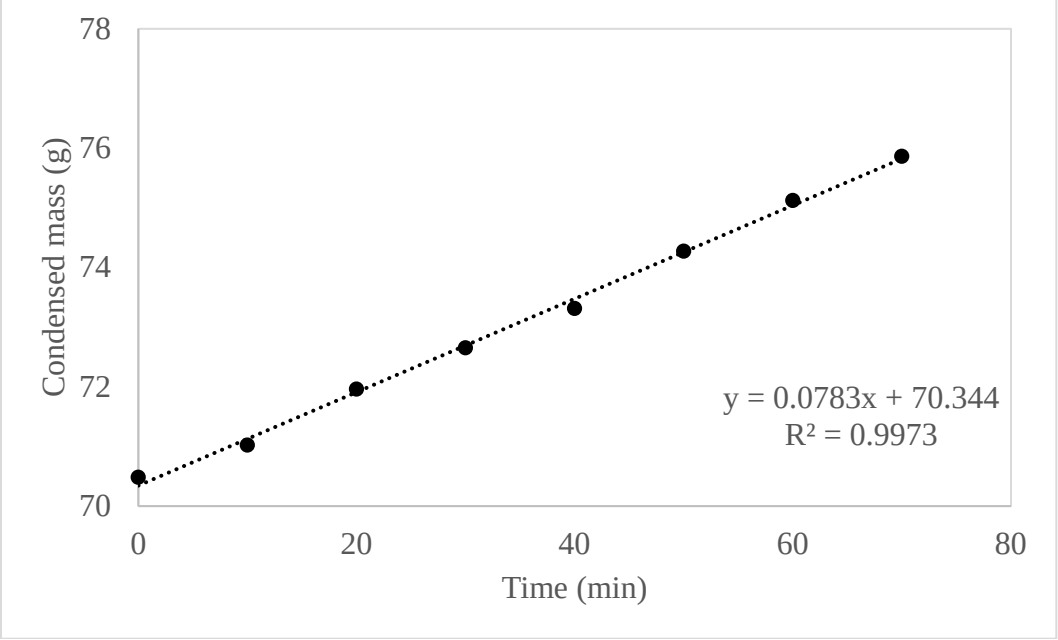
78
76
74
72
70
Condensed mass (g)
0
20
40
60
80
Time (min)
y = 0.0783x + 70.344
R² = 0.9973

2. Airflow rate: 10 L min^{-1}

Time	Airflow (L min^{-1})		Water flow (mL min^{-1})		Outflow scale (g)	Air pressure (psi)		Water pressure (psi)		Condensed mass (g)	Calibrated water flow (mL min^{-1})	
	I	II	In	Out		In	Out	In	Out		In	Out
20:27	5	5	1.02	0.56	318.95	2	0	37	36	86.06	0.52	0.38
20:37	5	5	0.98	0.56	322.19	2	0	37	36	87.33	0.49	0.38
20:47	5	5	1.02	0.57	325.41	2	0	37	36	88.54	0.52	0.39
20:57	5	5	1.03	0.56	328.6	2	0	37	36	89.97	0.54	0.38
21:07	5	5	1.04	0.56	331.73	2	0	37	36	91.12	0.54	0.38
21:17	5	5	1.05	0.56	334.64	2	0	37	36	92.28	0.56	0.38
21:27	5	5	1.04	0.56	337.69	2	0	37	36	93.05	0.55	0.38
21:37	5	5	1.07	0.56	340.7	2	0	37	36	94.54	0.57	0.38
21:47	5	5	1.04	0.56	343.62	2	0	37	36	95.61	0.54	0.38
21:57	5	5	1.05	0.56	346.58	2	0	37	36	97.01	0.55	0.38
22:07	5	5	1.07	0.56	349.59	2	0	37	36	98.17	0.58	0.38

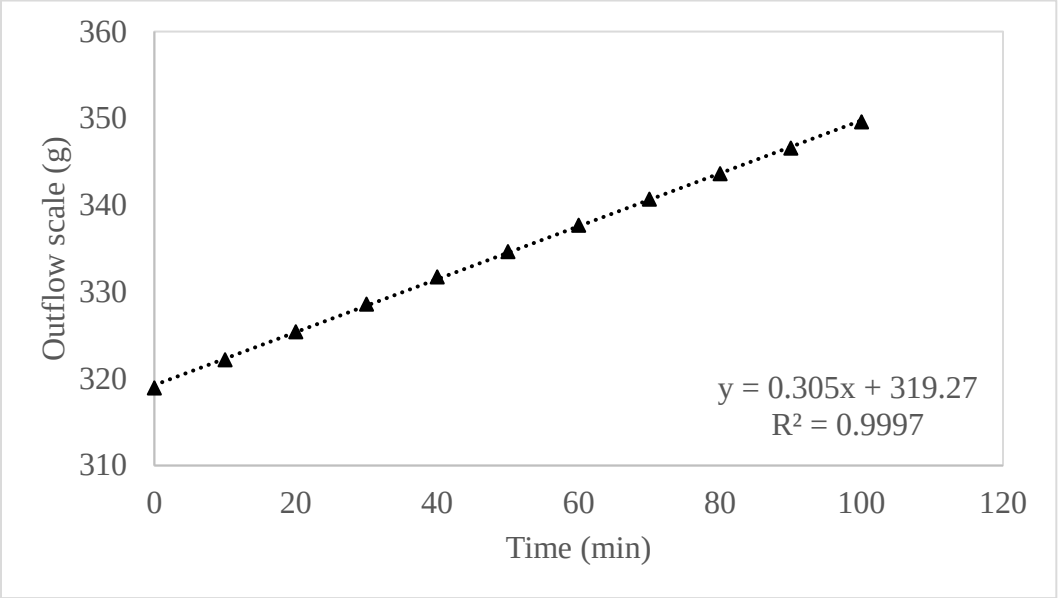
360
350
340
330
320
310
Outflow scale (g)
0
20
40
60
80
100
120
Time (min)
y = 0.305x + 319.27
R² = 0.9997

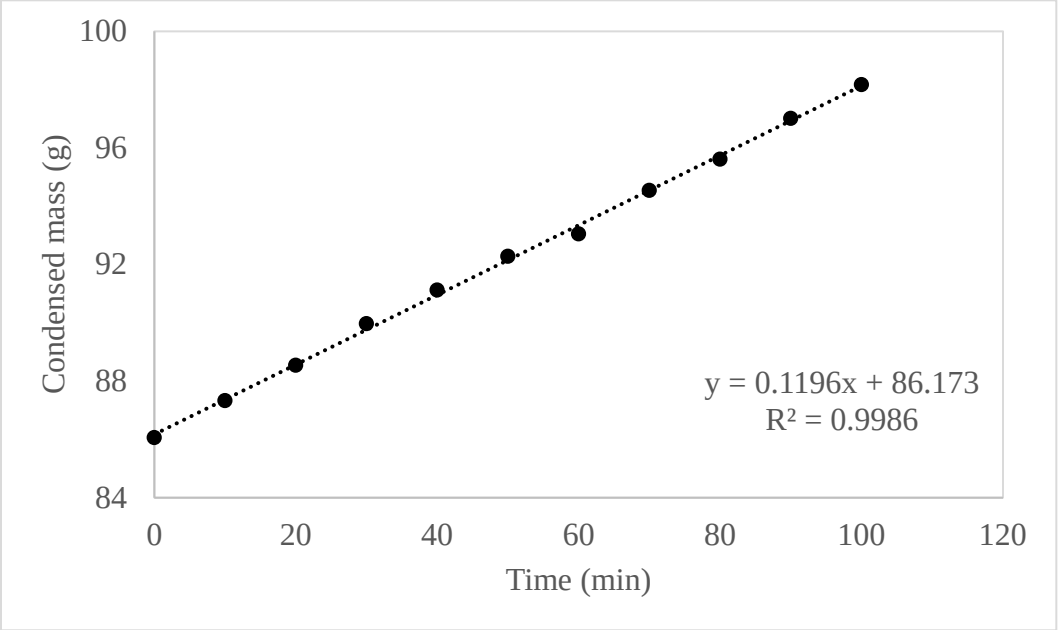
100
96
92
88
84
Condensed mass (g)
0
20
40
60
80
100
120
Time (min)
y = 0.1196x + 86.173
R² = 0.9986

3. Airflow rate: 15 L min^{-1}

Time	Airflow (L min^{-1})		Water flow (mL min^{-1})		Outflow scale (g)	Air pressure (psi)		Water pressure (psi)		Condensed mass (g)	Calibrated water flow (mL min^{-1})	
	I	II	In	Out		In	Out	In	Out		Inflow	Outflow
19:26	5	10	1.14	0.56	892.35	4	0	46	46	142.19	0.65	0.38
19:36	5	10	1.13	0.56	895.92	4	0	46	45	143.31	0.64	0.38
19:46	5	10	1.13	0.57	899.49	4	0	45	45	145.23	0.64	0.38
19:56	5	10	1.15	0.57	903.19	4	0	45	44	146.58	0.66	0.38
20:06	5	10	1.12	0.56	906.75	4	0	45	44	147.92	0.63	0.38
20:16	5	10	1.14	0.56	910.36	4	0	44	44	150.04	0.65	0.38

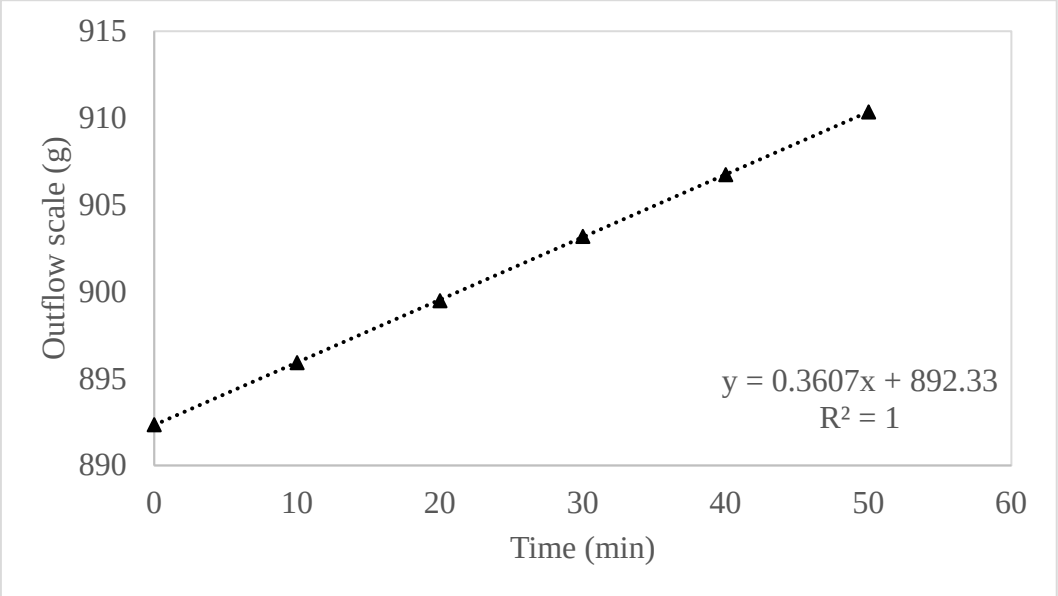
915
910
905
900
895
890
Outflow scale (g)
0
10
20
30
40
50
60
Time (min)
y = 0.3607x + 892.33
R² = 1

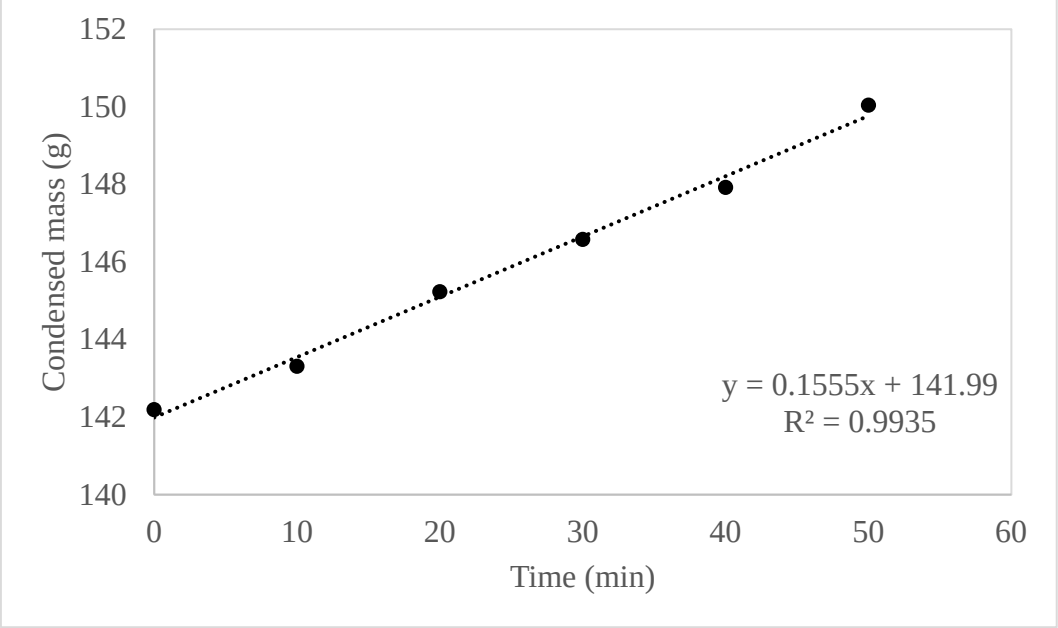
152
150
148
146
144
142
140
Condensed mass (g)
0
10
20
30
40
50
60
Time (min)
y = 0.1555x + 141.99
R² = 0.9935

4. Airflow rate: 20 L min-1

Time	Airflow (L min^{-1})		Water flow (mL min^{-1})		Outflow scale (g)	Air pressure (psi)		Water pressure (psi)		Condensed mass (g)	Calibrated water flow (mL min^{-1})	
	I	II	In	Out		In	Out	In	Out		In	Out
19:26	10	10	1.08	0.56	144	6	0	37	36	70.62	0.59	0.38
19:36	10	10	1.09	0.56	147.04	6	0	37	36	72.51	0.59	0.38
19:46	10	10	1.08	0.56	150.07	6	0	37	36	74.34	0.58	0.38
19:56	10	10	1.08	0.56	153.12	6	0	37	36	76.26	0.59	0.38
20:06	10	10	1.07	0.56	156.22	6	0	37	36	78.13	0.57	0.38
20:16	10	10	1.07	0.56	159.2	6	0	37	36	80.07	0.57	0.38
20:26	10	10	1.07	0.58	162.21	6	0	37	36	81.89	0.58	0.39

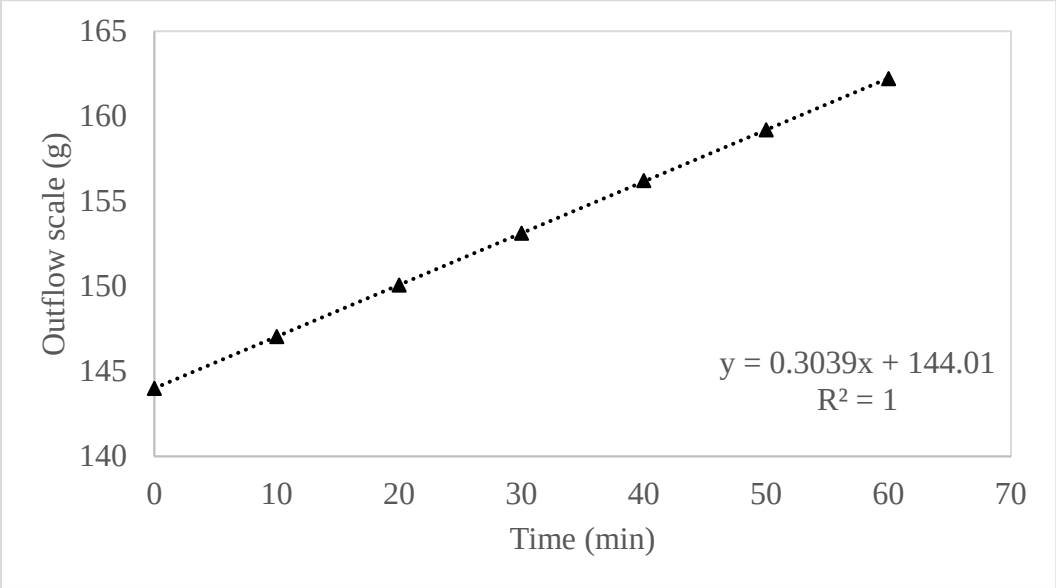
165
160
155
150
145
140
Outflow scale (g)
0
10
20
30
40
50
60
70
Time (min)
y = 0.3039x + 144.01
R² = 1

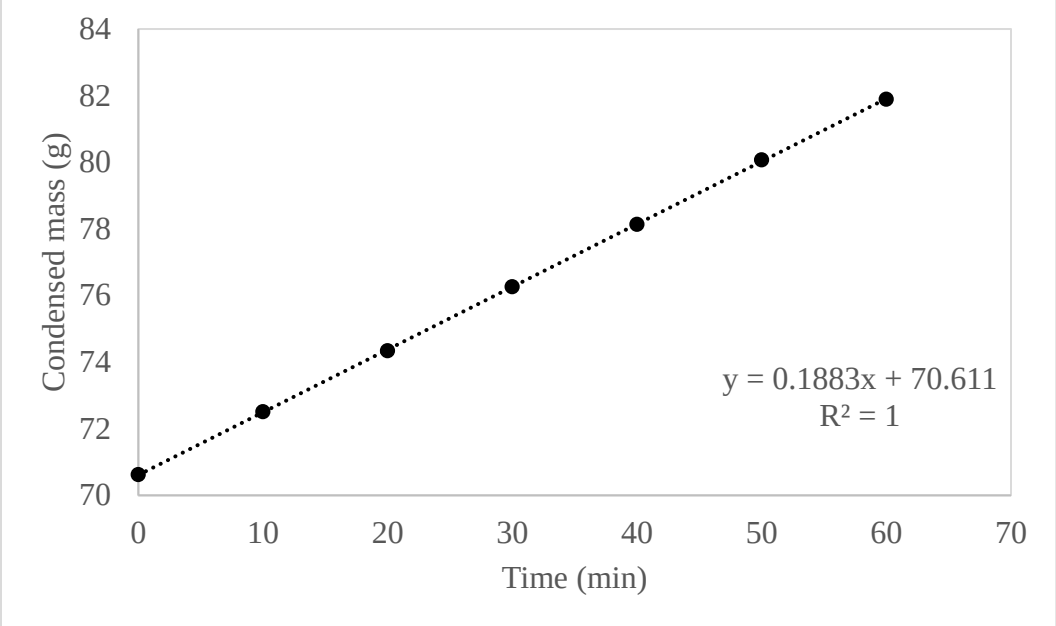
84
82
80
78
76
74
72
70
Condensed mass (g)
0
10
20
30
40
50
60
70
Time (min)
y = 0.1883x + 70.611
R² = 1

5. Airflow rate: 25 L min^{-1}

Time	Airflow (L min^{-1})		Water flow (mL min^{-1})		Outflow scale (g)	Air pressure (psi)		Water pressure (psi)		Condensed mass (g)	Calibrated water flow (mL min^{-1})	
	I	II	In	Out		In	Out	In	Out		In	Out
18:05	15	10	1.12	0.56	862.84	9	0	51	50	132.03	0.62	0.38
18:15	15	10	1.17	0.56	866.39	9	0	53	52	133.44	0.68	0.38
18:25	15	10	1.16	0.57	870.1	9	0	52	51	134.59	0.66	0.39
18:35	15	10	1.17	0.56	873.61	9	0	51	50	136.66	0.68	0.38
18:45	15	10	1.17	0.56	877.33	9	0	50	49	137.42	0.67	0.38
18:55	15	10	1.20	0.56	880.99	9	0	49	48	139.32	0.71	0.38

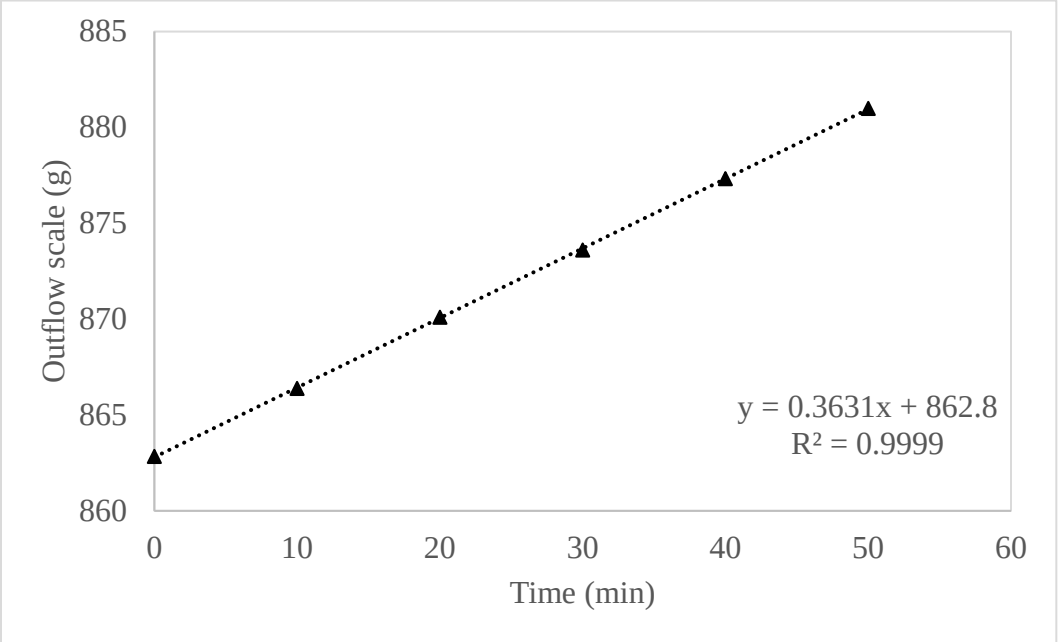
885
880
875
870
865
860
Outflow scale (g)
0
10
20
30
40
50
60
Time (min)
y = 0.3631x + 862.8
R² = 0.9999

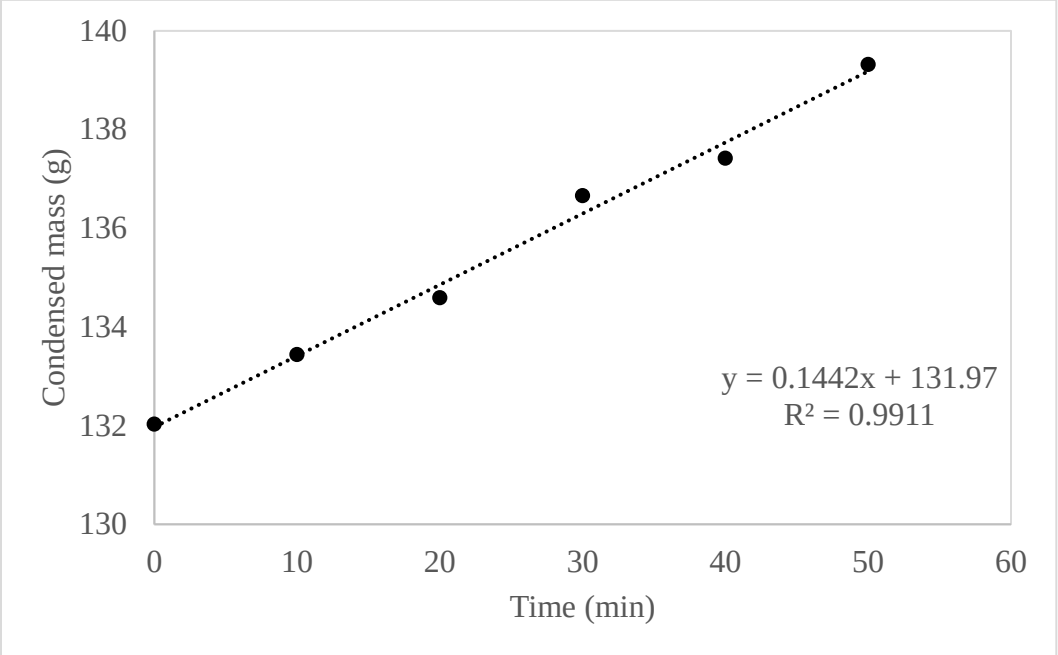
140
138
136
134
132
130
Condensed mass (g)
0
10
20
30
40
50
60
Time (min)
y = 0.1442x + 131.97
R² = 0.9911

6. Airflow rate: 30 L min^{-1}

Time	Airflow (L min^{-1})		Water flow (mL min^{-1})		Outflow scale (g)	Air pressure (psi)		Water pressure (psi)		Condensed mass (g)	Calibrated water flow (mL min^{-1})	
	I	II	In	Out		In	Out	In	Out		In	Out
11:02	15	15	1.34	0.56	15.66	11	0	36	36	12.62	0.85	0.38
11:12	15	15	1.30	0.57	18.75	11	0	36	36	14.59	0.81	0.39
11:22	15	15	1.30	0.56	21.89	11	0	36	36	16.35	0.81	0.38
11:32	15	15	1.31	0.56	25.13	11	0	37	36	18.16	0.82	0.38
11:42	15	15	1.31	0.56	28.36	11	0	36	36	20.15	0.82	0.38
11:52	15	15	1.29	0.56	31.59	11	0	36	36	21.92	0.80	0.38

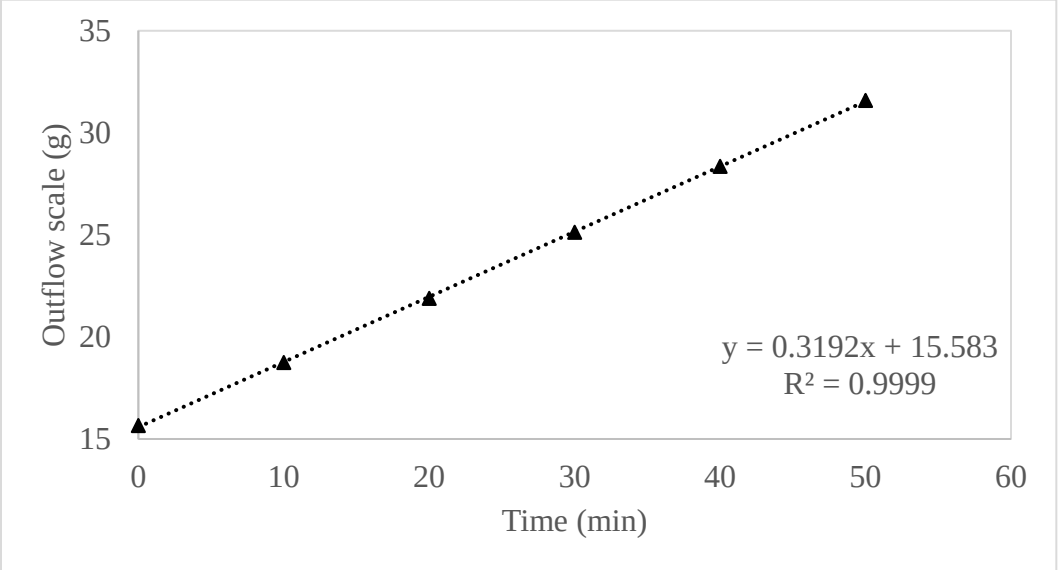
35
30
25
20
15
Outflow scale (g)
0
10
20
30
40
50
60
Time (min)
y = 0.3192x + 15.583
R² = 0.9999

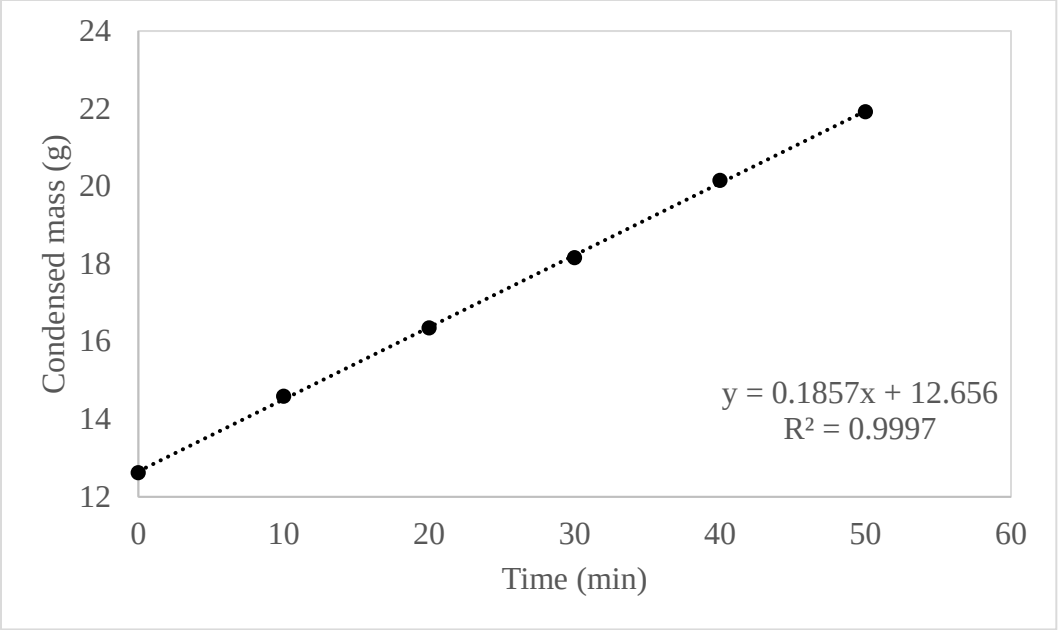
24
22
20
18
16
14
12
Condensed mass (g)
0
10
20
30
40
50
60
Time (min)
y = 0.1857x + 12.656
R² = 0.9997

Appendix III: Data record for variable air temperature (DI water)

1. Air temperature: 23 °C

Time	Airflow (L min^{-1})		Water flow (mL min^{-1})		Outflow scale (g)	Air pressure (psi)		Water pressure (psi)		Condensed mass (g)	Calibrated water flow (mL min^{-1})	
	I	II	In	Out		In	Out	In	Out		In	Out
20:24	10	10	0.90	0.56	137.4	5	0	36	36	59.2	0.41	0.38
20:34	10	10	0.95	0.56	140.76	5	0	37	36	59.43	0.46	0.38
20:44	10	10	0.99	0.56	144	5	0	36	36	59.63	0.50	0.38
20:54	10	10	0.90	0.57	147.17	5	0	36	36	59.88	0.41	0.39
21:04	10	10	0.86	0.56	150.46	5	0	36	36	60.11	0.37	0.38
21:14	10	10	0.83	0.56	153.7	5	0	36	36	60.25	0.33	0.38
21:24	10	10	0.83	0.57	156.96	5	0	36	36	60.48	0.33	0.38
21:34	10	10	0.84	0.56	160.34	5	0	36	36	60.58	0.34	0.37
21:44	10	10	0.81	0.56	163.81	5	0	36	36	60.72	0.31	0.38
21:54	10	10	0.82	0.56	167.02	5	0	36	36	60.99	0.32	0.37
22:04	10	10	0.83	0.56	170.26	5	0	37	36	60.98	0.33	0.38
22:14	10	10	0.85	0.56	173.49	5	0	36	36	61.09	0.36	0.38
22:24	10	10	0.84	0.56	176.69	5	0	36	36	61.16	0.34	0.38

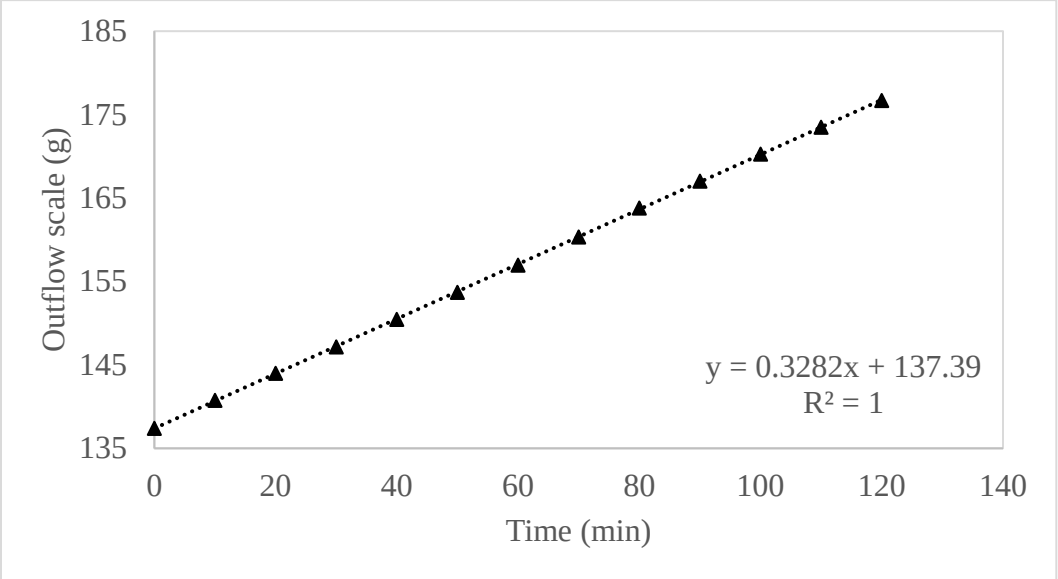
185
175
165
155
145
135
Outflow scale (g)
0
20
40
60
80
100
120
140
Time (min)
y = 0.3282x + 137.39
R² = 1

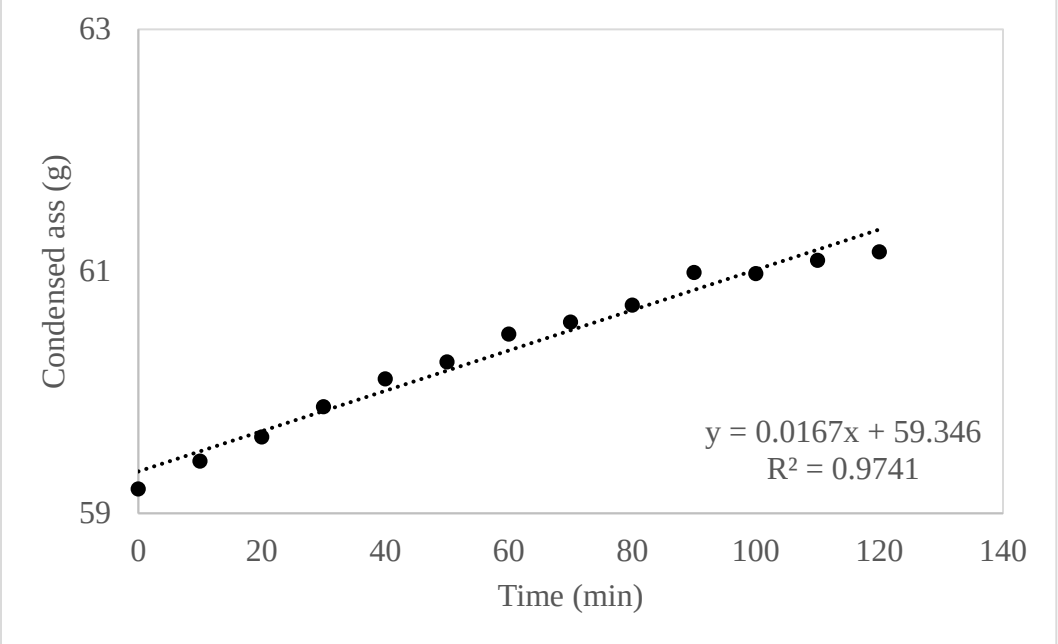
63
61
59
Condensed ass (g)
0
20
40
60
80
100
120
140
Time (min)
y = 0.0167x + 59.346
R² = 0.9741

2. Air temperature: 45 °C

Time	Airflow (L min^{-1})		Water flow (mL min^{-1})		Outflow scale (g)	Air pressure (psi)		Water pressure (psi)		Condensed mass (g)	Calibrated water flow (mL min^{-1})	
	I	II	In	Out		In	Out	In	Out		In	Out
15:47	10	10	1.04	0.57	176.4	5	0	37	36	83.32	0.55	0.39
15:57	10	10	1.05	0.57	179.66	5	0	37	36	84.45	0.55	0.38
16:07	10	10	1.05	0.56	182.77	5	0	37	36	85.69	0.56	0.38
16:17	10	10	1.04	0.56	186	5	0	37	36	86.87	0.54	0.38
16:27	10	10	1.04	0.56	189.18	5	0	37	36	88.06	0.55	0.38
16:38	10	10	1.04	0.56	192.7	5	0	37	36	89.41	0.55	0.38
16:48	10	10	1.04	0.56	195.92	5	0	37	36	90.58	0.55	0.38
16:58	10	10	1.04	0.56	199.17	5	0	37	36	91.9	0.55	0.38
17:08	10	10	1.04	0.56	202.34	5	0	37	36	93.11	0.55	0.38
17:18	10	10	1.04	0.56	205.55	5	0	37	36	94.38	0.55	0.38
17:28	10	10	1.04	0.56	208.84	5	0	37	36	95.53	0.55	0.38

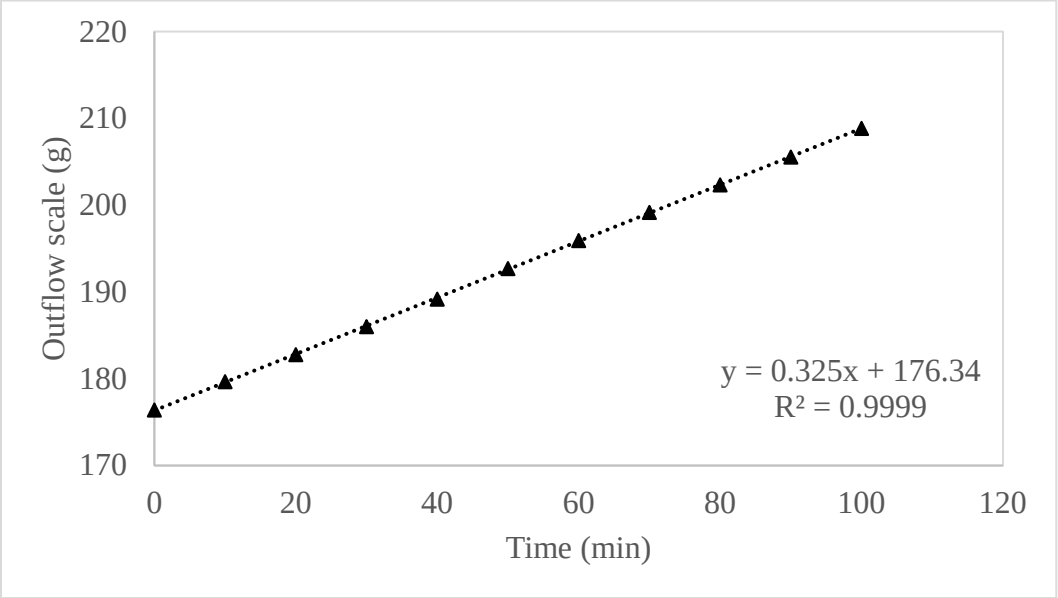
220
210
200
190
180
170
Outflow scale (g)
0
20
40
60
80
100
120
Time (min)
y = 0.325x + 176.34
R² = 0.9999

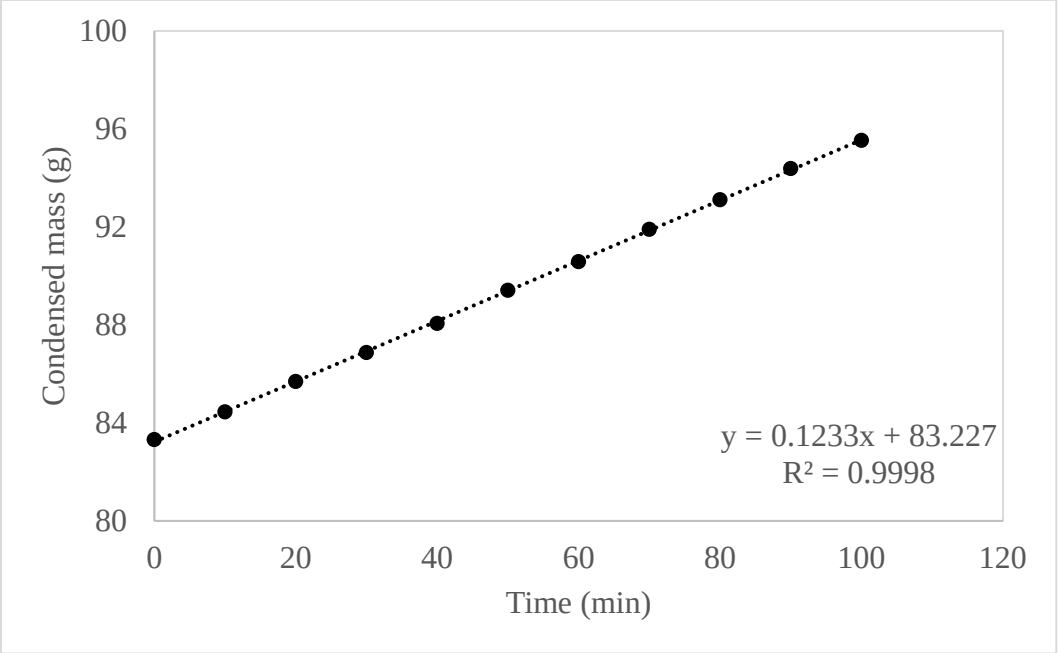
100
96
92
88
84
80
Condensed mass (g)
0
20
40
60
80
100
120
Time (min)
y = 0.1233x + 83.227
R² = 0.9998

3. Air temperature: 60 °C

Time	Airflow (L min^{-1})		Water flow (mL min^{-1})		Outflow scale (g)	Air pressure (psi)		Water pressure (psi)		Condensed mass (g)	Calibrated water flow (mL min^{-1})	
	I	II	In	Out		In	Out	In	Out		In	Out
19:26	10	10	1.08	0.56	144	6	0	37	36	70.62	0.59	0.38
19:36	10	10	1.09	0.56	147.04	6	0	37	36	72.51	0.59	0.38
19:46	10	10	1.08	0.56	150.07	6	0	37	36	74.34	0.58	0.38
19:56	10	10	1.08	0.56	153.12	6	0	37	36	76.26	0.59	0.38
20:06	10	10	1.07	0.56	156.22	6	0	37	36	78.13	0.57	0.38
20:16	10	10	1.07	0.56	159.2	6	0	37	36	80.07	0.57	0.38
20:26	10	10	1.07	0.58	162.21	6	0	37	36	81.89	0.58	0.39

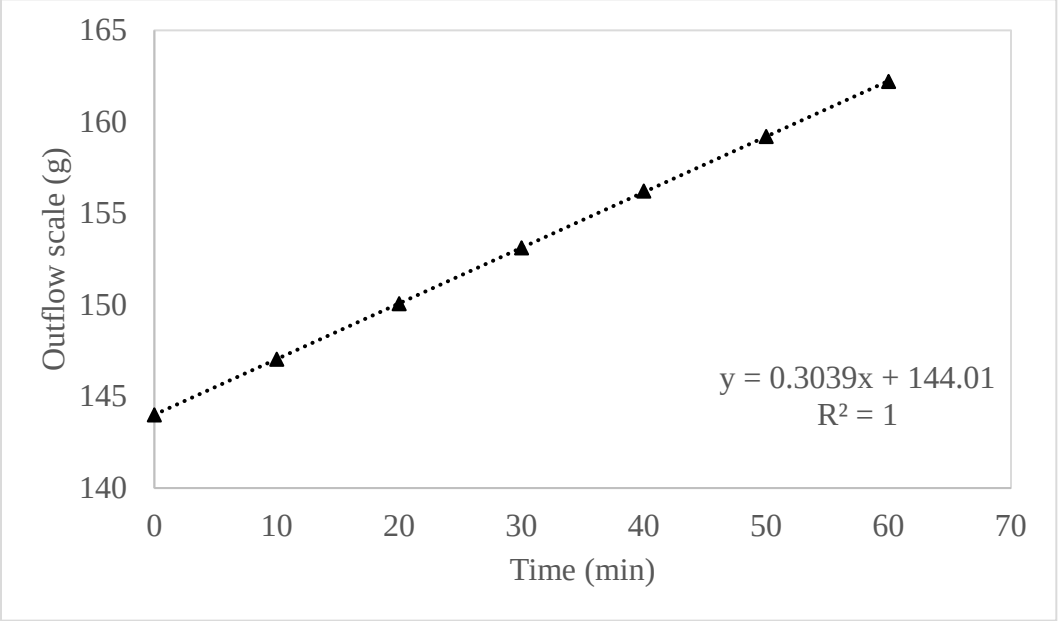
165
160
155
150
145
140
Outflow scale (g)
0
10
20
30
40
50
60
70
Time (min)
y = 0.3039x + 144.01
R² = 1

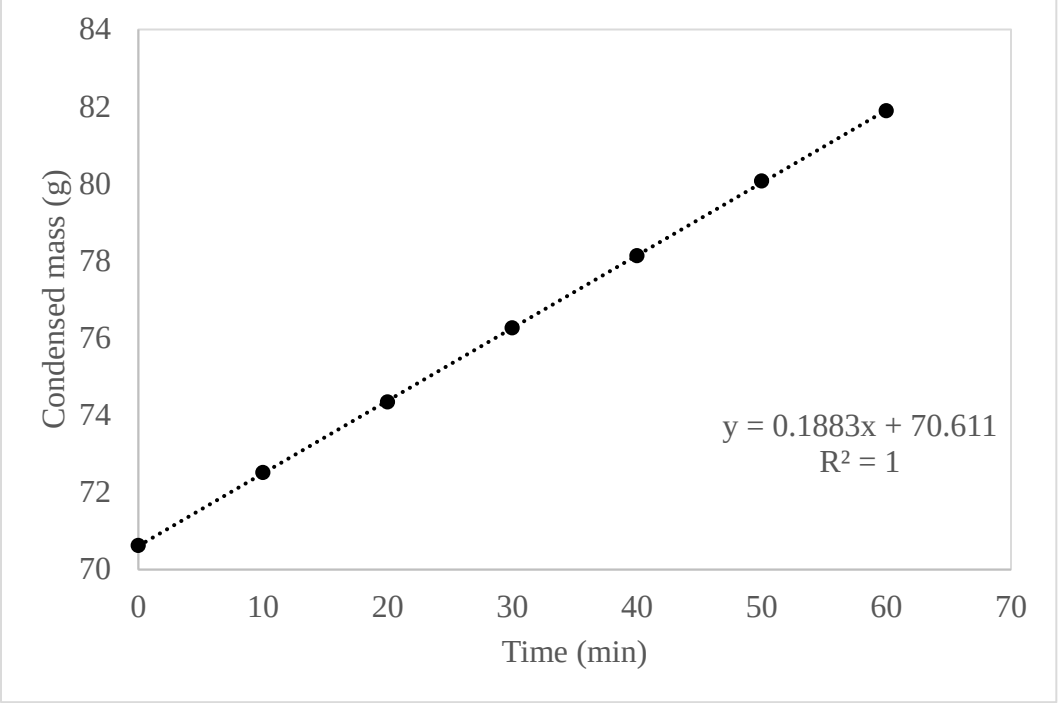
84
82
80
78
76
74
72
70
Condensed mass (g)
0
10
20
30
40
50
60
70
Time (min)
y = 0.1883x + 70.611
R² = 1

4. Air temperature: 70 °C

Time	Airflow (L min^{-1})		Water flow (mL min^{-1})		Outflow scale (g)	Air pressure (psi)		Water pressure (psi)		Condensed mass (g)	Calibrated water flow (mL min^{-1})	
	I	II	In	Out		In	Out	In	Out		In	Out
17:29	10	10	1.18	0.58	82	6	0	36	36	36.45	0.68	0.39
17:34	10	10	1.18	0.56	83.54	6	0	36	36	37.66	0.68	0.38
17:39	10	10	1.16	0.56	85.05	6	0	36	36	38.87	0.66	0.38
17:44	10	10	1.18	0.56	86.63	6	0	36	36	40.21	0.69	0.38
17:49	10	10	1.21	0.56	88.15	6	0	36	36	41.44	0.72	0.38
17:54	10	10	1.17	0.56	89.7	6	0	36	36	42.75	0.68	0.38
17:59	10	10	1.17	0.56	91.3	6	0	36	36	43.96	0.68	0.38

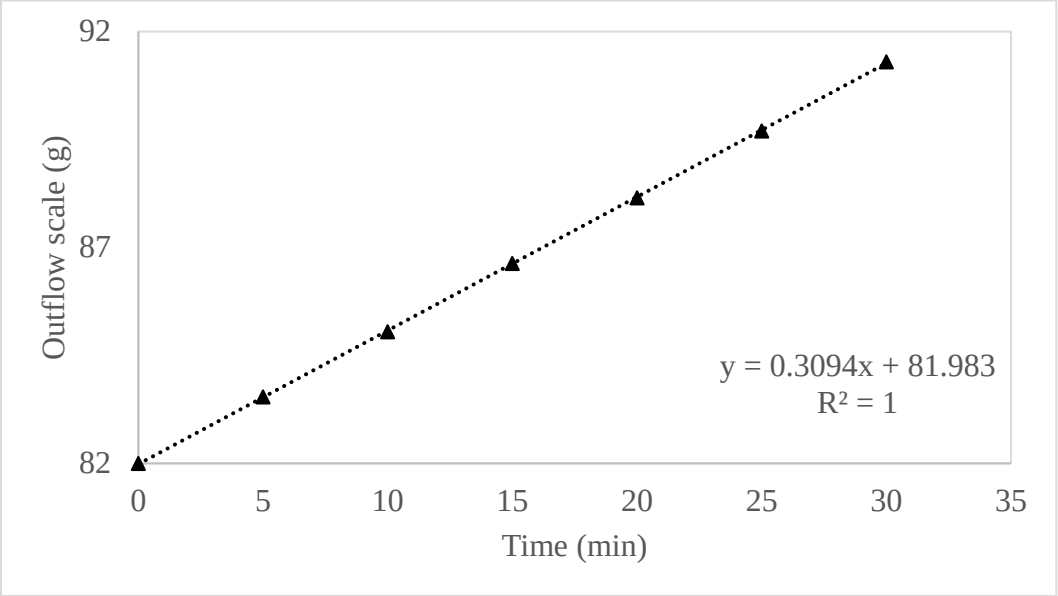
92
87
82
Outflow scale (g)
0
5
10
15
20
25
30
35
Time (min)
y = 0.3094x + 81.983
R² = 1

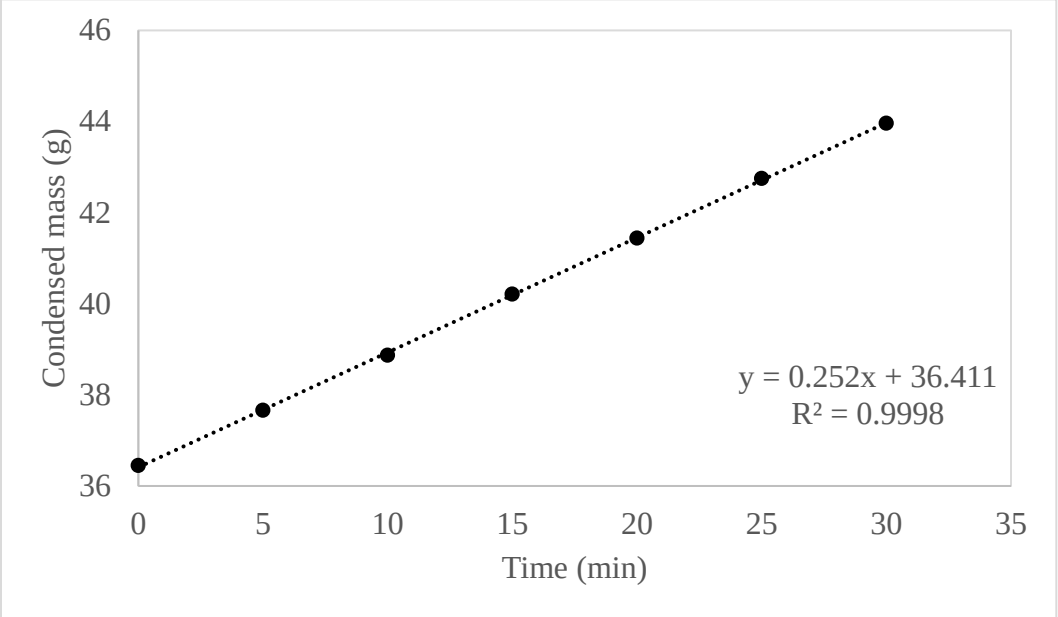
46
44
42
40
38
36
Condensed mass (g)
0
5
10
15
20
25
30
35
Time (min)
y = 0.252x + 36.411
R² = 0.9998

5. Air temperature: 80 °C

Time	Airflow (L min^{-1})		Water flow (mL min^{-1})		Outflow scale (g)	Air pressure (psi)		Water pressure (psi)		Condensed mass (g)	Calibrated water flow (mL min^{-1})	
	I	II	In	Out		In	Out	In	Out		In	Out
19:00	10	10	1.34	0.57	213.48	6	0	37	36	52.74	0.85	0.38
19:05	10	10	1.34	0.58	215.04	6	0	37	36	54.71	0.85	0.39
19:10	10	10	1.33	0.56	216.64	6	0	37	36	56.26	0.84	0.38
19:15	10	10	1.34	0.56	218.27	6	0	37	36	57.75	0.85	0.38
19:20	10	10	1.33	0.56	219.9	6	0	37	36	59.45	0.84	0.38
19:25	10	10	1.33	0.56	221.5	6	0	37	36	61.12	0.84	0.38
19:30	10	10	1.31	0.56	223.11	6	0	37	36	62.66	0.82	0.38
19:35	10	10	1.31	0.56	224.75	6	0	37	36	64.14	0.82	0.38

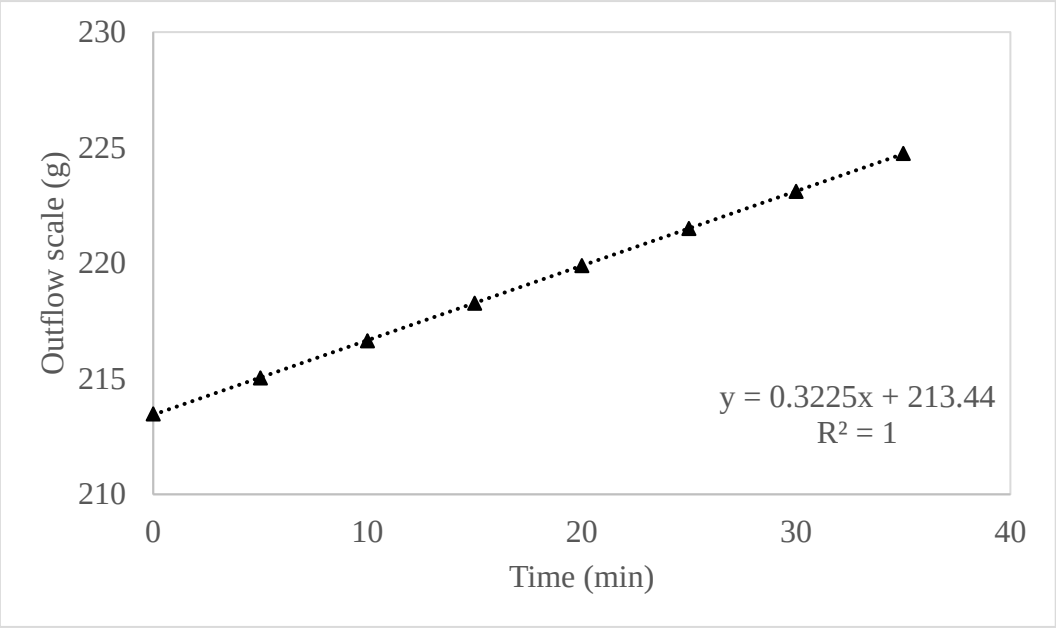
230
225
220
215
210
Outflow scale (g)
0
10
20
30
40
Time (min)
y = 0.3225x + 213.44
R² = 1

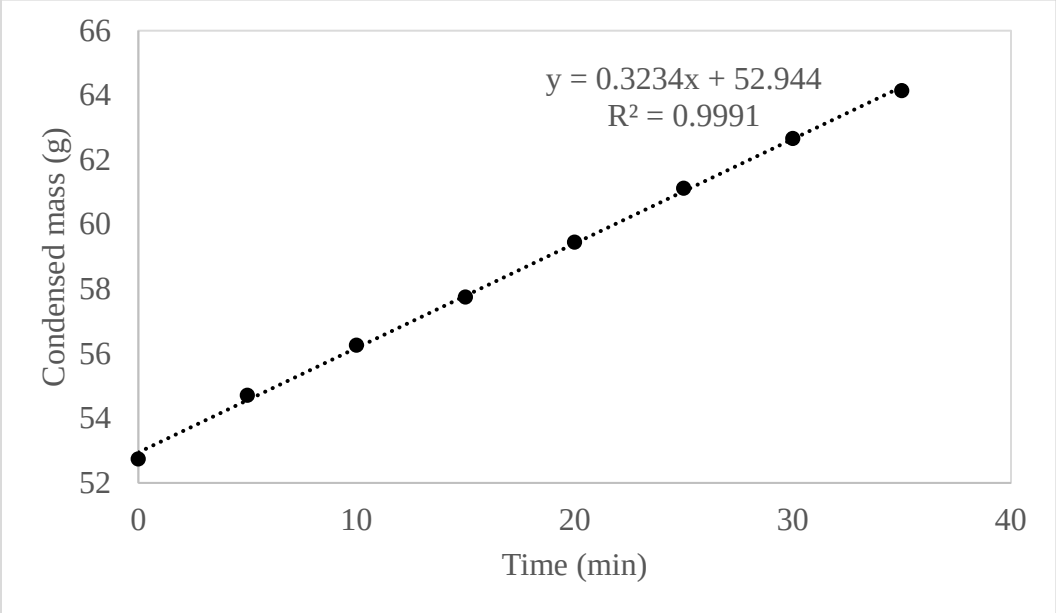
66
64
62
60
58
56
54
52
Condensed mass (g)
0
10
20
30
40
Time (min)
y = 0.3234x + 52.944
R² = 0.9991

Appendix IV: Data record for module 1 (Brine concentrate)

Time	Airflow (L min^{-1})		Water flow (mL min^{-1})		Outflow scale (g)	Air pressure (psi)		Water pressure (psi)		Conductivity (mS cm^{-1})	Condensed mass (g)	Calibrated water flow (mL min^{-1})	
	I	II	In	Out		In	Out	In	Out			In	Out
16:57	10	10	0.92	0.51	80.43	7	0	31	31	13.75	33.84		0.42
17:57	10	10	1.12	0.51	103.56	8	0	31	31	13.79	41.24	0.66	0.42
18:57	10	10	1.11	0.50	126.13	8	0	32	31	14.14	48.9	0.64	0.41
19:57	10	10	1.12	0.50	148.88	8	0	32	31	14.62	56.09	0.65	0.41
20:57	10	10	1.11	0.52	172.5	8	0	32	31	16.09	63.46	0.65	0.42
21:57	10	10	1.07	0.50	196.11	8	0	32	30	18.14	70.2	0.60	0.41
22:57	10	10	1.01	0.51	219.42	8	0	32	30	19.44	75.77	0.54	0.42
23:57	10	10	1.03	0.51	241.99	8	0	32	30	19.40	81.18	0.56	0.42
0:57	10	10	1.02	0.50	264.26	8	0	32	30	19.26	85.43	0.55	0.41
1:57	10	10	1.00	0.50	287.37	8	0	32	30	19.10	89.45	0.53	0.41
2:57	10	10	0.98	0.50	310.31	8	0	32	30	18.96	92.36	0.50	0.41
3:57	10	10	0.96	0.50	332.69	8	0	32	30	18.87	94.72	0.48	0.41
4:57	10	10	0.93	0.52	354.79	8	0	32	29	18.74	96.4	0.44	0.42
5:57	10	10	0.93	0.50	376.48	8	0	32	29	18.58	97.32	0.45	0.41
6:57	10	10	0.91	0.50	398.44	8	0	32	29	18.62	98.14	0.43	0.41
7:57	10	10	0.90	0.50	420.62	8	0	32	29	18.48	98.34	0.41	0.41
8:57	10	10	0.89	0.50	442.39	8	0	32	29	18.38	98.15	0.40	0.41
9:57	10	10	0.89	0.50	464.14	8	0	32	29	18.28	97.74	0.40	0.41
10:57	10	10	0.93	0.51	485.89	8	0	32	28	18.14	97.32	0.45	0.42

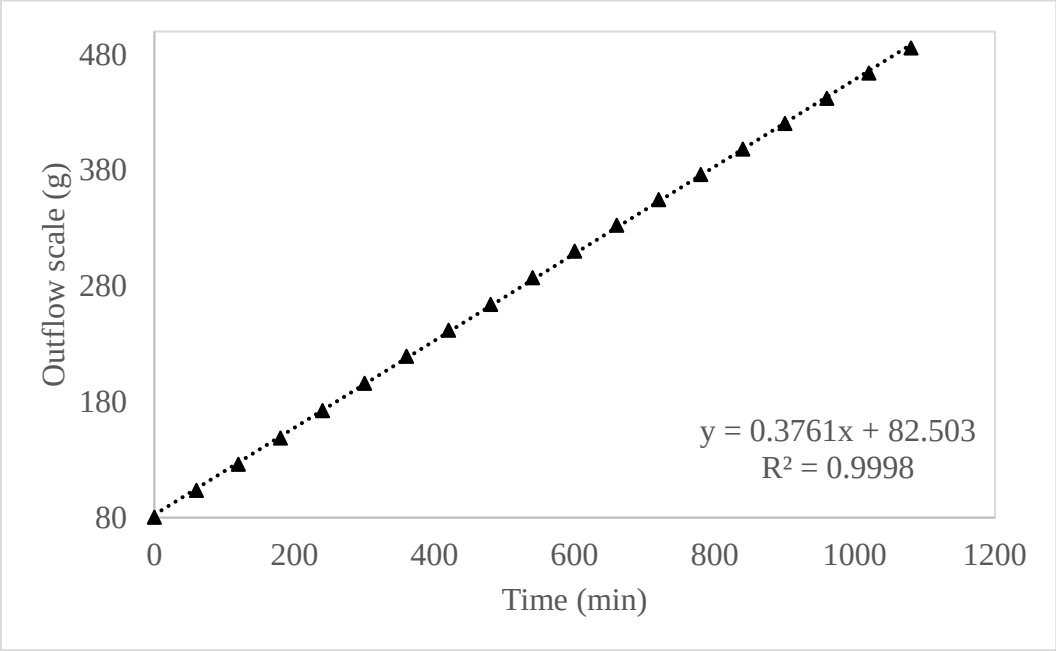
480
380
280
180
80
Outflow scale (g)
0
200
400
600
800
1000
1200
Time (min)
y = 0.3761x + 82.503
R² = 0.9998

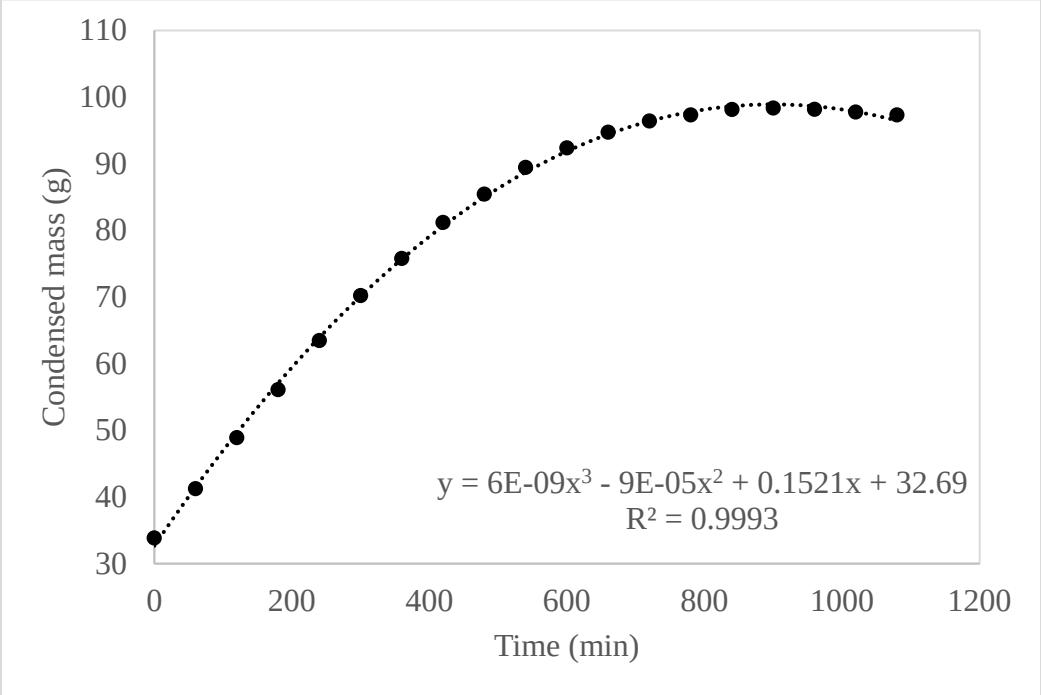
110
100
90
80
70
60
50
40
30
Condensed mass (g)
0
200
400
600
800
1000
1200
Time (min)
y = 6E-09x³ - 9E-05x² + 0.1521x + 32.69
R² = 0.9993

Appendix V: Data record for module 2 (Brine concentrate)

Time	Airflow (L min^{-1})	Water flow (mL min^{-1})		Outflow scale (g)	Air pressure (psi)		Water pressure (psi)		Conductivity (mS cm^{-1})	Condensed mass (g)	Calibrated water flow (mL min^{-1})	
		In	Out		In	Out	In	Out			In	Out
23:45	15	0.88	0.59	5.19	4	0	19	19	14.15	139.22		0.50
0:45	15	1.07	0.59	27.67	4	0	19	19	14.36	146.7	0.66	0.50
1:45	15	1.06	0.59	51.52	5	0	19	18	14.64	153.61	0.65	0.50
2:45	15	1.10	0.60	74.86	5	0	19	18	15.67	161.12	0.69	0.51
3:45	15	1.06	0.60	98.45	5	0	19	18	17.71	168.3	0.65	0.51
4:45	15	1.08	0.61	121.61	5	0	19	18	19.16	175.27	0.67	0.52
5:45	15	1.07	0.59	143.77	5	0	19	18	19.78	182.51	0.66	0.50
6:45	15	1.07	0.60	165.59	5	0	19	18	19.83	188.76	0.66	0.51
7:45	15	1.07	0.59	187.93	5	0	19	18	19.90	194.98	0.66	0.50
8:45	15	1.07	0.59	209.98	5	0	19	18	19.84	201	0.66	0.50
9:45	15	1.06	0.60	232.08	5	0	19	18	19.70	206.67	0.65	0.51
10:45	15	1.04	0.59	254.33	5	0	19	18	19.60	211.81	0.63	0.50
11:45	15	1.00	0.59	276.95	6	0	19	18	19.53	216.32	0.59	0.50
12:45	15	1.00	0.60	299.19	6	0	19	18	19.44	220.38	0.59	0.51
13:45	15	1.01	0.60	321.34	6	0	19	18	19.40	224.72	0.60	0.51
14:45	15	0.97	0.59	343.86	6	0	19	18	19.24	228.21	0.56	0.50
15:45	15	0.99	0.60	366.43	6	0	19	18	19.17	231.43	0.58	0.51
16:45	15	0.99	0.59	388.85	6	0	19	18	19.08	234.73	0.58	0.50
17:45	15	0.98	0.59	411.1	6	0	19	18	18.97	237.32	0.57	0.50
18:45	15	0.99	0.59	433.45	7	0	19	18	18.86	240.06	0.58	0.50
19:45	15	0.99	0.61	456.25	7	0	19	18	18.80	242.86	0.58	0.52
20:45	15	0.97	0.59	479.38	7	0	19	18	18.70	245.45	0.56	0.50

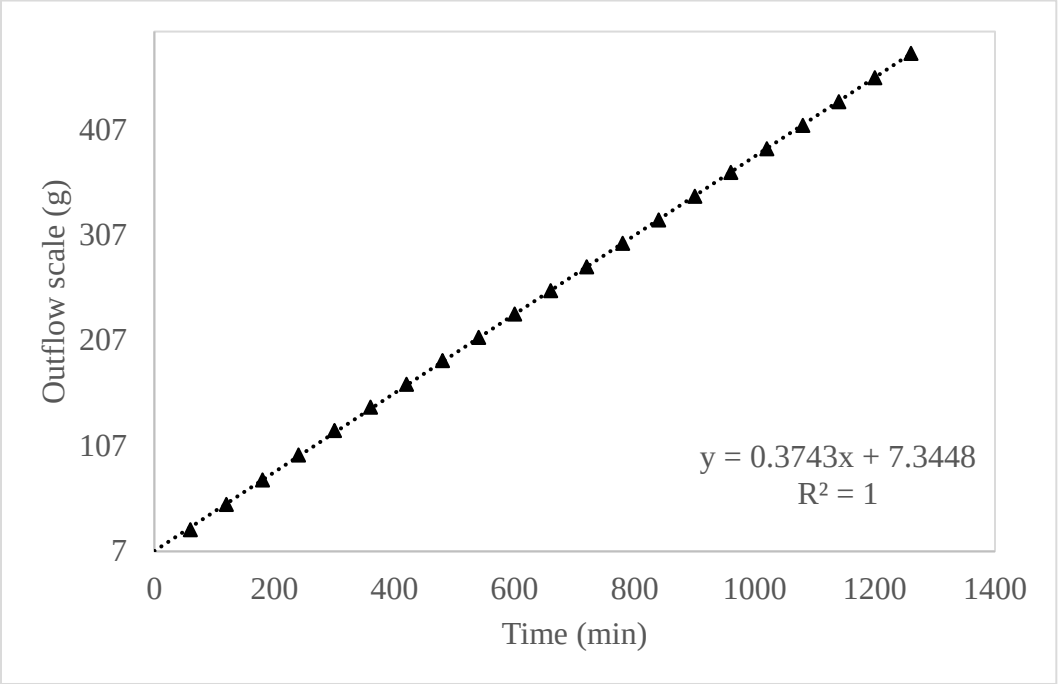
Outflow scale (g)
407
307
207
107
7
0
200
400
600
800
1000
1200
1400
Time (min)
y = 0.3743x + 7.3448
R² = 1

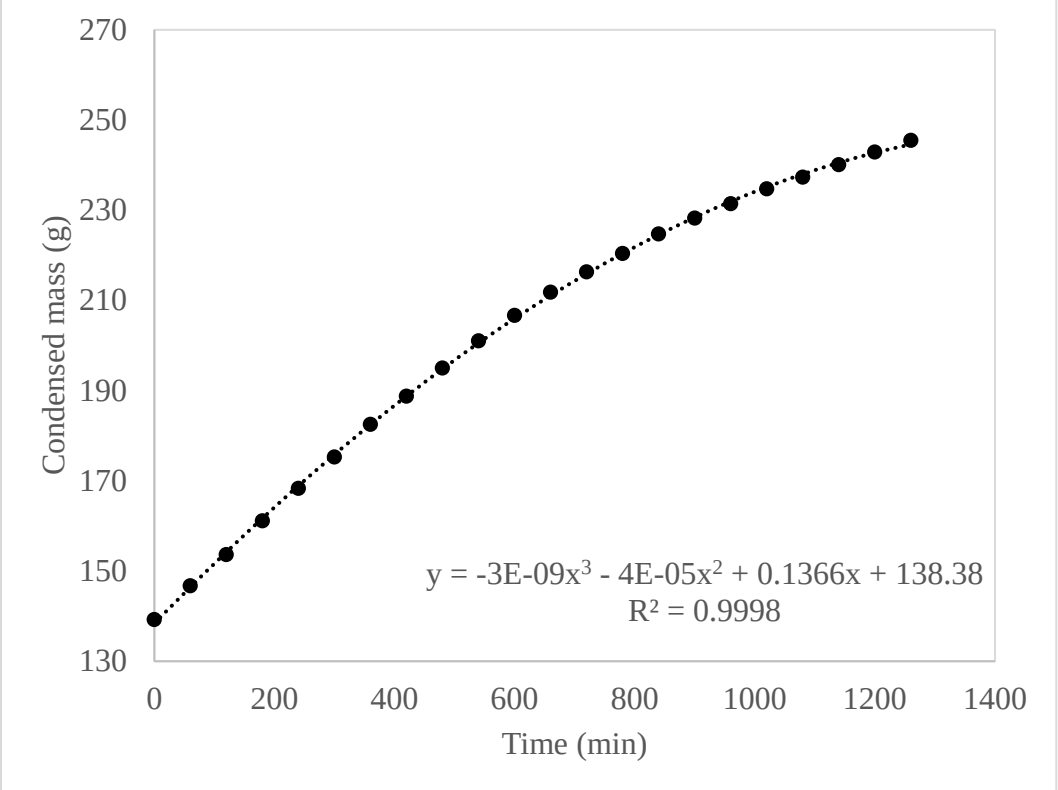
Condensed mass (g)
270
250
230
210
190
170
150
130
0
200
400
600
800
1000
1200
1400
Time (min)
y = -3E-09x³ - 4E-05x² + 0.1366x + 138.38
R² = 0.9998

Appendix VI: Data record for module 3 (Brine concentrate)

Time	Airflow (L min^{-1})	Water flow (mL min^{-1})		Outflow scale (g)	Air pressure (psi)		Water pressure (psi)		Conductivity (mS cm^{-1})	Condensed mass (g)	Calibrated water flow (mL min^{-1})	
		In	Out		In	Out	In	Out			In	Out
17:10	15	0.73	0.50	68.51	3	0	30	29	14.12	191.36	0.22	0.41
18:10	15	1.00	0.51	82.23	3	0	32	32	14.22	198.18	0.53	0.42
19:10	15	0.96	0.50	95.91	4	0	32	31	14.31	204.33	0.48	0.41
20:10	15	0.99	0.51	109.64	4	0	32	31	14.42	211.04	0.51	0.42
21:10	15	0.97	0.50	123.82	4	0	32	31	14.65	217.22	0.49	0.41
22:10	15	0.95	0.50	137.43	4	0	32	32	15.24	222.85	0.46	0.41
23:10	15	0.93	0.50	150.91	4	0	32	32	16.15	228.97	0.44	0.41
0:10	15	0.93	0.50	164.54	4	0	32	32	17.59	234.7	0.45	0.41
1:10	15	0.93	0.51	178.71	4	0	32	32	19.09	240.18	0.44	0.42
2:10	15	0.92	0.51	193.04	4	0	32	32	20.26	246.1	0.43	0.42
3:10	15	0.91	0.50	207.08	4	0	32	32	21.25	250.63	0.42	0.41
4:10	15	0.90	0.50	220.91	4	0	32	32	21.85	255.48	0.41	0.41
5:10	15	0.90	0.51	234.82	4	0	32	31	22.11	260.55	0.41	0.42
6:10	15	0.91	0.50	248.95	4	0	32	31	22.09	265.22	0.43	0.41
7:10	15	0.89	0.50	263.62	4	0	32	31	22.21	269.86	0.39	0.41
8:10	15	0.83	0.50	277.39	4	0	32	31	22.14	273.84	0.34	0.41
9:10	15	0.84	0.50	291.09	4	0	32	30		277.86	0.34	0.41
12:10	15	0.86	0.51	526.5	4	0	32	25	20.92	285.62	0.37	0.41
13:10	15	0.80	0.50	539.83	4	0	32	18	20.76	288.62	0.30	0.41
14:10	15	0.75	0.50	552.65	4	0	32	9	20.59	290.84	0.24	0.41
15:10	15	0.69	0.50	564.35	4	0	32	1	20.46	293.24	0.17	0.41
16:10	15	0.64	0.51	571.09	4	0	32	1	20.35	294.92	0.11	0.41

Time	Airflow (L min^{-1})	Water flow (mL min^{-1})		Outflow scale (g)	Air pressure (psi)		Water pressure (psi)		Conductivity (mS cm^{-1})	Condensed mass (g)	Calibrated water flow (mL min^{-1})	
		In	Out		In	Out	In	Out			In	Out
17:10	15	0.58	0.50	573.98	4	0	32	1	20.33	296.63	0.05	0.40
18:10	15	0.58	0.50	575.52	4	0	32	0	20.30	297.62	0.05	0.41
19:10	15	0.59	0.51	576.18	4	0	32	0	20.27	298.64	0.06	0.42
20:10	15	0.57	0.51	576.8	4	0	33	0	20.29	298.58	0.04	0.42
21:10	15	0.55	0.52	577.34	4	0	33	0	20.32	298.84	0.01	0.42
22:10	15	0.53	0.51	577.86	4	0	33	0	20.33	298.56	-0.01	0.42

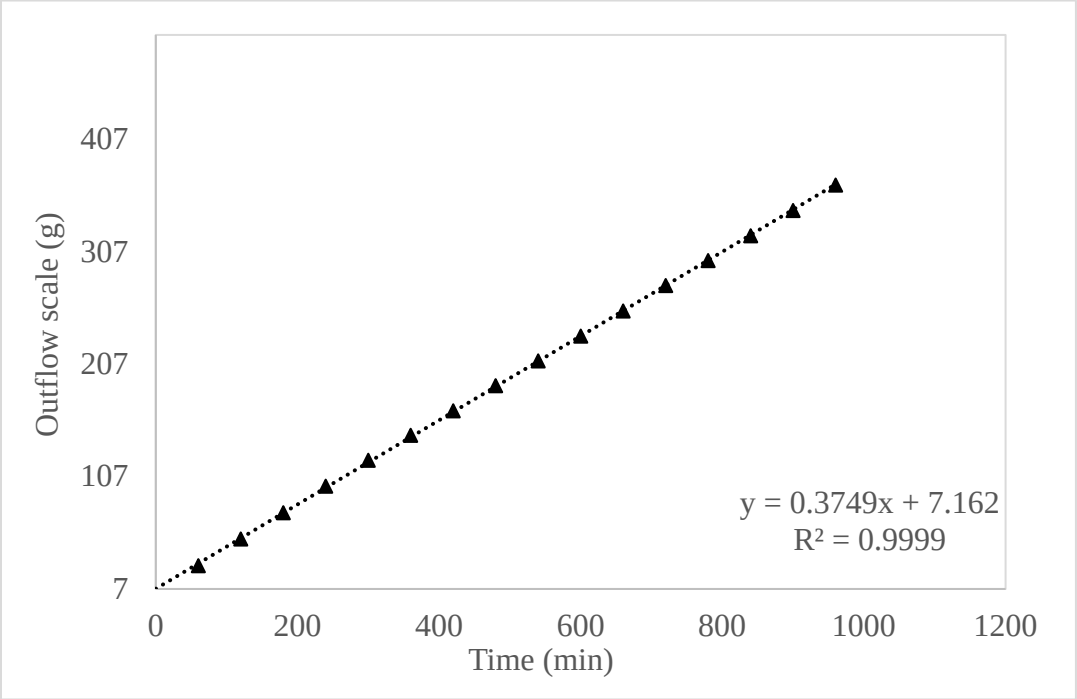
Outflow scale (g)
407
307
207
107
7
0
200
400
600
800
1000
1200
Time (min)
y = 0.3749x + 7.162
R² = 0.9999

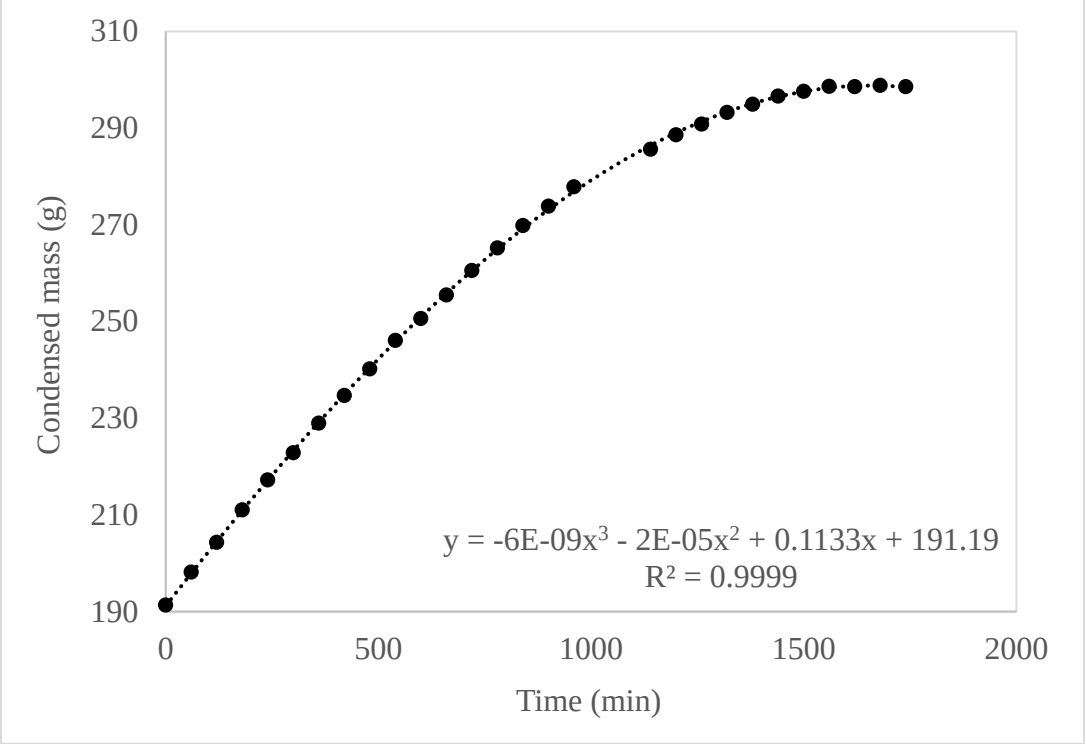
Condensed mass (g)
310
290
270
250
230
210
190
0
500
1000
1500
2000
Time (min)
y = -6E-09x³ - 2E-05x² + 0.1133x + 191.19
R² = 0.9999

16. Appendix VII: Data Record for Module 4 (Brine Concentrate)

Time	Airflow (L min^{-1})	Water flow (mL min^{-1})		Outflow scale (g)	Air pressure (psi)		Water pressure (psi)		Conductivity (mS cm^{-1})	Condensed mass (g)	Calibrated water flow (mL min^{-1})	
		In	Out		In	Out	In	Out			In	Out
20:07	15	1.13	0.80	2	4	0	32	32	15	18.61	0.58	0.52
22:07	15	1.16	0.80	46.47	4	0	32	32	17	33.69	0.61	0.52
12:08	15	1.12	0.81	372.73	4	0	32	31	22	135.36	0.56	0.53
14:08	15	1.11	0.80	418.92	4	0	31	31	22	150.33	0.55	0.51
16:08	15	1.12	0.80	464.6	4	0	31	31	22	165.05	0.56	0.52
18:08	15	1.11	0.80	509.57	4	0	31	31	22	179.8	0.55	0.52
20:08	15	1.09	0.80	554.33	4	0	31	30	22	194.09	0.53	0.52
22:08	15	1.07	0.80	598.51	4	0	31	30	22	207.7	0.51	0.52
0:08	15	1.09	0.80	642.48	4	0	31	30	22	221.65	0.53	0.52
2:08	15	1.08	0.80	686.33	4	0	31	30	22	235.37	0.51	0.51
4:08	15	1.09	0.81	730.17	4	0	31	30	22	249.4	0.53	0.53
6:08	15	1.11	0.80	773.78	4	0	31	30	22	263.96	0.55	0.52
8:08	15	1.14	0.80	816.94	4	0	31	30	22	278.77	0.59	0.52
10:08	15	1.16	0.80	860.49	4	0	30	30	22	293.33	0.61	0.52
12:08	15	1.17	0.80	903.75	4	0	30	30	22	308.21	0.62	0.52
14:08	15	1.22	0.82	947.04	4	0	30	30	23	323.09	0.68	0.53
16:08	15	1.25	0.81	990.23	4	0	30	29	22	338.49	0.72	0.53
18:08	15	1.25	0.80	1033.6	4	0	30	30	23	353.85	0.71	0.52
20:08	15	1.27	0.82	1076.8	4	0	30	30	23	368.91	0.73	0.53
22:08	15	1.29	0.82	1120.3	4	0	30	30	22	384.06	0.76	0.53

Time	Airflow (L min^{-1})	Water flow (mL min^{-1})		Outflow scale (g)	Air pressure (psi)		Water pressure (psi)		Conductivity (mS cm^{-1})	Condensed mass (g)	Calibrated water flow (mL min^{-1})	
		In	Out		In	Out	In	Out			In	Out
0:08	15	1.33	0.80	1163.8	4	0	30	30	22	399.25	0.81	0.52
2:08	15	1.33	0.80	1207.4	4	0	30	30	23	414.07	0.80	0.52
4:08	15	1.33	0.80	1251	4	0	30	30	23	429.07	0.81	0.52
6:08	15	1.33	0.80	1294.7	4	0	30	30	23	443.44	0.81	0.52

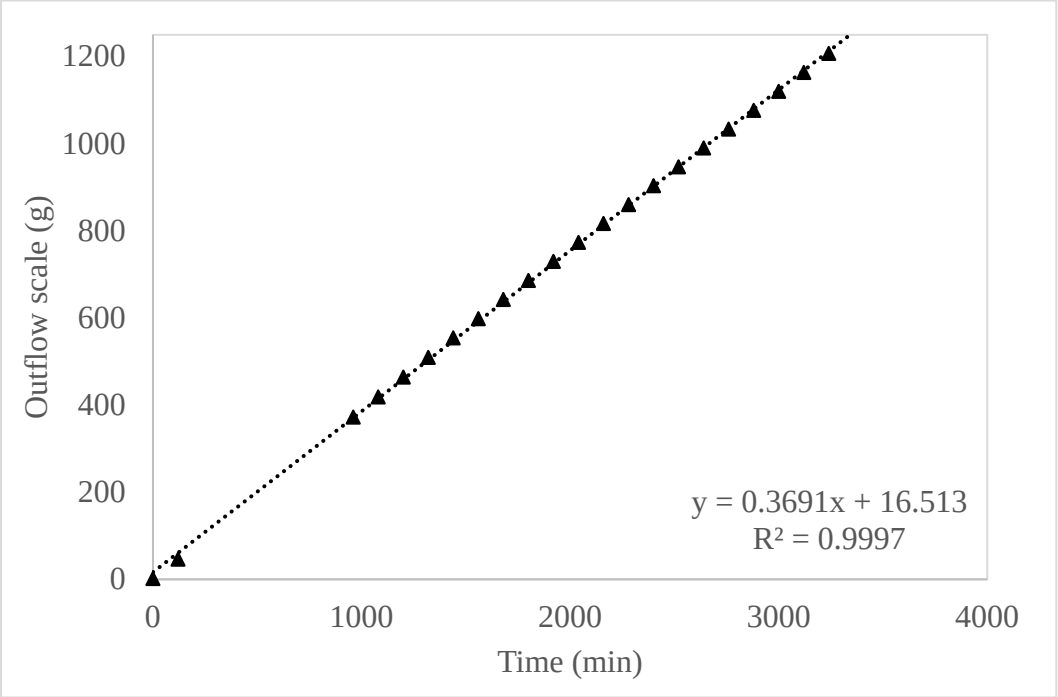
1200
1000
800
600
400
200
0
Outflow scale (g)
0
1000
2000
3000
4000
Time (min)
y = 0.3691x + 16.513
R² = 0.9997

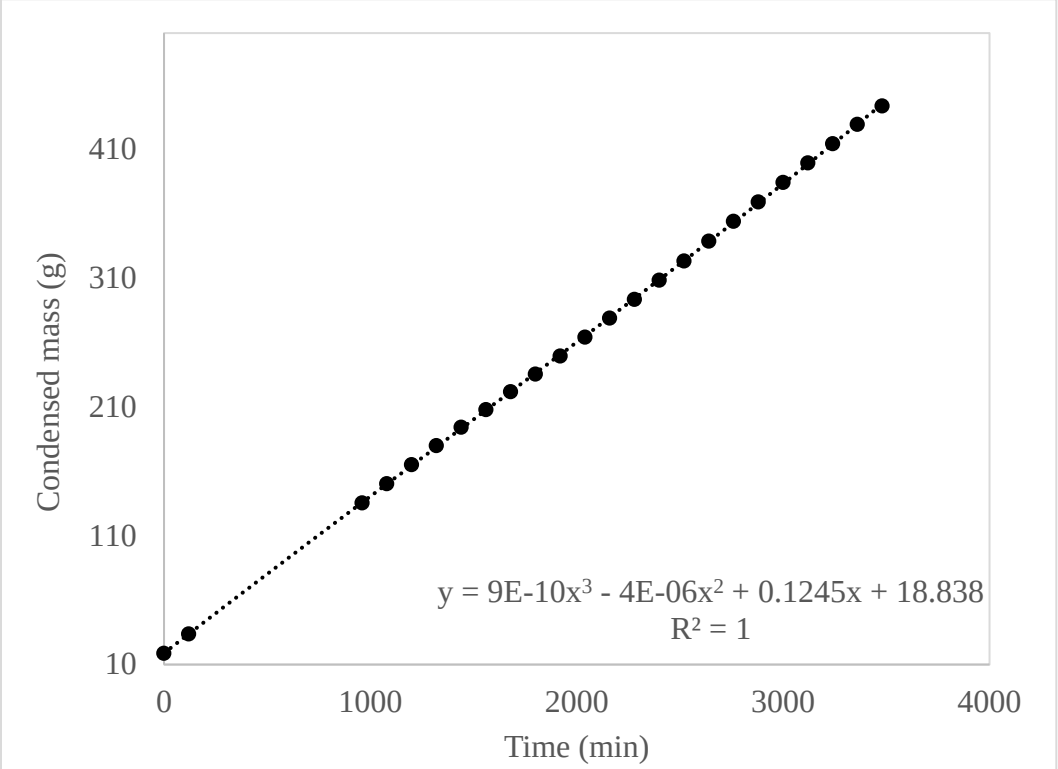
410
310
210
110
10
Condensed mass (g)
0
1000
2000
3000
4000
Time (min)
y = 9E-10x³ - 4E-06x² + 0.1245x + 18.838
R² = 1